Olea Imagein

The Diffusion saga

Olea MEDICAL

#2 - November 2016 - RSNA Edition

CONTENTS

NEWS

Olea Medical® strongly supports research

Olea Medical® supports research in medical imaging as Gold sponsor of SFR-CERF research grants in 2016

Legal representative:
Fayçal Djeridane
Olea Medical® is a subsidiary of Toshiba Medical Systems Corporation
Printer: Création Communication Impression (CCI) – 9 avenue Paul Heroult 13015 Marseille – France
Director:
Anca Mitulescu
Editor-in-Chief:
Sarah Quenet

Content Manager:
Brianna Bucciarelli
Graphics:
Christophe Rebesco
Selling price:
free of charge
Date of legal deposit:
March 2016
Publication date:
November 27th, 2016
ISSN Number: 2492-7260

EDITO

Denis Le Bihan, MD, PhD

Director of NeuroSpin, CEA Saclay-Center, Gif-sur-Yvette, France;
Professor at Human Brain Research Center,
Kyoto University Graduate School of Medicine, Kyoto, Japan.

I am delighted that Olea Medical® has chosen Diffusion MRI for their second Olea Imagein issue. Diffusion MRI was born in 1985 with a thought-provoking goal: provide non-invasively information of tissues at a microscopic level, while MR images remain at a macroscopic (millimetric) resolution. Beyond the invention of diffusion MRI, this is the *motto* which has driven, and is still driving today, my efforts and those of many teams around the world, to develop and apply this powerful concept to biomedical research and clinical practice. From their first days, focusing on the management of stroke patients, Olea Medical® has built upon diffusion MRI, and its child, IVIM MRI, to provide robust and efficient software solutions for the healthcare community, and this makes me very proud. While it took years for diffusion MRI to emerge in the clinical field, as its concept was without doubt very innovative at the time and "out of the box", diffusion MRI has become a cornerstone of modern medical imaging, first for the management of neurological disorders, but now increasingly for a broad variety of body illnesses, especially cancer, wherever in breast, prostate, or liver. The field of diffusion MRI has matured considerably over the last 30 years, benefiting from hardware development from MRI manufacturers (notably for the gradient systems hardware allowing larger "b-values" to be available), but also from a better understanding of the diffusion processes at play in tissues, resulting in models which are becoming more and more sophisticated. Needless to say, post-processing is central to diffusion MRI, to extract its full juice and the rich information it conveys, as we would be missing a lot by merely looking at simple "diffusion-weighted" MR images, hence the crucial role Olea Medical® has played in the field.

Still, the basic principles of diffusion MRI, and their limitations, remain the same and must be well kept in mind when interpreting results. Unfortunately, or fortunately, there are many ways to acquire and process diffusion MR images, which has led to clinical results which have been highly variable across the literature, giving sometimes the misleading impression that diffusion MRI might not be so reliable. Hence, if one wants to have diffusion MRI accepted (as many think that it should) as a reference method, for instance for the development, validation and approval by regulatory agencies of new therapies, especially in oncology, efforts must be made by manufacturers, software developers and clinicians to standardize diffusion MRI protocols. This should now be a priority in the own interests of all those players, but, above all, for patients' benefit. Thanks to the partnership with Toshiba Medical, Olea will be in a leading position, mastering the entire chain, from MR sequences and MRI hardware to data processing algorithms and software. However, this is only a step, as diffusion MRI has not yet spoken its last words. Big surprises are around the corner, as the concepts of IVIM and diffusion MRI can be extended to cross borders, for instance to perform MR angiography without contrast agents, or MR elastography without using mechanical vibrations.

Enjoy your reading!

Open Letter

Fayçal Djeridane
CEO, Olea Medical®

Dear friends,

Since the very beginning, at Olea Medical® we've been fueled by our quest for the scientific truth and greater knowledge. Scientific truth is timeless and the greater knowledge quest is infinite. Therefore, our constant challenge is to bring reliable and efficient tools in the hands of radiologists and radiographers, our most valuable partners in our mission.

Our innovation capacity is now well established and recognized in our field and it is part of our DNA at Olea. Sharing such innovation worldwide for the utmost patients' benefit has always been our credo. Therefore, although Olea Medical® joined the Toshiba Medical family last year, we will not amend our vendor-neutral approach, since this is the only way to deliver our innovation to the greatest number of patients. By the same reasoning, Olea Medical® keeps the door wide open to collaboration with various MR vendors because such collaborations will exponentially enhance knowledge, accelerate innovation and, ultimately, improve patient care. We strongly encourage all MR manufacturers to share our innovation for patients' sake.

Each of us alone is merely the master luthier. But we all need to work with the whole orchestra to bring out the best of sounds. Come join us and we will make a finer music together!

Sincerely yours,
Fayçal Djeridane

Olea Innovators Award Laureates

2016 TOPIC:
Innovative MRI medical imaging techniques for diagnosis and follow up of devastating diseases.

TECHNOLOGICAL INDUSTRIALIZATION CATEGORY

Todd Parrish, PhD

Professor of Radiology and BME at Northwestern University, Chicago, USA

ACQUISITION OF PERMEABILITY AND PERFUSION IN TUMORS USING A SINGLE INJECTION OF CONTRAST

"I have developed a new imaging method that will allow the collection of both perfusion and permeability data without additional contrast or compromising either study with a split dose."

INCUBATORS CATEGORY

Gabrielle Fournet

PhD candidate at Neurospin (CEA Saclay) INRIA Saclay, France

APPLICATION OF INTRAVOXEL INCOHERENT MOTION (IVIM) IMAGING TO THE EARLY DIAGNOSIS OF ALZHEIMER'S DISEASE (AD)

"The main goal is to investigate how early IVIM is able to detect changes in the microvasculature related to the presence of amyloid plaques in AD."

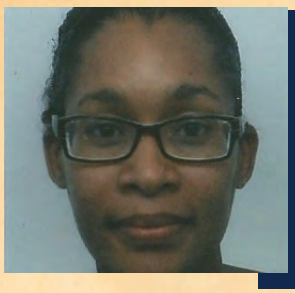

Aude Pavilla

PhD candidate at University of Rennes 1, France

CEREBRAL ISCHEMIC STROKE INTRAVOXEL INCOHERENT MOTION (CISIVIM)

"Stroke management relies on the setting of a diffusion-perfusion "discrepancy" (...), the aim of this project is to establish this mismatch with the IVIM method using a single diffusion sequence."

Sotirios Bisdas, MD, PhD, MSc

Senior Lecturer in Neuroradiology at University College London, UK

TEXTURE ANALYSIS IN DIFFUSIONAL KURTOSIS IMAGING (DKI) COMBINED WITH SUPPORT VECTOR MACHINE FOR NON-INVASIVE DIAGNOSIS OF IDH MUTATIONAL STATUS AND HISTOLOGICAL GRADING OF GLIOMAS

"Integration of texture analysis in DKI is expected to increase the diagnostic accuracy of tumour grade differentiation at the pre-treatment stage assisting thus the clinical management of the patients."

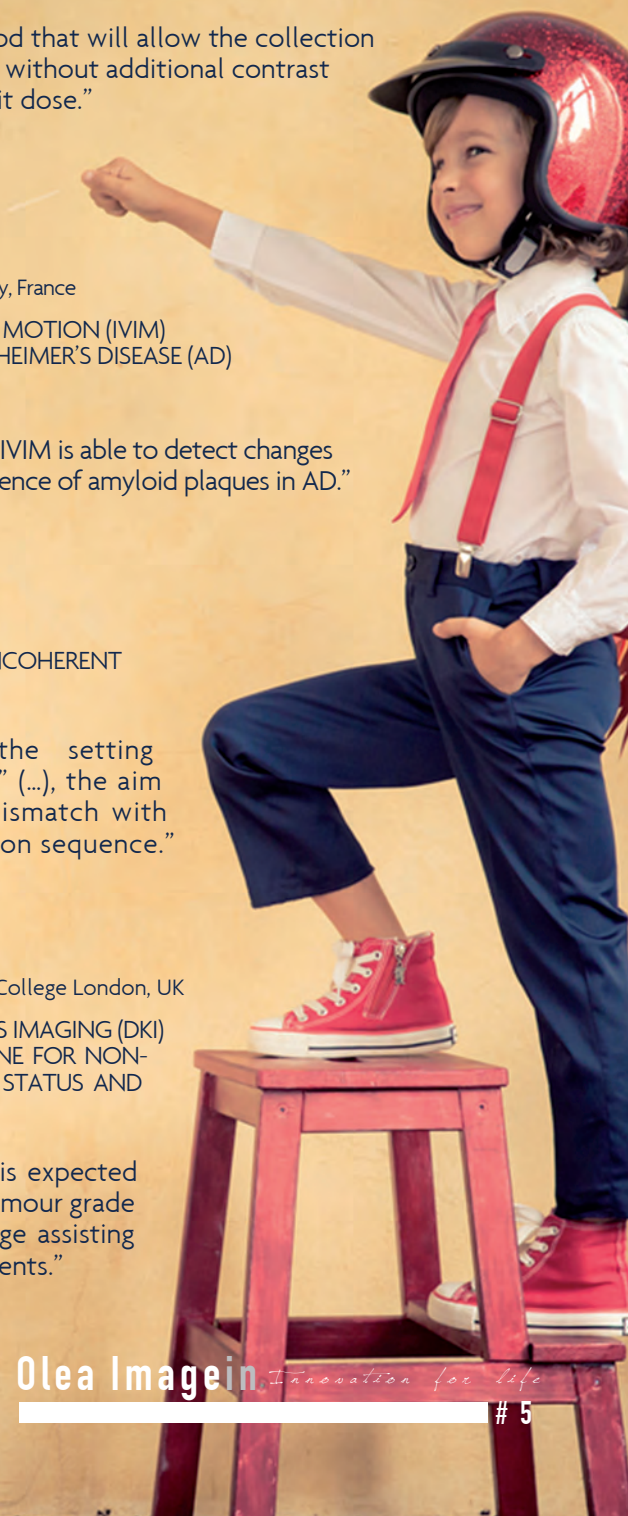

Pros & Cons | DWI in acute ischemic stroke

PROS

Jan Gralla, MD

Director and Chief Physician at University Institute of Diagnostic and Interventional Neuroradiology in Bern, Switzerland

"Acute ischemic stroke is an emergency: decision making is prompt and mainly based on clinical presentation and brain imaging. This decision, e.g. treatment modality or even no treatment, cannot be revised some hours later and has major impact on patients' future life.

MRI is more expensive and presumably more time consuming in many centers!

MRI including diffusion-weighted imaging (DWI) is an accurate imaging modality to access infarct core and mismatch in all patients; it furthermore provides an estimate of the time window in wake-up and unknown onset strokes. Therefore, we don't have to argue anymore about the necessity to evaluate patients with unknown onset of symptoms with MRI.

CT-CTP is equal for decision making in some obvious cases, but it fails to reproduce the clear delineation of the infarct core compared to DWI. Therefore, unconscious patients with basilar artery thrombosis are evaluated in MRI in many centers to estimate the mesencephalic and pons/brainstem lesion before advocating treatment.

CT-CTP also fails to illustrate the relevant changes in more peripheral vessel occlusion. Is the left sides M2/M3 occlusion beyond the time window of IV-tPA a reasonable target for mechanical thrombectomy, or do we put this patient with NIHSS of 4 at an unjustified risk? Would you like to make this decision based on a CT-CTP, or would you like to see a small and well delineated infarct core in DWI in combination with mismatch in MRI? Doesn't the same account for the large and growing number of "grey zone patients", e.g. elderly patients with various co-morbidities, heterogeneous quality of life and reduced potential for rehabilitation?

Decision making for stroke treatment is an emergency business and does not allow corrections later on. The impact for the patient is life-long with all its socioeconomic consequences – we should have the most accurate tools available."

CONS

Adam de Havenon, MD

Assistant Professor in Neurology and Program Director of Vascular Neurology Fellowship at University of Utah, UT, USA

"As a vascular neurologist at a tertiary academic medical center, I have 24/7 CT and MRI capability, immediately adjacent to our Emergency Department. Last year, we treated 600 acute ischemic stroke and transient ischemic attack (TIA) patients at my center, ~40 of which underwent our "Rapid" MRI protocol that includes DWI, FLAIR, GRE, DSC MRP, and a CE-MRA of the head, with a 9-minute scan time.

During the same time period, 100 patients had a "Brain Attack" CT protocol that includes CTA of the head/neck and CTP, with a comparable scan time to the MRI. I am a firm believer that the CT protocol is a superior tool for evaluating if stroke patients warrant treatment with intravenous tissue plasminogen activator (IV tPA) or endovascular thrombectomy.

The CRISP study, recently completed by Maarten Lansberg and colleagues at Stanford University, reported that CTP can reliably delineate the ischemic core and penumbra with automated threshold-based volumetric analysis in acute ischemic stroke patients.

In my experience, CTP is more practical from a workflow perspective, due to the difficulty of screening acute stroke patients for MRI safety.

An additional challenge with acute stroke MRI is that the combined head/neck MRI coils provide inferior neck vessel imaging compared to CTA. Switching between the high-performance, but separate, head and neck coils is not an option in this clinical setting. Finally, the widespread availability of modern multidetector CT scanners in small- and medium-sized hospitals that lack MRI capability provides a viable pathway for expansion of volumetric CTP analysis in the future, which will become increasingly important if the time window for endovascular treatment of ischemic stroke extends to 16 hours based on results of the ongoing DEFUSE-3 study. In conclusion, a combined acute ischemic stroke CT protocol with CTA and CTP, processed with automated volumetric software such as Olea Sphere®, is a reliable and expedient means of assessing stroke patients that provides comparable information to MRI with multiple real-world advantages."

Let's start from scratch!

PROS

Christophe Cognard, MD

Head of Neuroradiology Department at CHU Toulouse, Purpan hospital, Toulouse, France

"Mechanical thrombectomy (MT) within six hours of onset is nowadays the treatment of choice for large vessel occlusion stroke (LVOS). Decision to perform or not a MT in a patient presenting an acute LVOS is based on several clinical parameters: patient age, co-morbidity, modified Rankin scale before stroke onset, stroke severity evaluated by the NIHSS score, time from stroke onset, but also imaging parameters.

Imaging must at least show the presence of a LVOS and the core size. The minimum acceptable imaging techniques are a plain CT (giving the ASPECT score) and an angio-CT (giving the level of occlusion). In cases where the indication to perform MT is obvious, this limited protocol can be sufficient (young patient with a LVOS, early after stroke onset, with a huge deficit and a small core - ASPECT score › 7).

However, because of its extreme efficacy in increasing the rate of alive and independent patients at 3 months, MT is today proposed in many different situations where decision-making is difficult: very old patients (›90 YO) or younger ones (‹18 YO), low NIHSS score (2 to 6), distal thrombus (M2, A2), large core stroke (ASPECT‹7), long delay from onset (›6h). In all these situations, treating patients with a MT could be useless or even dangerous; on the contrary, deciding not to do a MT jeopardizes the chance for the patient to fully recover at 3 months. Decision-making process can be helped by performing more sophisticated imaging such as CT perfusion, for a better evaluation of stroke core, hypo-perfusion volumes and mismatch, or multiphase CTA for collaterals evaluation.

In some countries like the US, stroke imaging is only/mainly performed by CT, mostly because of MR cost and lack of availability in 24/7 emergency. In France, Germany and some other European countries however, MR is considered as the technique of choice for acute stroke management and MT decision-making. Indeed, a complete MR-exam can be done in 10 minutes including diffusion, FLAIR, T2*, TOF brain angiography, cervical vessel gadolinium angiography and perfusion. Moreover, some software can now automatically provide the volume of diffusion and perfusion anomalies for better quantifying the sizes of core and penumbra (mismatch).

In addition, the cost of a complete multimodal MR is less than 300 Euros in France, versus less than 150 Euros for a CT/CTA. Extra-cost for MR evaluation is then insubstantial. Therefore, in many Departments of Neuroradiology, the number of MR machines increases while the number of CT-scan machines decreases.

The advantages of MRI are tremendous for making a decision in a difficult situation. MRI gives information that is not available using CT or even CTA/CTP or multiphase CT:

- Diffusion sequences offer very precise information on the stroke core volume. Diffusion volume anomalies (computed by automated software) are much more reliable and accurate than the ASPECT score calculated on a plain CT done very early after the stroke onset. Location of the stroke core is also much more precise (deep, superficial eloquent/not eloquent territories).

- FLAIR may help determining stroke onset in wake up stroke and allows making the decision in patients with unknown stroke onset time.

- T2* shows the location and size of the clot. It may indicate small distal emboli in the same or different territory that the CT cannot detect. It shows signs of micro-bleeds in hypertensive patients. It will probably in the future help predicting clot origin and etiology (TOAST, CCS, ASCO classifications) and ability to retrieve the clot and later help in deciding the MT technique depending on clot features.

- Cerebral MR angiography shows clot location and vessels anatomy; cervical MR angiography shows clot location, cervical lesion (carotid plaques, dissections, tortuosity) or intracranial stenosis.

- Perfusion images allow much better understanding of patients' brain hypo-perfusion and collaterals efficacy.

The decision to perform a MT is always made by a duo including a stroke neurologist and a neuro-interventionist. Decision has to be made as fast as possible on images acquired rapidly and easy to interpret. Even if evidence of the tremendous efficacy of MT were given by randomized clinical trials, patient selection is difficult in many situations. MR allows much better understanding of stroke core and tissue at risk giving further arguments to decide to perform a MT or not. It is particularly true in the following situations: patients with low NIHSS score, patients with large infract core, stroke onset › 6h, distal thrombus.

It is of high importance to keep working on MR sequences and on automatized software able to provide quantitative information on patient brain damage and salvageable tissue. In the future, we could imagine that both MR and software will enable to foresee the 3 months mRS score in case of persistent arterial occlusion or complete recanalization."

CONS

Anne Vanbinst, MD
& Koenraad Nieboer, MD

Neuroradiologists at UZ-Brussel, Belgium

"It is known that DWI imaging is more sensitive than unenhanced CT scan of the brain in detecting acute ischemic stroke. However, we prefer and advocate the use of CT scan in our institution.

The pre-hospital notification is set up to alarm the emergency ward CT team to keep the scanner free from activity. Arriving at the hospital the patient passes the triage in the emergency department and is directly placed on the CT table, without thinking about possible contraindications like pacemakers.

The neurologist can do a quick evaluation of the patient. Modern 256 slice CT scans create an unenhanced CT of the brain in 0.5 s, with real-time reconstructions to rule out intracranial hemorrhage within seconds.

In the meanwhile, the iv-thrombolysis is prepared and in the case of a negative CT for hemorrhage the nurse enters the CT room and injects the iv-thrombolysis bolus. This procedure allows us to reach door-to-needle times of less than 10 minutes.

Perfusion and angiographic imaging with late phase collateral evaluation are done within 10 minutes. During the perfusion acquisition, a possible ACM (M1-M2) occlusion is easy to depict, marking the patient as a potential candidate for a thrombectomy procedure.

With dedicated perfusion and angiographic software, we confirm the diagnosis of acute ischemic stroke, the expansion of the ischemic region, the prediction of the core lesion, the extent of the responsible thrombus and the collateral circulation or suggest stroke-mimics like epilepsy.

So, despite the high sensitivity of DWI, we do not keep an MRI scanner empty waiting for an announced patient. We do not have to think about contraindications for MRI or to bother about a nurse entering the magnetic field to give the iv-thrombolysis. Moreover, last but not least in our institutional setting, we can treat the patient faster according to the Time = Brain paradigm."

The Diffusion saga

for a good Sunday read

Yasmina Chaibi, PhD
Sophie Campana Tremblay, PhD
Brianna Bucciarelli

First described by Rabi in 1938 [1], nuclear magnetic resonance progressively led to the emergence of MR imaging for medical applications, serving in the early 1980s as a primary essential diagnostic modality. Over the past 30 years, the flexible and dynamic MRI technology kept evolving to become a gold standard in brain and soft tissue imaging, leading to increasingly complex acquisition sequences. Early conventional weighted techniques, such a T1-w or T2-w used for morphologic assessments, were enriched in the mid-1980s when Le Bihan et al. [2] laid the theoretical foundations of diffusion imaging applied to human brain. 10 years later, diffusion-weighted imaging had become a powerful clinical tool able to investigate neurologic disorders, particularly in patients with acute stroke, but also cancers and metastases in whole-body organs. Diffusion imaging covers a broad spectrum of techniques, from the mapping of apparent diffusion coefficient (ADC) values to diffusion tensor imaging (DTI), Intravoxel incoherent motion (IVIM) or Kurtosis imaging. All these applications are based on a single physicochemical property: water motion at the cellular level.

DIFFUSION BASICS

Isotropic and anisotropic diffusion

Molecules in tissue move around over time, changing direction as they bump into each other. Some of this motion is related to active processes such as circulation of blood, while other motion is simply randomly driven due to thermal agitation. This phenomenon is the result of Brownian motion, without any net direction of flow - molecules simply shake and bounce around in solution, moving along a meandering path. This movement is referred as molecular *free diffusion* and was first observed by the Scottish botanist Robert Brown in 1827 [3], through spontaneous vibration of pollen particles under the microscope; it was later explained by Einstein in 1905 [4].

However, as opposed to *free diffusion* of water kept inside a container, diffusion inside a voxel of tissue (e.g. brain) is primarily hindered by cell membranes boundaries. In fact, the motion of these water molecules is *restricted* by the presence of those barriers. Therefore, in physiological tissues, it would be more accurate to speak about *restricted diffusion* [5]. The degree of diffusion restriction can be quantified by a diffusion coefficient, which reflects the average distance a particle will cover in a second. Technically, it is measured in mm^2/s because it refers to the movement of particles grouped within an area per second. The measured diffusion coefficients with MRI represent averages of the entire voxel in all directions of diffusion [6]. At 25°, for instance, the *diffusion coefficient* of pure water is about $2.3 \times 10^{-3} mm^2/s$ [7].

Soft tissues tend to behave like aqueous protein solutions; due to boundaries with various degrees of permeability and reduced mobility of water molecules, their corresponding diffusion coefficient is generally smaller than that of pure water. Applying the Brownian motion model in that case leads to an *Apparent Diffusion Coefficient* (ADC) [2,8], to be distinguished from the diffusion coefficient of free water molecules [9]. The hindrance mechanism hence results in lower ADC values in highly cellular tumors [10].

Conventional DWI assumes that all water molecules behave the same within a voxel, resulting in a single ADC per voxel. However, this is not accurate: water molecules experience vastly different environments even within a single voxel. Molecules in flowing blood have a baseline velocity, and when the capillary bed is very dense and randomly orientated (e.g. in some kind of tumors), this latter can mimic a random walk, which induces a fast pseudo-diffusion involving a signal attenuation. In addition, intra- and extracellular compartments also have different diffusivities. While a simplistic model is sufficient for most clinical purposes (stroke assessment for example), emerging data suggest that some clinically relevant findings may be found in more complex models. The two main categories of advanced diffusion modeling are *intravoxel incoherent motion* (IVIM) [11-13] and *diffusion kurtosis imaging* [14-16].

IVIM phenomenon is most noticeable in the liver [17,18], and is believed to be related to blood flow in capillaries [6]. It describes the microscopic motions that occur in diffusion imaging and might allow separation between the water molecular diffusion (due to thermal Brownian motion) and the microcirculation of blood (also called pseudo-diffusion). IVIM metrics involve the extraction of three coefficients with specific modeling described later in this paper: one related to molecular diffusion restriction (D), another related to the tissue perfusion (D*) and finally the vascular volume fraction (f).

Diffusion kurtosis imaging depicts the non-Gaussian diffusion arising from diffusion barriers, such as cell membranes and organelles or other hindrance due to complex and restricted structures in tissues [19]. This approach holds therefore the potential to better reflect the complexity of the microscopic structure of tissues. Kurtosis metrics rely on a dimensionless coefficient K that characterizes the degree of deviation of the signal behavior from a Gaussian distribution. K kurtosis, equal to zero when molecular displacements follow a Gaussian law, is a marker of the heterogeneity of the diffusion environment.

1. Rabi II, Millman S, Kusch P, Zacharias JR. The Magnetic Moments of $_3Li^6$, $_3Li^7$ and $_9F^{19}$. Physical Review. 1938; 53(6):495.
2. Le Bihan D, Breton E, Lallemand D, Grenier P, Cabanis E, Laval-Jeantet M. MR imaging of intravoxel incoherent motions: application to diffusion and perfusion in neurologic disorders. Radiology. 1986 Nov;161(2):401-7.
3. Brown R. XXVII. A brief account of microscopical observations made in the months of June, July and August 1827, on the particles contained in the pollen of plants; and on the general existence of active molecules in organic and inorganic bodies. Philosophical Magazine Series 2. 1828;4(21):61-173.
4 . Einstein A. The theory of the brownian movement. Ann. der Physik. 1905;17-549.
5. Koh DM, Collins DJ. Diffusion-weighted MRI in the body: applications and challenges in oncology. AJR Am J Roentgenol. 2007 Jun;188(6):1622-35.
6. http://xrayphysics.com/dwi.html
7. James TL, McDonald GG. Measurement of the self-diffusion coefficient of each component in a complex system using pulsed-gradient Fourier transform NMR. J Magn Reson Imaging. 1973; 11:58-61.
8. Moseley ME, Cohen Y, Kucharczyk J, Mintorovitch J, Asgari HS, Wendland MF, Tsuruda J, Norman D. Diffusion-weighted MR imaging of anisotropic water diffusion in cat central nervous system. Radiology. 1990 Aug;176(2):439-45.
9. Luypaert R, Boujraf S, Sourbron S, Osteaux M. Diffusion and Perfusion MRI: basic Physics. Eur J Radiol. 2001 Apr;38(1):19-27.
10. http://radiopaedia.org/articles/diffusion-weighted-imaging-1
11. Yablonskiy DA, Sukstanskii AL. Theoretical models of the diffusion weighted MR signal. NMR Biomed. 2010 Aug;23(7):661-81.

Isotropic diffusion described above assumes that water molecules diffuse equally in all directions. Indeed, in some tissues such as brain gray matter, it is sufficient to describe the diffusion characteristics with a single scalar such as the apparent diffusion coefficient (ADC), the molecular diffusion restriction coefficient (D) or the tissue perfusion related coefficient (D*). In other words, within those tissues, the measured apparent diffusivity is independent of the matter orientation at the voxel scale.

However, diffusion is direction-dependent in *anisotropic* media such as highly structured tissues, particularly nerves, skeletal and cardiac muscle [20-22] and white matter [8,23,24]. In that case, the measured diffusivity is known to depend upon the orientation of the tissue, so that a single ADC cannot fully characterize the direction of water mobility. Furthermore, if white matter diffusion is measured in a specific direction, different values will be obtained for different parts of the same healthy tissue, depending on the axons orientation [25]. A solution to this issue was proposed by measuring diffusion in several directions and computing different metrics reflecting this anisotropic behavior. Such modeling considers diffusion not as a scalar or single number, but as a 3D symmetrical tensor. The simplest method is called *diffusion tensor imaging* (DTI), using 2nd-order 3D diffusional tensor represented as an ellipsoid with a principal direction (see DTI box). An extension of DTI is *diffusional kurtosis tensor imaging* (DKTI), using a 4th-order 3D tensor to characterize restricted diffusion in all directions.

Clinical interest and applications of conventional DWI

Over the past two decades, magnetic resonance imaging has proven to be a valuable diagnostic tool in stroke and oncology [26-30]. Rapid improvements in MRI techniques have resulted in MR images with excellent spatial resolution and soft tissue contrast, which contribute to the differentiation of suspected tumors [31].

MR diffusion-weighted imaging (DWI), a part of the MRI clinical protocol, provides qualitative and quantitative analysis of Brownian motion, which may be altered as a result of pathological processes. This specificity allows collecting information that is not readily available on conventional or morphological series, more focused on anatomical details. A significant characteristic of such imaging is its reliance on inherent tissue contrast rather than on the administration of exogenous contrast medium, which can be of particular importance in patients with renal failure or contrast allergies. In addition, DWI sequences can be performed quickly with echo planar single shot pulse sequences, allowing substantial and useful information to be gathered at relatively little additional imaging time expense.

The applications of DWI in neuroradiology are increasingly widespread, chiefly in ischemic strokes, but also in tumor, infectious, and inflammatory brain pathologies. Indeed, DWI is commonly used in the detection of irreversible infarct in acute stroke, since it is the earliest (within less than one hour) and most sensitive method for ischemic core diagnosis. It has been shown that in ischemic brain tissue, proton spins motion was restricted due to cytotoxic edema, leading to an ADC decrease coupled with a diffusion-weighted signal intensity incqrease in areas of acute ischemic injury [26]. Moreover, DWI is used to date the stroke event and distinguish between acute and subacute strokes. Finally, this technique improves the diagnosis of different categories of brain pathologies: tumor disease with cerebral lymphoma, epidermoid and cholesteatoma cysts; infectious disease with pyogenic brain abscess, herpes encephalitis and Creutzfeldt-Jakob's; inflammatory disease with multiple sclerosis; traumatic injury [32].

Though essentially used for brain exploration in clinical practice, advances in MR technology permit its application outside the brain, in musculoskeletal radiology and oncology. Particularly, DWI can be applied for tumor detection and characterization, and for monitoring the response to chemotherapy and radiation treatment [5]. The development of whole-body DWI is ongoing.

12. Niendorf T, Dijkhuizen RM, Norris DG, van Lookeren Campagne M, Nicolay K. Biexponential diffusion attenuation in various states of brain tissue: Implications for diffusion-weighted imaging. Magn Reson Med. 1996 Dec;36(6):847-57.
13. Clark CA, Le Bihan D. Water diffusion compartmentation and anisotropy at high b values in the human brain. Magn Reson Med. 2000 Dec;44(6):852-9.
14. Chabert S, Meca CC, Le Bihan D. Relevance of the information about the diffusion distribution in vivo given by kurtosis in q-space imaging. In: Proceedings of the 12th Annual Meeting of ISMRM. 2004; (Kyoto, Japan).
15. Jensen JH, Helpern JA. MRI quantification of non-Gaussian water diffusion by kurtosis analysis. NMR Biomed. 2010 Aug;23(7):698-710.
16. Huang Y, Chen X, Zhang Z, Yan L, Pan D, Liang C, Liu Z. MRI quantification of non-Gaussian water diffusion in normal human kidney: a diffusional kurtosis imaging study. NMR Biomed. 2015 Feb;28(2):154-61.
17. Luciani A, Vignaud A, Cavet M, Nhieu JT, Mallat A, Ruel L, Laurent A, Deux JF, Brugieres P, Rahmouni A. Liver cirrhosis: intravoxel incoherent motion MR imaging pilot study. Radiology. 2008 Dec;249(3):891-9.
18. Dyvorne H, Jajamovich G, Kakite S, Kuehn B, Taouli B. Intravoxel incoherent motion diffusion imaging of the liver: optimal b-value subsampling and impact on parameter precision and reproducibility. Eur J Radiol. 2014 Dec;83(12):2109-13.
19. de Santis S, Gabrielli A, Palombo M, Maraviglia B, Capuani S. Non-Gaussian diffusion imaging: a brief practical review. Magn Reson Imaging. 2011 Dec;29(10):1410-6.
20. Cleveland GG, Chang DC, Hazlewood CF, Rorschach HE. Nuclear magnetic resonance measurement of skeletal muscle: anisotropy of the diffusion coefficient of the intracellular water. Biophys J. 1976 Sep;16(9):1043-53.

FOCUS ON ISOTROPIC DIFFUSION

In the following section, focus is raised on isotropic diffusion by describing the most commonly known and useful models in clinical practice: mono-exponential (ADC), bi-exponential (IVIM) and Kurtosis. For each model, the techniques, clinical applications, pros and cons are presented. Before detailing these different modeling approaches, an overview of the imaging basics of DWI is proposed.

DWI basics: pulse sequence, b-value and ADC

Diffusion-weighted (DW) sequences all originate from the *pulsed gradient spin echo* technique developed by E. Stejskal and J. Tanner in the mid-1960's [33]. In each space direction (x,y,z), two successive strong gradient pulses are applied:

- the first one dephases the magnetization of both mobile and static spins;

- the second one is subsequently applied with the same direction and time period, but with an opposite magnitude so that the dispersion can be refocused or rephased.

As shown in Figure 1, both symmetric and strong *diffusion-sensitizing gradients* (DG) are applied on either side of the 180°-pulse. The phases of stationary spins are unaffected by the DG pair since any phase accumulation from the first gradient lobe is reversed by the second. Diffusing spins, however, move into different locations between the first and second lobes, falling out of phase and losing signal.

Immediately following the second DG, an image acquisition starts. This is typically an echo-planar sequence using rapidly oscillating phase and frequency gradients that generate multiple gradient echoes.

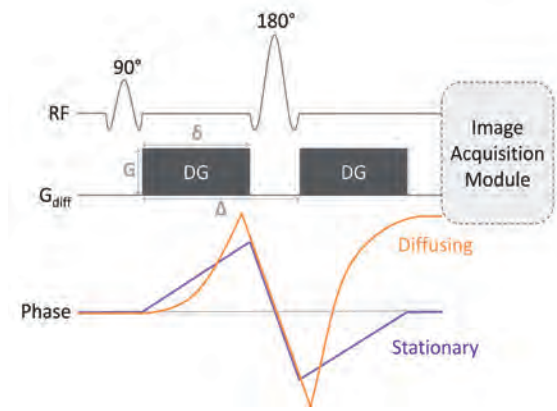

Figure 1: Pulsed Gradient Spin Echo Technique. From [34,35]

Rapid image acquisition is generally required to minimize the effects of bulk motion (such as vascular pulsations) on the DW images. Other modules (such as fast spin echo) are possible. The amount of diffusional signal lost by the gradient application is known to obey the following equation [2]:

$$\frac{S}{S_0} = e^{-\gamma^2 G^2 \delta^2 \left(\Delta - \frac{\delta}{3}\right) D} = e^{-bD}$$ Equation 1

Where:
S_0 is the signal intensity at the baseline (without diffusion gradient application);
S is the signal with the gradient application;
γ is the gyromagnetic ratio;
G is the amplitude of the two diffusion gradient pulses;
δ is the duration of the pulses;
Δ is the time between the two pulses;
D is a diffusion constant (diffusion coefficient as a measure of the strength of diffusion in tissue).

$$b = \gamma^2 G^2 \delta^2 \left(\Delta - \frac{\delta}{3}\right)$$

is the b-value, i.e. the factor that reflects the strength and timing of the gradients used to generate diffusion-weighted images.

21. Garrido L, Wedeen VJ, Kwong KK, Spencer UM, Kantor HL. Anisotropy of water diffusion in the myocardium of the rat. Circ Res. 1994 May;74(5):789-93.
22. Tanner JE. Self-diffusion of water in frog muscle. Biophys J. 1979 Oct;28(1):107-16.
23. Henkelman RM, Stanisz GJ, Kim JK, Bronskill MJ. Anisotropy of NMR properties of tissues. Magn Reson Med. 1994 Nov;32(5):592-601.
24. Moseley ME, Kucharczyk J, Asgari HS, Norman D. Anisotropy in diffusion-weighted MRI. Magn Reson Med. 1991 Jun;19(2):321-6.
25. http://users.fmrib.ox.ac.uk/~karla/reading_group/lecture_notes/TheoryofDiffusion.pdf
26. Wittsack HJ, Ritzl A, Fink GR, Wenserski F, Siebler M, Seitz RJ, Mödder U, Freund HJ. MR imaging in acute stroke: diffusion-weighted and perfusion imaging parameters for predicting infarct size. Radiology. 2002 Feb;222(2):397-403.
27. Bazot M, Darai E, Nassar-Slaba J, Lafont C, Thomassin-Naggara I. Value of magnetic resonance imaging for the diagnosis of ovarian tumors: a review. J Comput Assist Tomogr. 2008 Sep-Oct;32(5):712-23.
28. Schima W. MRI of the pancreas: tumours and tumour-simulating processes. Cancer Imaging. 2006 Dec 20;6:199-203.
29. Saar B, Kellner-Weldon F. Radiological diagnosis of hepatocellular carcinoma. Liver Int. 2008 Feb;28(2):189-99.
30. Kuhl CK. Concepts for differential diagnosis in breast MR imaging. Magn Reson Imaging Clin N Am. 2006 Aug;14(3):305-28.
31. Vermoolen MA, Kwee TC, Nievelstein RA. Apparent diffusion coefficient measurements in the differentiation between benign and malignant lesions: a systematic review. Insights Imaging. 2012 Aug;3(4):395-409.
32. Kremer S, Oppenheim C, Schmitt E, Dietemann JL. Diffusion MRI: technique and clinical applications. J Radiol. 2007 Mar;88(3 Pt 2):428-43.

The higher the b-value, the stronger the diffusion effects. The b-value depends on the strength, duration, and spacing of the pulsed gradients. A larger b-value is achieved by increasing the gradient amplitude and duration, and/or by widening the interval between gradient pulses.

Equation 1 offers two precious indications about what governs signal loss.

First, the higher the diffusion coefficient, the larger the signal loss. Indeed, the amount of signal loss depends on the time between two pulses, i.e. the time granted to water molecules to diffuse. The longer they diffuse, the less perfect will be their refocusing, the larger will be the signal loss.

Second, the stronger and/or longer the gradient pulses, the larger the signal loss. Therefore, the strength of gradients needs to be changed in order to obtain various amounts of diffusion weighting. This is why the b-value (s/mm^2) indicates the sensitivity to diffusion.

Finally, to compute isotropic images, the diffusion gradients must have been applied sequentially in three orthogonal axes in the directions of the section-select, phase-encoding, and readout gradients, in order to generate a set of three orthogonal-axis diffusion-weighted echo-planar images. The signal intensities of the *x*-, *y*-, and *z*-direction source images are given by [36]:

$$S_x = S_0 e^{-b\,D_{xx}}$$
$$S_y = S_0 e^{-b\,D_{yy}}$$
$$S_z = S_0 e^{-b\,D_{zz}}$$

Where S_0 is the signal intensity of a point in the b0 image and D_{xx}, D_{yy} and D_{zz} are the directionally-specific diffusion coefficients at the same point.

Thus, the isotropic diffusion-weighted image (S_{Iso}), or Trace DW image, is calculated as follows:

$$S_{iso} = \sqrt[3]{S_x\,S_y\,S_z}$$

$$S_{iso} = S_0\, e^{-\frac{b\,(D_{xx}+D_{yy}+D_{zz})}{3}} = S_0\, e^{-\frac{b\,D_{Trace}}{3}} = S_0\, e^{-b\,ADC}$$

One must note that the equations described above are true only when, for each voxel, the eigenvectors of the diffusion tensor are aligned with the principal (*X*-, *Y*- and *Z*-) axes.

We mentioned earlier that most of biological tissues are anisotropic. This means that they have multiple diffusion coefficients that vary within different directions; they can be represented by the *diffusion tensor*, a 3x3 array of numbers. The term "*Trace*" comes from matrix algebra which means the sum of diagonal elements of such an array, so $D_{Trace} = D_{xx} + D_{yy} + D_{zz}$. Using the average value of the trace, $D_{Trace}/3$, reduces the multi-directional diffusivity at each point into a single number that can be considered as the ADC. This is why the terms average trace and ADC are often used interchangeably [37].

The isotropic DW image is not a map of diffusion; it is only diffusion-weighted. Isotropic DW images possess considerable T2-weighting. As such, lesions with either very long or very short T2 values may "contaminate" the isotropic DW images, making them appear artificially bright or dark. These important phenomena are known as "T2-shine-through" and "T2-black-out". T2-effects can be mathematically removed from the DW image to create a pure parametric image of apparent diffusion coefficients, most commonly known as the *ADC Map*.

This quantitative parameter characterizes the mean amplitude of the water molecules motion. The signal intensity of each voxel in an isotropic diffusion-weighted (or Trace DW images) is inversely related to its ADC value. Pathologies that restrict diffusion (stroke) lower the ADC and appear bright. Conversely, substances with unrestricted diffusion and high ADC (e.g. cerebrospinal fluid) appear dark [37].

33. Stejskal EO, Tanner JE. Spin diffusion measurements: spin echoes in the presence of time-dependent field gradient. J Chem Phys. 1965;42:288-292.
34. http://mri-q.com/making-a-dw-image.html
35. http://mri-q.com/what-is-the-b-value.html
36. Chong J, Lu D, Aragao F, Singer MB, Schonewille WJ, Silvers A, Tuhrim S, Atlas SW. Diffusion-weighted MR of acute cerebral infarction: comparison of data processing methods. AJNR Am J Neuroradiol. 1998 Oct;19(9):1733-9.
37. http://mri-q.com/trace-vs-adc-map.html
38. Le Bihan D. Apparent diffusion coefficient and beyond: what diffusion MR imaging can tell us about tissue structure. Radiology. 2013 Aug;268(2):318-22.
39. Sugahara T, Korogi Y, Kochi M, Ikushima I, Shigematu Y, Hirai T, Okuda T, Liang L, Ge Y, Komohara Y, Ushio Y, Takahashi M. Usefulness of diffusion-weighted MRI with echo-planar technique in the evaluation of cellularity in gliomas. J Magn Reson Imaging. 1999 Jan;9(1):53-60.
40. Kang Y, Choi SH, Kim YJ, Kim KG, Sohn CH, Kim JH, Yun TJ, Chang KH. Gliomas: histogram analysis of apparent diffusion coefficient maps with standard- or high-bvalue diffusion-weighted MR imaging—correlation with tumor grade. Radiology. 2011 Dec;261(3):882-90.
41. Tsuruda JS, Chew WM, Moseley ME, Norman D. Diffusion-weighted MR imaging of extra-axial tumors Magn Reson Med. 1991 Jun;19(2):316-20.
42. Tien RD, Felsberg GJ, Friedman H, Brown M, MacFall J. MR imaging of high-grade cerebral gliomas: valu of diffusion-weighted echoplanar pulse sequences. AJR Am J Roentgenol. 1994 Mar;162(3):671-7.
43. Namimoto T, Yamashita Y, Sumi S, Tang Y, Takahashi M. Focal liver masses: characterization with diffusion-weighted echo-planar MR imaging. Radiology. 1997 Sep;204(3):739-44.

Mono-exponential Model

In the mono-exponential model, the ADC is computed by linear regression from the isotropic images based on all b-values according to the formula hereafter [2,38]:

$$S_{Iso} = S_0\, e^{-b\,ADC} \rightarrow ADC = -\frac{1}{b} ln(\frac{S_{Iso}}{S_0})$$

When plotted against the b-values, the diffusion MR signal ($\ln(S_{Iso}/S_0)$) would follow a straight line whose slope is the ADC. For this purpose, a set of at least two different b-values images (e.g. b=0 and b=1000 s/mm^2) is needed. However, a computation from three (or more) different b-values is more accurate than from two b-values only.

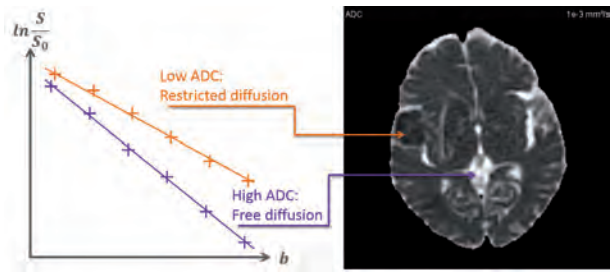

Figure 2: Illustration of two different mono-exponential fits. In orange: Low ADC (low slope of the fit) means that water molecules have more difficulties to diffuse, like in a tumor, or the core of a stroke. In purple: High ADC (high slope of the fit) means that water molecules diffuse freely, as in the Cerebral Spinal Fluid, or in an edema.

Nevertheless, ADC estimation is very sensitive to noise and sampling. Thus Bayesian probability theory is used in the Olea Sphere® application in order to better estimate this parameter (see Bayesian box).

The isotropic ADC obtained from DWI with a mono-exponential model is used to grade gliomas [39,40] and distinguish cystic and edematous from solid tumors [41-43]. Among other applications, ADC also allows for the classification of brain disorders [44].

However, as mentioned earlier, the most important clinical application of DW MR imaging remains the detection and characterization of cerebral ischemia [45-48]. Recently, some studies were published to determine the value of DW MRI in healthy parotid glands and associated disorders by measuring ADC values under physiologic and pathologic conditions, or after irradiation [49-51], or for noninvasive quantification of functional changes in the parotid glands [52].

This technique was also applied for breast pathologies, where the challenge is to obtain the best compromise between lesion detection and characterization [53-55]. Several studies applied this technique for prostate cancer detection [56-58] and diagnostic imaging of the kidney [59] and ovaries [60]. With recent advances in technology, DW MR imaging is also reaching a potential for clinical use in the abdomen, particularly in the liver with promising results for liver lesion detection and characterization [61] and many other clinical applications.

However, several researchers reported contradictory findings about the ADC values for glioma grading [39,40,62]. For instance, Catalaa et al. [63] found that ADC could not be used to separate different tumor grades and Zonari et al. [64] found no significant difference in the ADC of low- versus high-grade glial tumors. Zhang et al. [65] reported that the use of a mono-exponential function for DW imaging analysis was playing a substantial role in causing the variability in ADC of healthy kidneys.

In addition, ADC values calculated by using a mono-exponential model may not be able to accurately reflect water molecular diffusion *in vivo*, because it is influenced by the microcirculation of blood in capillaries [66].

Finally, the complex microstructures in biological tissue result in hindered and restricted diffusion of water molecules, which leads to a non-Gaussian distribution [67]. Hence, ADC has limitations in the accurate evaluation of water molecular diffusion [68].

44. Sener RN. Diffusion MRI: apparent diffusion coefficient (ADC) values in the normal brain and a classification of brain disorders based on ADC values. Comput Med Imaging Graph. 2001 Jul-Aug;25(4):299-326.
45. Warach S, Chien D, Li W, Ronthal M, Edelman RR. Fast magnetic resonance diffusion-weighted imaging of acute human stroke. Neurology. 1992 Sep;42(9):1717-23.
46. Fiehler J, Fiebach JB, Gass A, Hoehn M, Kucinski T, Neumann-Haefelin T, Schellinger PD, Siebler M, Villringer A, Röther J. Diffusion-weighted imaging in acute stroke – a tool of uncertain value? Cerebrovasc Dis. 2002;14(3-4):187-96.
47. Copen WA, Schaefer PW, Wu O. MR perfusion imaging in acute ischemic stroke. Neuroimaging Clin N Am. 2011 May;21(2):259-83.
48. Olivot JM, Mlynash M, Inoue M, Marks MP, Wheeler HM, Kemp S, Straka M, Zaharchuk G, Bammer R, Lansberg MG, Albers GW; DEFUSE 2 Investigators. Hypoperfusion intensity ratio predicts infarct progression and functional outcome in the DEFUSE 2 Cohort. Stroke. 2014 Apr;45(4):1018-23.
49. Yoshino N, Yamada I, Ohbayashi N, Honda E, Ida M, Kurabayashi T, Maruyama K, Sasaki T. Salivary glands and lesions: evaluation of apparent diffusion coefficients with split-echo diffusion-weighted MR imaging – initial results. Radiology. 2001 Dec;221(3):837-42.
50. Sumi M, Takagi Y, Uetani M, Morikawa M, Hayashi K, Kabasawa H, Aikawa K, Nakamura T. Diffusion-weighted echoplanar MR imaging of the salivary glands. AJR Am J Roentgenol. 2002 Apr;178(4):959-65.

This is the reason why some researchers have suggested that bi-exponential or stretched exponential DWI models and diffusion kurtosis imaging (DKI) might provide more accurate information about water diffusion [2,19,69]. Le Bihan et al. [2,70] described the bi-exponential intravoxel incoherent motion DWI model. This latter might allow separation of water molecular diffusion from microcirculation. Bennett et al. [69] introduced the stretched exponential DWI model, which has been used to describe the heterogeneity of intravoxel diffusion rates and the distributed diffusion effect (see Stretched-exponential Model box). Finally, DKI has been used to measure non-Gaussian diffusion, which has the potential to characterize both normal and pathologic tissue better than diffusion-tensor imaging [71,72].

Stretched-exponential model

The stretched-exponential model [69] has been introduced to offer a more complex description of the water diffusion behavior compared to the simple mono-exponential model. This model is described as follows:

$$S(b) = S_0\, e^{-(b\,DDC)^{\alpha}}$$

Where:

S(b) is the signal at a given b-value;
S_0 is the reference signal at b = 0;
DDC is the Distributed Diffusion Coefficient;
α is a heterogeneity index.

In Olea Sphere®, the Bayesian probability theory is used in order to estimate the parameters more robustly, similarly to the bi-exponential model (see Bayesian box).

Bi-exponential model

As mentioned previously, the computation of ADC from the mono-exponential equation does not fully describe the tissue behavior [73]. As a result, intravoxel incoherent motion (IVIM) imaging was introduced and developed by Le Bihan et al. to quantitatively assess all the microscopic translational motions that occur in biological tissues [2]. These displacements are essentially due to molecular water diffusion (thermal Brownian motion) and microcirculation of blood in the capillary network that mimics a random walk (also called pseudo-diffusion or perfusion). These two phenomena lead to a signal loss in diffusion MRI, which depends on the velocity of the flowing blood and the vascular architecture.

As for molecular diffusion, pseudo-diffusion effect on signal attenuation depends on the b-value. However, the rate of signal loss resulting from pseudo-diffusion is typically an order of magnitude greater than that of molecular diffusion in tissues, so its relative contribution to the diffusion-weighted MRI signal becomes significant only at very low b-values, allowing diffusion and perfusion effects to be separated [66,74]. Indeed when different diffusion b-values are applied, a bi-exponential decay of the signal is observed on diffusion-weighted plot (Figure 3).

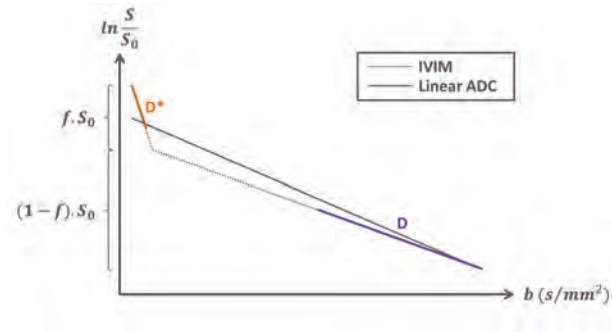

Figure 3: Bi-exponential decay of the signal

51. Patel RR, Carlos RC, Midia M, Mukherji SK. Apparent diffusion coefficient mapping of the normal parotid gland and parotid involvement in patients with systemic connective tissue disorders. AJNR Am J Neuroradiol. 2004 Jan;25(1):16-20.
52. Habermann CR, Cramer MC, Graessner J, Gossrau P, Reitmeier F, Fiehler J, Schoder V, Jaehne M, Adam G. Functional imaging of parotid glands: diffusion-weighted echo-planar MRI before and after stimulation. Rofo. 2004 Oct;176(10):1385-9.
53. Thomassin-Naggara I, De Bazelaire C, Chopier J, Bazot M, Marsault C, Trop I. Diffusion-weighted MR imaging of the breast: advantages and pitfalls. Eur J Radiol. 2013 Mar;82(3):435-43.
54. de Bazelaire C, Pluvinage A, Chapelier M, Hamy AS, Albiter M, Farges C, Bourrier P, Zagdanski AM, Espié M, de Kerviler E, Frija J. Diffusion-weighted MR imaging of the breast J Radiol. 2010 Mar;91(3 Pt 2):394-404.
55. Abdulghaffar W, Tag-Aldeen MM. Role of diffusion weighted imaging (DWI) and apparent diffusion coefficient (ADC) in differentiating between benign and malignant breast lesions. The Egyptian Journal of Radiology and Nuclear Medicine. 2013;44(4): 945–951.
56. Gibbs P, Tozer DJ, Liney GP, Turnbull LW. Comparison of quantitative T2 mapping and diffusion weighted imaging in the normal and pathologic prostate. Magn Reson Med. 2001 Dec;46(6):1054-8.
57. Morgan VA, Kyriazi S, Ashley SE, DeSouza NM. Evaluation of the potential of diffusion-weighted imaging in prostate cancer detection. Acta Radiol. 2007 Jul;48(6):695-703.
58. Jacobs MA, Ouwerkerk R, Petrowski K, Macura KJ. Diffusion-weighted imaging with apparent diffusion coefficient mapping and spectroscopy in prostate cancer. Top Magn Reson Imaging. 2008 Dec;19(6):261-7.

The acquisition intended to depict IVIM phenomenon allows the extraction of three metrics: two diffusion coefficients, one related to molecular diffusion restriction (D), another related to the tissue perfusion (D*); and one vascular volume fraction (f). The decay is described by the following equation:

$$S(b) = S_0 \left[f e^{-bD^*} + (1-f) e^{-bD} \right]$$

Where:
S(b) is the signal;
S_0 is the reference signal;
D is the molecular diffusion restriction coefficient;
*D** is the tissue perfusion related coefficient;
f is the perfusion fraction.

The perfusion fraction (f) indicates the relative influence of the first perfusion term and is correlated to the perfusion (microcirculation in the capillaries) of the tissue.

Regarding the number and the magnitude of b-values to be used, no consensus has been reached yet. At least 4 b-values are needed to characterize the bi-exponential phenomenon but more are recommended. A compromise is to use between 6 to 8 values by sampling more the low b-values range (lower than 100 s/mm^2). Indeed, low b-values are crucial to obtain reliable estimate of *D** [73].

However, as for mono-exponential model, parameters estimation (especially *D**) is very sensitive to noise and sampling. To overcome this limitation, the Bayesian probability theory was applied in Olea Sphere® application, in order to better estimate such parameters (see Bayesian box).

IVIM was initially used to evaluate perfusion in brain activation studies before the introduction of fMRI, and to focus on clinical applications such as stroke and brain tumors [75-77]. Some studies have proven the validity of IVIM concept from fMRI, with an increase in the IVIM perfusion parameters in brain activated regions; the potential of the approach could help in the understanding of the different vascular contributions to the fMRI signal [78]. IVIM concept has also been used to improve other applications like arterial spin labeling (ASL) [79] or to suppress signal from extracellular flowing fluid in perfused cell systems [80]. IVIM has then undergone a striking revival for applications out of the brain [70].

Following earlier encouraging results in kidneys [81] or even heart [82], IVIM really took off for liver applications. For instance, Luciani et al. [17] found that D* was significantly reduced in cirrhotic patients which, according to the IVIM model, points out the reduction of blood velocity and flow. The perfusion fraction f, linked to blood volume in the IVIM model, remained normal, confirming earlier results by Yamada et al. [83], though blood volume is expected to be reduced in liver cirrhosis. Many other applications are currently under investigation, especially for imaging of patients suspected of cancer outside brain (prostate, liver, kidney, pancreas, etc.) [73]. Clinical studies have shown the potential value of IVIM parameters for disease assessment, particularly in oncology [73].

There is growing interest in applying analytic techniques beyond simple ADC calculations to tease out the effects of microcapillary perfusion from DW-MRI data [70]. IVIM imaging provides quantitative information on perfusion without the need of administration of exogenous contrast agent whose toxicity is not negligible. In addition, the method does not depend on the geometry of the capillary bed compared to other methods described in the literature [84]. IVIM sequences can be performed quickly. However the acquisition is longer than for conventional DWI since more b-values are required. Furthermore, as mentioned, so far there is no consensus regarding the number and the magnitude of b-values to use, and the non-Gaussian effects are not taken into account in this model.

59. Goya C, Hamidi C, Bozkurt Y, Yavuz A, Kuday S,Gümüş H, Türkçü G,5 Hattapo-lu S, Bilici A. The role of apparent diffusion coefficient quantification in differentiating benign and malignant renal masses by 3Tesla magnetic resonance imaging. Balkan Medical Journal. 2015;32(3):273–278.
60. Mukuda N, Fujii S, Inoue C, Fukunaga T, Tanabe Y, Itamochi H, Ogawa T. Apparent diffusion coefficient (ADC) measurement in ovarian tumor: effect of region-of interest methods on ADC values and diagnostic ability. J Magn Reson Imaging. 2016 Mar;43(3):720-5.
61. Taouli B, Koh DM. Diffusion-weighted MR imaging of the liver. Radiology. 2010 Jan;254(1):47-66.
62. Lam WW, Poon WS, Metreweli C. Diffusion MR imaging in glioma: does it have any role in the pre-operation determination of grading of glioma? Clin Radiol. 2002 Mar;57(3):219-25.
63. Catalaa I, Henry R, Dillon WP, Graves EE, McKnight TR, Lu Y, Vigneron DB, Nelson SJ. Perfusion, diffusion and spectroscopy values in newly diagnosed cerebral gliomas. NMR Biomed. 2006 Jun;19(4):463-75.
64. Zonari P, Baraldi P, Crisi G. Multimodal MRI in the characterization of glial neoplasms: the combined role of single-voxel MR spectroscopy, diffusion imaging and echoplanar perfusion imaging. Neuroradiology. 2007 Oct;49(10):795-803.
65. Zhang JL, Sigmund EE, Chandarana H, Rusinek H, Chen Q, Vivier PH, Taouli B, Lee VS. Variability of renal apparent diffusion coefficients: limitations of the monoexponential model for diffusion quantification. Radiology. 2010 Mar;254(3):783-92.
66. Le Bihan D, Breton E, Lallemand D, Aubin ML, Vignaud J, Laval-Jeantet M. Separation of diffusion and perfusion in Intravoxel incoherent motion MR imaging. Radiology. 1988 Aug;168(2):497-505.
67. Raab P, Hattingen E, Franz K, Zanella FE, Lanfermann H. Cerebral gliomas: diffusional kurtosis imaging analysis of microstructural differences. Radiology. 2010 Mar;254(3):876-81.

Kurtosis model

Keystone of the DW protocol, b-value characterizes the diffusion rate of a subpopulation of hydrogen spins [85]. It measures the degree of diffusion weighting applied, as a function of several MR acquisition parameters: b-value is proportional to the product of the diffusion time interval with the square of the strength of the diffusion gradient. If the interval time is very short (low b-value), water will tend to diffuse in a similar way and with the same speed in every direction, resulting in a bell-shaped Gaussian displacement distribution [86]. However, when longer time intervals are considered (high b-value), some molecules will slow down or even stop due to tissue obstacles, while others will maintain a relatively free diffusion path with minor disturbance [38]. Increasing the interval time will therefore highlight the heterogeneities of the aqueous medium, leading to two major phenomena.

First, water displacement deviates from a strict Gaussian distribution, becoming more peaked and making the ADC inadequate to depict the diffusion properly [87]. To describe the shape difference compared to the normal distribution, the statistics terminology uses the term *kurtosis*: positive kurtosis refers to higher peaks and heavier tails (leptokurtic curves), while negative kurtosis refers to lower peaks and lighter tails (platykurtic curves). In the diffusion model, empirical evidence indicates that kurtosis is always positive [88].

Secondly, the presence of obstacles, or hindrance effect, reduces the average distance covered by the molecules during the fixed interval time: mean spins velocity is smaller than if considered earlier; high b-values settings therefore sense slower moving water than low b-values do [89]; it allows to target what is called the *slow component*, as opposed to the *fast component* characterized by a Gaussian unrestricted and slightly hindered diffusion. In other words, increasing the diffusion time also increases the weighting of the slow component, composed of restricted diffusion-driven molecules [90]. It is still unclear whether slow component should be related to intracellular space and fast component to extracellular one [38].

How could the slow component provide valuable clinical insights? As stated earlier, water displacement is affected by intracellular microenvironment. Tissue damage often enhances local heterogeneities, such as in ischemic brain where cellular death includes nuclear fragmentation, chromatin condensation or cell body shrinkage [91]. High b-value diffusion images are sensitive to the specific areas where diffusion is slowed due to those microstructure alterations, they hence reveal the lesions at locations where conventional ADC mapping does not capture changes [92].

To achieve the tissue complexity detection, special quantitative kurtosis metrics are necessary. Indeed, raw diffusion-weighted images contain qualitative information, but their interpretation is not intuitive [86]. Therefore, as for ADC and IVIM phenomena, kurtosis modeling is based on the acquisition of multiple images, in order to plot the signal attenuation as a function of b-values. By processing this graph, a third compartment, consecutive to the IVIM (low b-values) and ADC (intermediate b-values) compartments, appears for high b-values with a curvature reflecting the non-Gaussian nature of diffusion (Figure 4).

To fit this complex signal decay, several models have been proposed; among them the phenomenological kurtosis model [15] described by 4 parameters:

$$S(b) = S_0 \left[f e^{-bD^*} + (1-f) e^{-bADC_0 + (bADC_0)^2 \frac{K}{6}} \right]$$

Where:

S(b) is the signal;
S_0 is the reference signal;
ADC_0 is the apparent diffusion coefficient;
*D** is the tissue perfusion related coefficient;
f is the perfusion fraction;
K is the apparent kurtosis coefficient.

68. Bai Y, Lin Y, Tian J, Shi D, Cheng J, Haacke EM, Hong X, Ma B, Zhou J, Wang M. Grading of Gliomas by Using Monoexponential, Biexponential, and Stretched Exponential Diffusion-weighted MR Imaging and Diffusion Kurtosis MR Imaging. Radiology. 2016 Feb;278(2):496-504.
69. Bennett KM, Schmainda KM, Bennett RT, Rowe DB, Lu H, Hyde JS. Characterization of continuously distributed cortical water diffusion rates with a stretched exponential model. Magn Reson Med. 2003 Oct;50(4):727-34.
70. Le Bihan D. Intravoxel incoherent motion perfusion MR imaging: a wake-up call. Radiology. 2008 Dec;249(3):748-52.
71. Jensen JH, Helpern JA, Ramani A, Lu H, Kaczynski K. Diffusional kurtosis imaging: the quantification of non-gaussian water diffusion by means of magnetic resonance imaging. Magn Reson Med. 2005 Jun;53(6):1432-40.
72. Lu H, Jensen JH, Ramani A, Helpern JA. Three-dimensional characterization of non-gaussian water diffusion in humans using diffusion kurtosis imaging. NMR Biomed. 2006 Apr;19(2):236-47.
73. Koh DM, Collins DJ, Orton MR. Intravoxel incoherent motion in body diffusion-weighted MRI: reality and challenges. AJR Am J Roentgenol. 2011 Jun;196(6):1351-61.
74. Le Bihan D. Magnetic resonance imaging of perfusion. Magn Reson Med. 1990 May;14(2):283-92.
75. Wirestam R, Brockstedt S, Lindgren A, Geijer B, Thomsen C, Holtås S, Ståhlberg F. The perfusion fraction in volunteers and in patients with ischaemic strok
Acta Radiol. 1997 Nov;38(6):961-4.
76. Le Bihan D, Douek P, Argyropoulou M, Turner R, Patronas N, Fulham M. Diffusion and perfusion magnetic resonance imaging in brain tumors. Top Magn Reson Imaging. 1993 Winter;5(1):25-31.
77. Neil JJ, Bosch CS, Ackerman JJ. An evaluation of the sensitivity of the intravoxel incoherent motion (IVIM) method of blood flow measurement to changes in cerebral blood flow. Magn Reson Med. 1994 Jul;32(1):60-5.

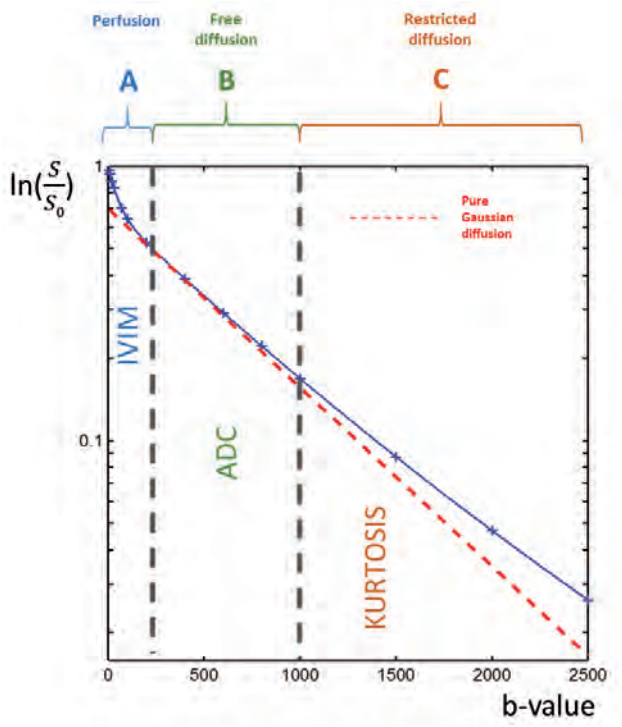

Figure 4: Plot of the signal attenuation logarithm against b-values. Three compartments A, B and C respectively stand for IVIM, ADC and kurtosis phenomena.

This model, an extension of the IVIM bi-exponential equation, combines the three diffusion phenomena contributions with 4 quantitative parameters, the kurtosis compartment being fully described by *K* dimensionless coefficient.

Parameters estimation commonly uses the classical least squares or non-linear least squares approach, to fit (*f, D*, ADC$_0$, K*) by minimizing the squares discrepancies between observed data and their expected value. However, this method presents several drawbacks: it is time-consuming and prone to images artifacts; it presents robustness issues since it strongly depends on image quality and Signal to Noise Ratio (SNR). As a consequence, this method tends to misestimate parameters, especially *D** [93]. The Bayesian processing is therefore under development for kurtosis at Olea

The Bayesian method in diffusion imaging: Technical overview

Unlike the least-squares algorithm, the Bayesian approach yields more robust parameter estimates, i.e. more stable and more accurate. Rather than minimizing a residual error, the Bayesian method estimates the uncertainty of each parameter separately, with a narrow probability density function indicating a well-resolved value [93].

The Bayesian method relies on the computation of the joint posterior probability of the parameters Θ to be estimated, given the data X:

$$P(\Theta, S_0, \sigma \mid X) \quad [112]$$

where:
Θ is the set of parameters to be evaluated ([ADC, D*, f, K] for example);
σ is the noise standard deviation;
S_0 is the reference signal;
X is the data.
As discribed by Neil et al. [112], uninformative priors are used. Then, the marginal posterior distribution of each parameter θ_i is computed, for example:

$$P(\theta_i|X) = \int P(\Theta, S_0, \sigma \mid X)\, d\sigma\, dS_0\, d\Theta_{\setminus i}$$

Where $d\Theta_{\setminus i}$ is the integral over all parameters of the set Θ but θ_i.
The parameter estimate $\langle\theta_i\rangle$ and the error on the estimate σ_i^2 are chosen respectively as the mathematical expectation and the standard deviation of the marginal posterior distribution:

$$\langle\theta_i\rangle = \int \theta_i\, P(\theta_i \mid X)\, d\theta_i$$

$$\sigma_i^2 = \int (\theta_i - \langle\theta_i\rangle)^2\, P(\theta_i \mid X)\, d\theta_i$$

It is possible to specify the limits of the integral as well as the number of sampling points. In Olea Sphere®, default values have been chosen to find the best compromise between precision and computation time.
The minimum and maximum values have to be chosen in agreement with the physiological values, so that, outside the integration limits, the joint probability is equal to zero. The computation time is proportional to the number of sampling points; this is why it is recommended to refrain from using very high values.

78. Song AW, Woldorff MG, Gangstead S, Mangun GR, McCarthy G. Enhanced spatial localization of neuronal activation using simultaneous apparent-diffusion-coefficient and blood-oxygenation functional magnetic resonance imaging. Neuroimage. 2002 Oct;17(2):742-50.
79. Silva AC, Williams DS, Koretsky AP. Evidence for the exchange of arterial spin-labeled water with tissue water in rat brain from diffusion-sensitized measurements of perfusion. Magn Reson Med. 1997 Aug;38(2):232-7.
80. Van Zijl PC, Moonen CT, Faustino P, Pekar J, Kaplan O, Cohen JS. Complete separation of intracellular and extracellular information in NMR spectra of perfused cells by diffusion-weighted spectroscopy. Proc Natl Acad Sci U S A. 1991 Apr 15;88(8):3228-32.
81. Powers TA, Lorenz CH, Holburn GE, Price RR. Renal artery stenosis: in vivo perfusion MR imaging. Radiology. 1991 Feb;178(2):543-8.
82. Callot V, Bennett E, Decking U.K.M, Balaban RS, Wen H. In vivo study of microcirculation in canine myocardium using the IVIM method. Magn Reson Med. 2003 Sep;50(3):531-40.
83. Yamada I, Aung W, Himeno Y, Nakagawa T, Shibuya H. Diffusion coefficients in abdominal organs and hepatic lesions: evaluation with intravoxel incoherent motion echo-planar MR imaging. Radiology. 1999 Mar;210(3):617-23.
84. Le Bihan D. Imagerie de diffusion/perfusion. Traité de Radiodiagnostic VI - Principes et techniques d'imagerie. 1990;35-251-A-10.
85. Hall MG, Barrick TR. From diffusion-weighted MRI to anomalous diffusion imaging. Magn Reson Med. 2008 Mar;59(3):447-55.
86. Hagmann P, Jonasson L, Maeder P, Thiran JP, Wedeen VJ, Meuli R. Understanding diffusion MR imaging techniques: from scalar diffusion-weighted imaging to diffusion tensor imaging and beyond. Radiographics. 2006 Oct;26 Suppl 1:S205-23.

Medical®, to compute more stable parameters that will be calculated within an acceptable processing time in clinical settings (see Bayesian box).

Extended mapping can be achieved to take into account the *anisotropic* nature of water diffusion. If the signal is captured in 15 different directions, a fourth-order 3D symmetric tensor can describe the full non-Gaussian behavior [15,91,92]. New metrics can then be computed: mean kurtosis (MK), axial kurtosis (AK) and radial kurtosis (RK). Therefore, a natural generalization of diffusion kurtosis imaging (DKI) is diffusional kurtosis tensor imaging (DKTI).

DKI offers numerous interesting diagnostic possibilities in neuroradiology. It has been suggested that it provides a better detection in neural tissues than conventional DWI especially in cerebral infarction [92], schizophrenia [94], Parkinson's disease [95] or gliomas [87]. In case of cerebral ischemia for example, DKI was able to show high intensity at the periphery of the ischemic lesion at an early stage, when conventional DWI was producing a homogeneous signal in the area of gliosis [96]. Encouraging results have also been reported for Alzheimer disease [97,98] and age-related patterns in the prefrontal brain region [99].

Besides neural tissues, several studies investigated the potential of DKI metrics in detecting prostate cancers [100,101], increasing the diagnostic confidence for characterizing breast lesions [102], or adding value to head and neck carcinoma analysis [103]. DKI preliminary studies are also conducted on lung [104], liver [105] and bladder [106].

DKI provides unique and supplementary information to detect microstructural alterations, with a wide spectrum of potential applications. It is a clinically feasible process that requires minor changes in data acquisition compared to conventional DWI: b-values are only larger than those usually employed. However, as a novel technique, links between DKI parameters and pathologic findings still need further investigation and validation [92].

Estimation of the kurtosis tensor can generate relatively long acquisition time (7 – 10 minutes) since at least 15 diffusion directions have to be acquired for each b-value, with increased susceptibility to patient motion [89]. However, if only mean kurtosis is of interest, fast DKI (1 – 2 minutes) can be performed [107].

Compared to apparent diffusion coefficient ADC_0, influenced by different factors such as macromolecules concentration, diffusional kurtosis is a true measure of tissue cellular compartments and membranes. This specificity makes the contrast to be high between white and gray matter on a K map, while lighter contrast appears on an ADC_0 mapping of the same area. As an illustration, apparent kurtosis coefficient in white matter is about 70% higher than in gray matter, reflecting the structural differences between these two types of cerebral tissues [15]. Finally, maximum b-values of about 2000 s/mm^2 are needed to compute DKI in the brain. Such values are now attainable on modern MRI scanners.

Yasmina Chaibi, PhD
Clinical & Scientific Research Manager
Olea Medical®

Sophie Campana Tremblay, PhD
Clinical & Scientific Research Engineer
Olea Medical®

Brianna Bucciarelli
Clinical Research Engineer
Olea Medical®

87. Van Cauter S, Veraart J, Sijbers J, Peeters RR, Himmelreich U, De Keyzer F, Van Gool SW, Van Calenbergh F, De Vleeschouwe S, Van Hecke W, Sunaert S. Gliomas: diffusion kurtosis MR imaging in grading. Radiology. 2012 May;263(2):492-501.
88. Tabesh A, Jensen JH, Ardekani BA, Helpern JA. Estimation of tensors and tensor-derived measures in diffusional kurtosis imaging. Magn Reson Med. 2011 Mar;65(3):823-36.
89. Steven AJ, Zhuo J, Melhem ER. Diffusion kurtosis imaging: an emerging technique for evaluating the microstructural environment of the brain. AJR Am J Roentgenol. 2014 Jan;202(1):W26-33.
90. Cohen Y, Assaf Y. Extracting Geometric properties of white matter with q-space diffusion MRI - "Diffusion MRI" - Oxford University Press - https://books.google.fr/books?id=dbZCMePD52AC. p126.
91. Nour M, Scalzo F, Liebeskind DS. Ischemia-reperfusion injury in stroke. Interv Neurol. 2013 Sep;1(3-4):185-99.
92. Hui ES, Fieremans E, Jensen JH, Tabesh A, Feng W, Bonilha L, Spampinato MV, Adams R,Helpern JA. Stroke assessment with diffusional kurtosis imaging. Stroke. 2012 Nov;43(11):2968-73.
93. Dyvorne HA, Galea N, Nevers T, Fiel MI, Carpenter D, Wong E, Orton M, de Oliveira A, Feiweier T, Vachon M, Babb JS, Taouli B. Diffusion-weighted imaging of the liver with multiple b values: effect of diffusion gradient polarity and breathing acquisition on image quality and intravoxel incoherent motion parameters-a pilot study. Radiology. 2013 Mar;266(3):920-9.
94. Baumann PS, Cammoun L, Conus P, Do KQ, Marquet P, Meskaldji D, Meuli R, Thiran JP, Hagmann F High b-value diffusion-weighted imaging: A sensitive method to reveal white matter differences in schizophrenia. Psychiatry Res. 2012 Feb 28;201(2):144-51.
95. Wang JJ, Lin WY, Lu CS, Weng YH, Ng SH, Wang CH Liu HL, Hsieh RH, Wan YL, Wai YY. Parkinson disease: diagnostic utility of diffusion kurtosis imaging. Radiolog 2011 Oct;261(1):210-7.

Diffusion Tensor Imaging: How? Technical and clinical overview

The computing of a diffusion tensor requires two separate sets of parameters: 1 - the direction of the fastest diffusion (i.e. the direction of the axon bundle) and 2 - the diffusion coefficients along and across the axons.

To define a direction in a 3D space, 3 coordinates are required; to fully describe the shape of an ellipsoid, 3 other metrics are required (1 per axis). This means that DTI requires measuring diffusion in 6 different directions. These measurements need to be achieved for each non-zero b-value [6].

Thus, the modeling of diffusion in complex materials is performed by creating a [3 x 3] array of numbers corresponding to diffusion rates in each combination of directions. The three diagonal elements (D_{xx} ,D_{yy}, D_{zz}) represent diffusion coefficients measured along each of the principal (X-, Y- and Z-) axes. The six off-diagonal terms (D_{xy} ,D_{xz}, etc.) reflect the correlation of random motions between each pair of principal directions:

$$D=\begin{bmatrix} Dxx & Dxy & Dxz \\ Dyx & Dyy & Dyz \\ Dzx & Dzy & Dzz \end{bmatrix} \quad \text{Equation A}$$

Because x→y and y→x diffusivities should be the same, mirror-image off-diagonal elements are equal, i.e. $D_{xy} = D_{yx}$, $D_{yz} = D_{zy}$, and $D_{xz} = D_{zx}$. The matrix is hence symmetric and has six degrees of freedom. As a result, at least six diffusion-weighted acquisitions in six non collinear directions are needed to acquire the tensor images.

This matrix is then diagonalized:

$$D\_diag=\begin{bmatrix} \lambda_1 & 0 & 0 \\ 0 & \lambda_3 & 0 \\ 0 & 0 & \lambda_3 \end{bmatrix} \quad \text{Equation B}$$

Where λ_1, λ_2, λ_3 are the three eigenvalues.
An ideal frame of reference for viewing the diffusion tensor can then be determined. This optimal coordinate system is based upon the diffusion ellipsoid, whose main axis is parallel to the principal diffusion direction within a voxel. This principal axis often corresponds to anatomic features such as white matter tracts or fascial planes. The major and minor axes of the diffusion ellipsoid are defined by the orthogonal unit vectors (ε_1, ε_2, ε_3) known as eigenvectors. The length of each eigenvector (ε_i) is multiplied by a factor λ_i. The eigenvalues of the ellipsoid are proportional to Einstein's root mean squared diffusion displacement in each direction. By convention, eigenvalues are labeled in descending order of magnitude ($\lambda_1 \geq \lambda_2 \geq \lambda_3$).

Specific DTI sequences are necessary to produce even and regular diffusion-weighted images in the brain - otherwise white matter tracts will look like they restrict diffusion.

From eigenvalues, 4 different DTI metrics can be computed:

- the Mean diffusivity (MD) map calculated by averaging the three eigenvalues; this parameter is typically used for DWI and ADC maps. MD describes the global motion of the molecules in a voxel and allows detecting diffusion obstacles.

- the Axial diffusivity (AD) map equal to the single scalar λ_1. AD represents the diffusion along the principal axis.

- the Radial diffusivity (RD) map calculated as the average of λ_2 and λ_3. RD represents the diffusivity along the two minor axes.

- the Fractional anisotropy (FA) map, calculated by comparing each eigenvalue with the mean of all eigenvalues. FA is a measure of anisotropy since large FA results in high anisotropic behavior.

Normal white matter tracts show high FA, a characteristic that is lost in many disease processes [109,110].

DTI can produce good low-resolution images of general white matter tract orientation; by calculating the principal direction of the tensor ellipsoid, it is possible to get the average direction of axonal bundles in the voxel.

Also, by coding the voxels with different colors according to the directions, a tractography map can be obtained.Axonal tracts are commonly mapped using a deterministic method known as FACT (Fiber Assignment by Continuous Tracking).

96. Hori M, Fukunaga I, Masutani Y, Taoka T, Kamagata K, Suzuki Y, Aoki S. Visualizing non-Gaussian diffusion: clinical application of q-space imaging and diffusional kurtosis imaging of the brain and spine. Magn Reson Med Sci. 2012;11(4):221-33.
97. Gong NJ, Wong CS, Chan CC, Leung LM, Chu YC. Correlations between microstructural alterations and severity of cognitive deficiency in Alzheimer's disease and mild cognitive impairment: a diffusional kurtosis imaging study. Magn Reson Imaging. 2013 Jun;31(5):688-94.
98. Struyfs H, Van Hecke W, Veraart J, Sijbers J, Slaets S, De Belder M, Wuyts L, Peters B, Sleegers K, Robberecht C, Van Broeckhoven C, De Belder F, Parizel PM, Engelborghs S. Diffusion Kurtosis Imaging: a possible MRI biomarker for AD diagnosis? J Alzheimers Dis. 2015;48(4):937-48.
99. Falangola MF, Jensen JH, Babb JS, Hu C, Castellanos FX, Di Martino A, Ferris SH, Helpern JA. Age-related non-Gaussian diffusion patterns in the prefrontal brain. J Magn Reson Imaging. 2008 Dec;28(6):1345-50.
100. Rosenkrantz AB, Sigmund EE, Johnson G, Babb JS, Mussi TC, Melamed J, Taneja SS, Lee VS, Jensen JH. Prostate cancer: feasibility and preliminary experience of a diffusional kurtosis model for detection and assessment of aggressiveness of peripheral zone cancer. Radiology. 2012 Jul;264(1):126-35.
101. Suo S, Chen X, Wu L, Zhang X, Yao Q, Fan Y, Wang H, Xu J. Non-Gaussian water diffusion kurtosis imaging of prostate cancer. Magn Reson Imaging. 2014 Jun;32(5):421-7.
102. Wu D, Li G, Zhang J, Chang S, Hu J, Dai Y. Characterization of breast tumors using diffusion kurtosis imaging (DKI). PLoS One. 2014 Nov 18;9(11):e113240.
103. Jansen JF, Stambuk HE, Koutcher JA, Shukla-Dave A. Non-Gaussian analysis of diffusion-weighted MR imaging in head and neck squamous cell carcinoma: a feasibility study. AJNR Am J Neuroradiol. 2010 Apr;31(4):741-8.

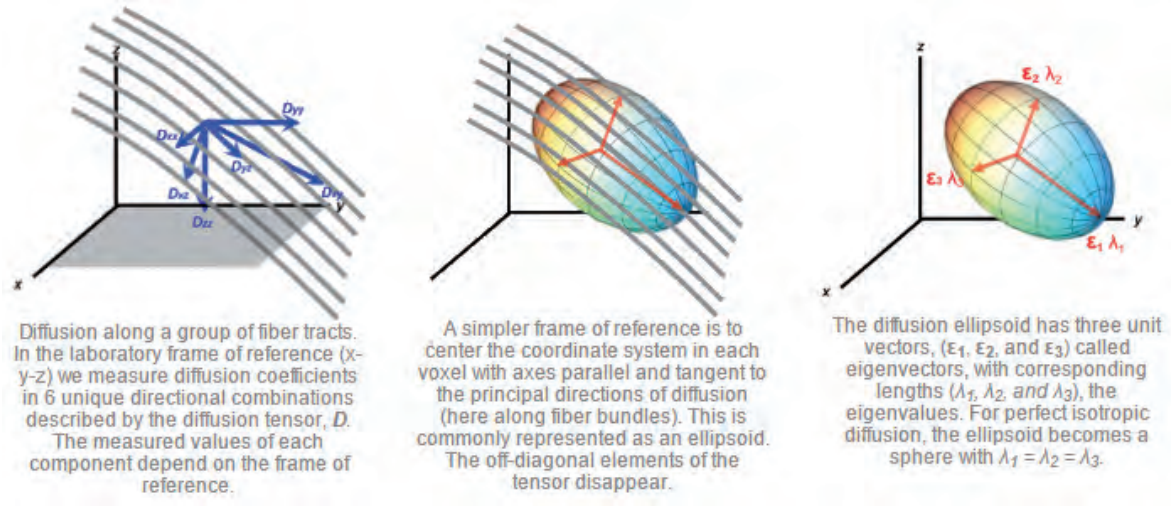

Figure 5: Diffusion along a group of fiber tracts. Representation of the diffusion coefficients, the diffusion ellipsoid and the eigenvectors and eigenvalues [108]

In this processing, the user selects "seed voxels" in a certain area of the organ (i.e brain) and an automated software computes fiber trajectories in and out of that area. This is accomplished by following the primary eigenvector (ε_1) in each voxel until it encounters a neighboring voxel, at which time the trajectory is changed to point in the direction of the new eigenvector.

Much more sophisticated and high resolution tractography can be obtained by measuring diffusion in more directions. This can take into account areas of crossing fiber bundles, which would just be averaged out in regular DTI.

Mainly applied in the brain, DTI enables the *in vivo* study of neural tissue microstructure. It gives indications about possible nerve fiber anomalies in white matter or spinal cord that are not visible in conventional imaging. Fiber tractography is the only method providing an indirect and *in vivo* view of the nerve fibers trajectories (Figure 6). It can be associated with fMRI to study the interconnections between nerve centers, used to analyze brain maturation and development (myelinization), assist in surgery planning for brain tumors (corticospinal bundle), or detect medullary compression. DTI can also be of interest in exploring Alzheimer's disease, some psychiatric conditions, inflammatory, tumoral, vascular, traumatic (irreversible comas) pathologies or drug-resistant epilepsies [111].

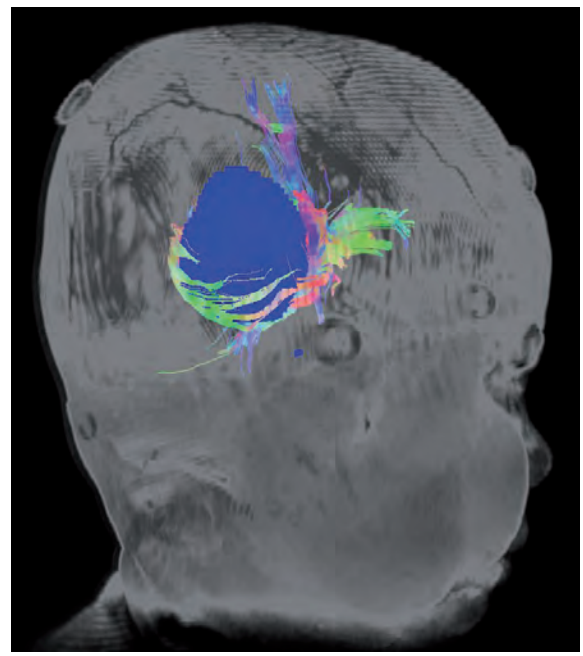

Figure 6: Tractography fused with tumor segmentation and 3D T1 gado series

104. Trampel R, Jensen JH, Lee RF, Kamenetskiy I, McGuinness G, Johnson G. Diffusional kurtosis imaging in the lung using hyperpolarized 3He. Magn Reson Med. 2006 Oct;56(4):733-7.
105. Rosenkrantz AB, Sigmund EE, Winnick A, Niver BE, Spieler B, Morgan GR, Hajdu CH. Assessment of hepatocellular carcinoma using apparent diffusion coefficient and diffusion kurtosis indices: preliminary experience in fresh liver explants. Magn Reson Imaging. 2012 Dec;30(10):1534-40.
106. Suo S, Chen X, Ji X, Zhuang Z, Wu L, Yao Q, Fan Y, Xu J. Investigation of the non-Gaussian water diffusion properties in bladder cancer using diffusion kurtosis imaging: a preliminary study. J Comput Assist Tomogr. 2015 Mar-Apr;39(2):281-5.
107. Hansen B, Lund TE, Sangill R, Jespersen SN. Experimentally and computationally fast method for estimation of a mean kurtosis. Magn Reson Med. 2013 Jun;69(6):1754-60.
108. http://mri-q.com/diffusion-tensor.html
109. Jellison BJ, Field AS, Medow J et-al. Diffusion tensor imaging of cerebral white matter: a pictorial review of physics, fiber tract anatomy, and tumor imaging patterns. AJNR Am J Neuroradiol. 2004 Mar;25(3):356-69.
110. Assaf Y, Pasternak O. Diffusion tensor imaging (DTI)-based white matter mapping in brain research: a review. J Mol Neurosci. 2008;34(1):51-61.
111. Oppenheim C, Ducreux D, Rodrigo S, Hodel J, Tourdias T, Charbonneau F, Pierrefitte S, Meder J. [Diffusion tensor imaging and tractography of the brain and spinal cord]. J. Radiol. 2007 Mar;88(3 Pt 2):510-20.
112. Neil JJ, Bretthorst GL. On the use of Bayesian probability theory for analysis of exponential decay data: an example taken from intravoxel incoherent motion experiments. Magn Reson Med. 1993 May;29(5):642-7.

Advanced Diffusion MRI models

Rachid Deriche, PhD
Research Director at Inria at Sophia Antipolis – Mediterranee Research Center, France

Rachid Deriche's research activities and expertise in Computational neuro-imaging, 3D Computer Vision and Mathematical Image Processing have been published in more than 60 journals and 180 conference papers with a Google Scholar h-index of 65, and recognized via several awards including the 2013 French Academy of Sciences Grand Prize of the EADS Corporate Foundation in Computer Science, the 2014 Doctorate Honoris Causa by Sherbrooke University and more recently the 2016 ERC Advanced Grant from the European Research Council (ERC) under the European Union's Horizon 2020 research and innovation program (ERC AdG agreement No 694665 "Computational Brain Connectivity Mapping" 09/2016-31/08/2021).

Olea Imagein: Could you please introduce INRIA to our readers and tell us more about your background?

Rachid Deriche: Inria, the French National Institute for computer science and applied mathematics, promotes "scientific excellence for technology transfer and society". At Inria, we do both theoretical and applied research in the computing and mathematical fields of digital sciences and Inria's missions are to produce both outstanding research and to ensure the impact of its research on the economy and society in particular. I am a former student of "Ecole Nationale Supérieure des Télécommunications" in Paris from which I graduated in 1979. I then received the PhD degree in Mathematics from the University of Paris IX, Dauphine in 1982 and the "Habilitation à Diriger des Recherches" (HDR degree) from Nice Sophia Antipolis University in 1991. I did my PhD thesis and started my research activity in computational image processing at Inria Rocquencourt, close to Paris, before moving in September 1988 to Inria Sophia-Antipolis, close to Nice in the French Riviera. So, I started contributing to the fields of computational image processing in the early 80's and then moved to the domain of 3D computer vision in the early 90's before shifting my research interest to the domain of computational neuro-imaging in the early 2000's.

O.I: What is the focus of your current academic activities?

R.D: I am currently Research Director at Inria in the Sophia Antipolis–Mediterranee Research Center where I lead the research activities of the Athena Project Team with the objectives to explore the Central Nervous System (CNS) using computational neuro-imaging. We focus on signal and image recording from Diffusion Magnetic Resonance Imaging (dMRI), Magneto-Encephalography (MEG) and Electro-Encephalography (EEG).

Our goal is to develop rigorous mathematical models and computational tools for acquiring, modeling and analyzing the complex CNS structure and function. These models and tools will help us to better understand the architecture and the functioning of the human CNS and will also help our collaborators such as Olea Medical® to use our expertise to provide innovative software solutions to healthcare professionals worldwide.

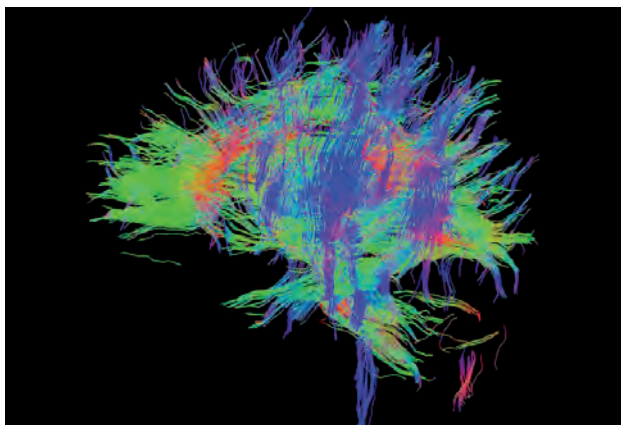

Figure 1: An example of tractography from brain dMRI data

O.I: Could you quickly explain diffusion imaging and the shifts over the past years?

R.D: Diffusion MRI (dMRI) is the unique *in vivo* and non-invasive MRI technique capable of providing the brain structural connectivity information. Its role is pivotal in investigating alterations and degeneration of the structural connections in the brain. The content of diffusion-weighted images is a signal sensitized to diffusion by using strong magnetic field gradient pulses. Since the first images of water diffusion in the human brain were published in ISMRM 1985 by D. Le Bihan et al., a plethora of models with increasing complexity and better accuracy have been proposed to characterize the integrity of the cerebral tissue, to understand its microstructure and to infer its connectivity. In dMRI, the acquisition and reconstruction of the diffusion signal allow for the reconstruction of the water molecules displacement probability, known as the Ensemble Average Propagator (EAP).

Historically, the first model in dMRI is the 2nd order diffusion tensor (DTI) proposed by Basser et al. in 1984 which assumes the EAP to be Gaussian centered at the origin. While practical, this assumption limited the ability of the DTI to describe complex, singular and intricate fiber configurations (U-shape, kissing or crossing fibers). To overcome this limitation, so-called Diffusion Spectrum Imaging (DSI) and High Angular Resolution Diffusion Imaging (HARDI) methods such as Q-ball imaging and other multi-tensors and compartment models were developed to resolve the orientationnality of more complicated fiber bundle configurations.

Overall, these last twenty years have seen an explosion of intensive scientific research which has vastly improved and literally changed the face of dMRI. These ground-breaking changes range from improved and more powerful gradients, scanner-technology to acquisition, post-processing and reconstruction schemes, resulting in shorter acquisitions and more accurate modeling of the brain-tissues microstructure and connectivity.

O.I: Why develop new models for accessing cerebral connectivity?

R.D: As well understood, dMRI is well adapted to detect, characterize and quantify possible white matter abnormalities of brain tissues that cannot be revealed by standard imaging techniques. The enormous potential of dMRI to probe human brain connectivity is also of great benefit in clinical practice. Since the inception of dMRI in the mid 1980's, increasingly more efficient and complex dMRI methods have been proposed to process and analyze measured diffusion signals and produce metrics describing in more detail the underlying brain connectivity.

However, so far, because the diffusion signal is highly complex, there is still room for improvement to take dMRI from the benchside to the bedside. The exact mechanisms governing water diffusion processes in the brain are still unclear and many interesting mathematical and computational challenges remain open. Therefore, new dMRI models have to be derived to gain deeper understanding of the dMRI signal in neural tissues. This will help to provide more insights and intrinsic parameters to precisely characterize white matter, in particular its intrinsic abnormalities that underpin disease states.

O.I: Could you simply present high order diffusion MRI modeling, and the resulting new biomarkers potentially available?

R.D: First we have to give back to Caesar what belongs to Caesar i.e. despite its intrinsic limitations in regions with complex fiber configurations, the DTI model has been, nonetheless, extremely successful in clinical practice, in acute brain stroke for instance, and biomarkers extracted from DTI as Mean Diffusivity (MD) and Fractional Anisotropy (FA) are still commonly used today. That being said, it is important to note that these biomarkers are extremely sensitive to confounding factors such as partial volume and axonal dispersion and severely lack specificity, meaning that room for improvement in dMRI remains.

> “Because the dMRI signal is highly complex, the mathematical tools required for processing it have to be commensurate in their complexity.”

Significant improvements have been introduced by acquiring HARDI data and analyzing them through non-Gaussian diffusion process models (Diffusion Kurtosis) and/or the reconstruction of the Ensemble Average Propagator (EAP), which represents the whole 3D diffusion process and offers the possibility to deduce valuable insights on the microstructural properties of the observed white matter tissue. Indeed, from a reconstructed EAP, one can compute the angular features of the diffusion in a diffusion Orientation Distribution Function (ODF), providing insight in axon orientation, calculate properties of the entire diffusion in a voxel such as the Mean Squared Diffusivity (MSD) and Return-To-Origin Probability (RTOP), or come forth with biomarkers detailing diffusion along a particular white matter bundle direction such as the Return-to-Axis or Return-to-Plane Probabilities (RTAP or RTPP). Because the dMRI signal is highly complex, the mathematical tools required for processing it have to be commensurate in their complexity. We can also rely on high order dMRI modeling, High Order Tensors and Diffusion Kurtosis Imaging for instance, to derive new sensitive imaging biomarkers based on orientationally invariants and intrinsic microstructural features. Examples of such biomarkers are axonal diameter and density that can quantify the complexity of the diffusion profile, irrespective of the orientation of the patient in the scanner or the local direction of white matter pathways and potentially able to detect and predict brain pathologies, exquisite and intrinsic brain connectivity quantification.

O.I: Could you tell us more about your research projects?

R.D: Since my research interest shifted from computer vision to computational neuro-imaging in the early 2000's, my contributions have been mainly focused on the computational dMRI field. This has led to fundamental, theoretical, methodological and practical contributions to DTI and HARDI with original and state-of-the-art algorithms in estimation, regularization, segmentation, tractography and clustering in DTI.

I have mainly introduced and advocated the use of new tools and concepts from Riemannian Geometry to efficient DTI and HARDI processing and developed a whole set of state-of-the-art algorithms in dMRI that include second as well as high order tensor and HARDI models. During the last years, I also tackled important applications such as optimizing dMRI acquisitions using Kalman filtering tools and compressed sensing theory, automatically clustering fiber paths to facilitate group-based statistical analysis and extend the Riemannian framework developed for the second order to high order tensor models, Ensemble Average Propagator (EAP) and Orientation Distribution Function (ODF) computing.

From now on and for the next years, I will be mainly involved in my 2016 ERC AdG awarded project “Computational Brain Connectivity Mapping” to develop a joint Dynamical Structural-Functional Brain Connectivity Network solidly grounded on advanced and integrated methods for dMRI, EEG & MEG.

O.I: Thanks for your contribution to Olea Imagein magazine and all the best with your projects.

R.D: Thank you very much. It has been a great pleasure to answer your questions. But if you will allow me, I would like to end by expressing my great thanks to my collaborators, colleagues and PhD students at Inria and also to Olea Medical® for your great contributions to medical imaging and for your excellent scientific magazine.

Diffusion for Breast application

Kaori Togashi, MD
Professor and Chair of the Department of Diagnostic Imaging and Nuclear Medicine at Kyoto University Graduate School of Medicine, Kyoto, Japan

She has been involved in MRI of the female pelvis for more than 30 years. She estimates herself lucky to have started her research at the very early stage of body MRI development. Initially she was excited to see detailed morphology and experience clinical usefulness of pelvic MRI. Then she gradually recognized the power of MRI beyond morphology; MRI as a functional imaging. Cine MRI is one of the field of her interests in which detailed movie image revealed uterus as a "Dynamic functional organ". After getting promoted to the current position in 2004, she has also been fascinated by the potential of DWI and FDG-PET imaging as other functional imaging modalities.

Olea Imagein: Could you quickly explain what DWI is?

Kaori Togashi: DWI is an image based on diffusion of water in the tissue. In the context of body MRI, the main role of DWI is evaluation of tumor. Along with FDG-PET, DWI is a powerful tool to detect unnoticed small metastasis or to estimate aggressiveness of tumor in various cancers including prostate cancer, uterine cancer, ovarian cancer, liver tumor, and breast cancer.

O.I: How do you use it in your daily routine for breast application? How does it help you in your diagnosis process?

K.T: In our institution, DWI is now incorporated into almost all of the routine body MR protocols. DWI helps radiologists in detecting known/unknown cancer site and improve our confidence in diagnosing malignancy, particularly when contrast enhanced images show inconclusive results or contrast agent is contraindicated. DWI does not need contrast agent and is, therefore, easy to add on with minimum burden to patients. In addition, apparent diffusion coefficient (ADC) value, a quantitative parameter, provides us with measurable information of the tumor cellularity, composition or structure. For example, ADC value is associated with cellularity and also with proliferative marker in certain types of breast cancer. Outside breasts, DWI sometimes helps in identifying unexpected metastasis to lymph nodes and bones.

O.I: Could you briefly present a case study to our readers?

K.T: A lady was diagnosed as bilateral fibroadenomas on ultrasound. MRI showed bilateral round circumscribed masses. However, one of the mass showed high signal intensity on DWI (b=1000 s/mm^2 right) with ADC value of 0.9 x 10^{-3} mm^2/s, which was too low for typical fibroadenoma. Pathological examination revealed this lesion as breast cancer.

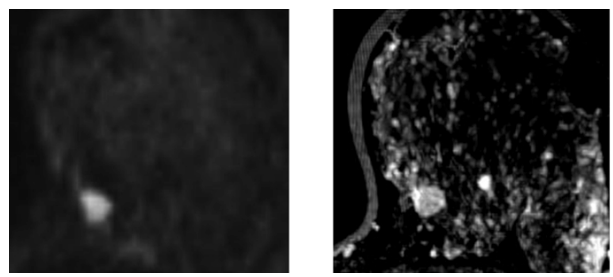

Figure 1: Round circumscribed mass pointed out on hyper-signal on b-1000 (left) and post-contrast T1-WI (right) series

Whole body Diffusion

Trevor La Folie, MD

Malignant tumors are the third most common cause of death worldwide, so accurate diagnosis and staging of cancer is imperative to optimize treatment strategies in order to improve long-term survival. For at least 10 years, whole-body magnetic resonance imaging (WBMRI) using conventional sequences has shown its superiority versus conventional modalities (e.g., bone scintigraphy, CT) and can be used alone or associated with PET/CT with excellent results. Unless acquired with high spatial resolution, these sequences also deliver numerous anatomical information and render it difficult for radiologists to screen the whole patient without missing a lesion. Initially developed for brain analysis, both diffusion-weighted imaging (DWI) and whole-body diffusion-weighted imaging (WB-DWI) exploit the random, translational motion of water protons in biologic tissue, which reflects tissue-specific diffusion capacity. Most tumor lesions are associated with architectural malformations and water diffusivity changes.

ACQUISITION AND INTERPRETATION

Generating a field of view from vertex to mid-thigh, either an integrated body coil or multiple phased array coils covering the entire zone are used, with or without particular devices for rapid table movement, with or without breathhold. Fat suppression or background body signal suppression is applied depending on machines and vendors. By performing multiple stations of axial slices a composite image of the whole body can be created using maximum intensity projection (MIP) (20 mm thickness) and displayed using a reversed black-and-white grey scale for convenient visualization (Figure 1).

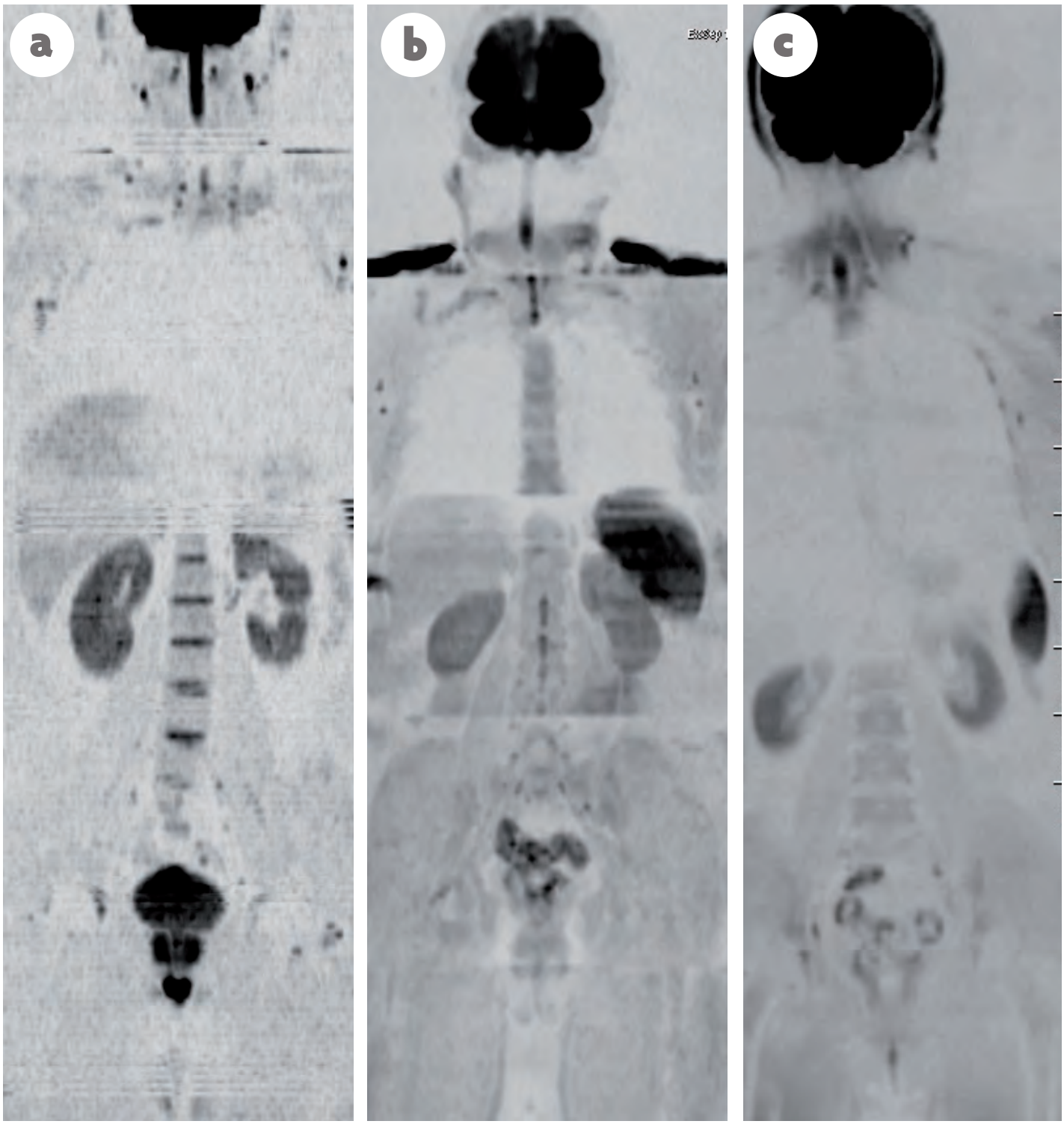

Figure 1: Whole-body coronal MIP grey-scale inverted DWI of normal subjects. (a) On a 1.5T GE MRI. Note that the dark signal of the brain, spleen, spinal cord and testicles is a normal finding, as are the small lymph nodes in the neck, axillae and groin; (b) On a 3T GE MRI; (c) On a 3T Siemens MRI.

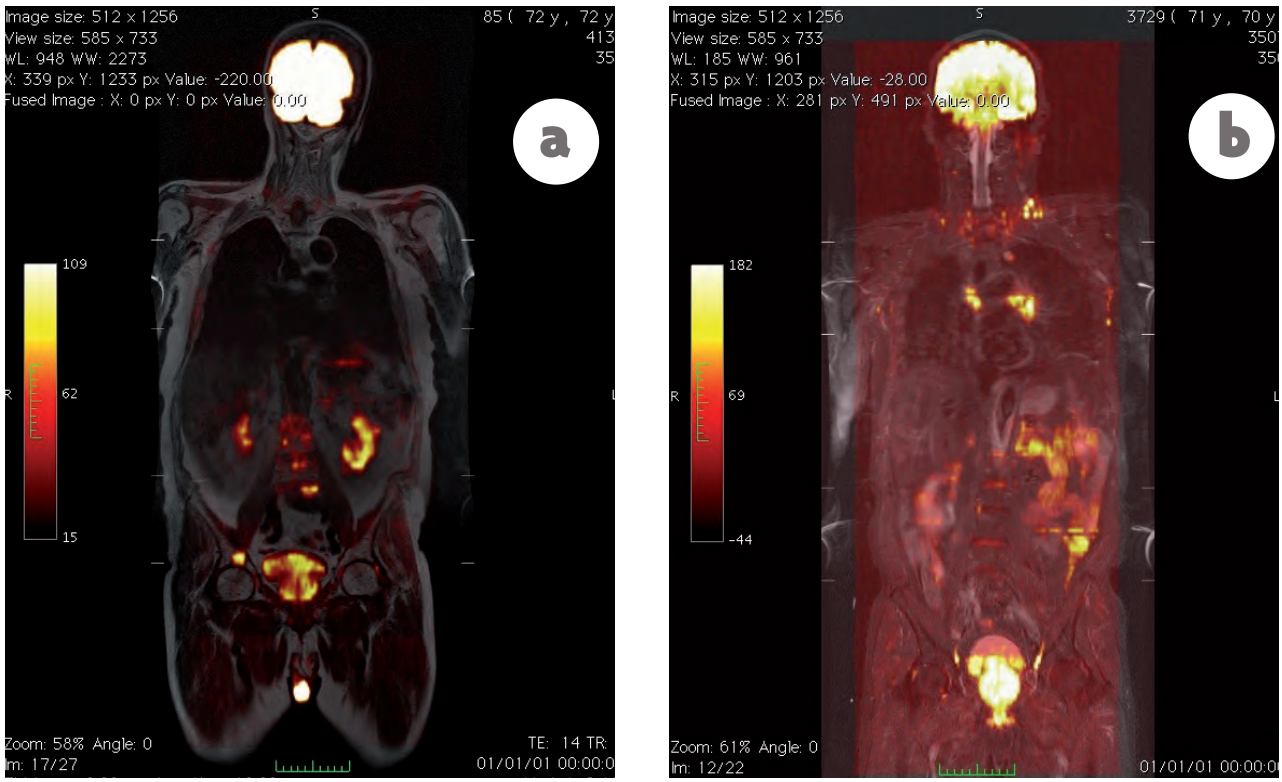

Figure 2: (a) Whole-body coronal T1-weighted image combined with coronal DWI b-600 (hot iron color) at 1.5T; (b) Whole-body coronal STIR combined with coronal DWI of the same patient at 1.5T

MIP images should not be used alone for disease assessments because false positive and false negative can occur. Every suspicious lesion on high b-value images should be evaluated using co-registration sequences. Two b-values usually suffice because increasing the number of b-values prolongs examination time. Because the technique is usually used as a contrast mechanism to identify cellular tissues, the higher b-value chosen is usually 600–1000 s/mm^2 (typically 600 with 1.5T machine and 800-1000 with 3T). Depending on the sequences used, comprehensive assessments can be completed within 45–50 min of table time. Dedicated workstation software and continuous moving table technologies are now widely available increasing acquisition process and post-acquisition [1]. These software tools stitch together images acquired at different anatomic stations and displayed as a single image to facilitate reading. Fusion images of DWI and conventional sequences have already been evaluated and proven useful in this way (Figure 2). Usual WB-DWI protocol could technically be: whole-body (skull base to mid-thighs)–axial, diffusion-weighted, STIR fat suppression, 5–7 mm contiguous slicing, multiple stations, 2 b-values (b50–100 and b800–1000), ADC calculations with mono-exponential data fitting, coronal b800–1000 multiplanar reconstructions and 3D-MIP reconstructions of highest b-value images.

QUANTIFICATION AND THERAPEUTIC FOLLOW-UP

The evaluation of source b800–1000 value images of DW-MRI sequences is based on comparing high b-value image intensity to adjacent muscle signal intensity, but assessment of Apparent Diffusion Coefficient (ADC) map is numeric (unit: 10^{-3}mm^2/s or μm^2/s). ADC is considered to reflect the tissue-specific diffusion capacity. This opens the way to an improved characterization of the lesions detected in a whole-body examination, especially useful during follow-up after therapy (Figures 3, 4 and 5). The need for standardisation of WB-MRI technology has always been expressed since 2005.

In this way, in 2009, a committee of experts reached consensus and made recommendations about DWI as a cancer biomarker [2] including: correlations with endpoints, data display, standardization, validation and reproducibility.

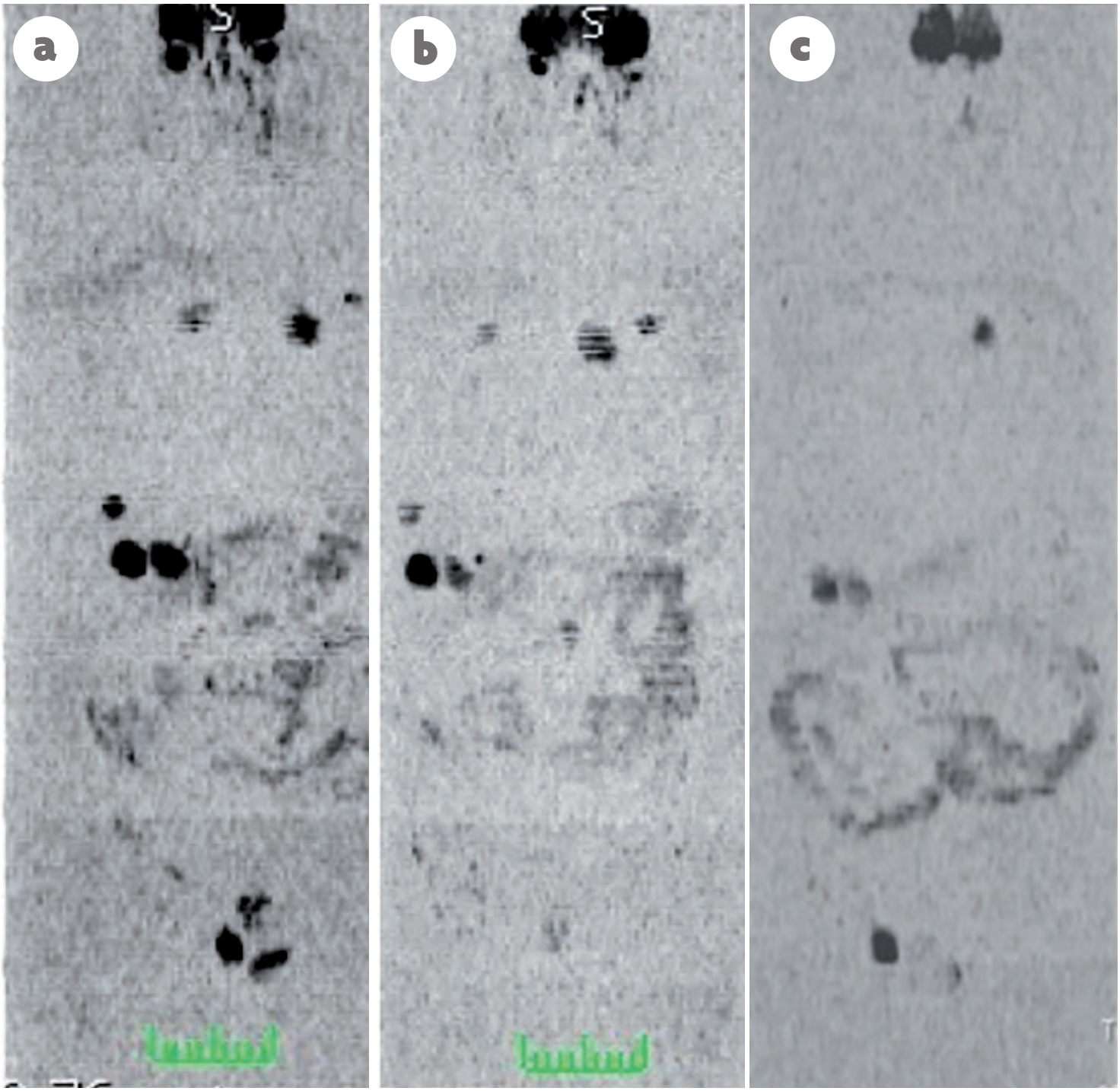

Figure 3: Whole-body coronal MIP grey-scale inverted DWI at 1.5T. (a) Initial exam. Note multiple masses in high signal. (b) After 1 month of chemotherapy: no changes. (c) After 2 months: loss of signal, same size of the masses.

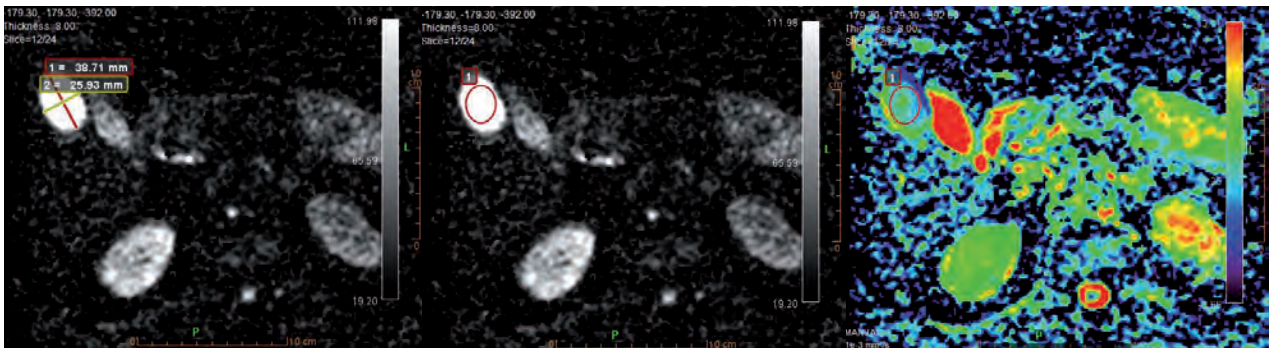

Figure 4: Same patient as in Figure 3, after 1 month of chemotherapy. Mass showing a high signal on axial DWI images and an ADC value near the initial one (1.34 x10^{-3} mm^2/s vs. 1.32 x10^{-3} mm^2/s initially).

Seven years later, in 2016 [3], considering that imaging depicted metastatic state is key to patient management for biomarker (BM) development and for therapeutic clinical trials, a panel of international experts has designed recommendations that promote standardization and diminish variations in the acquisition, interpretation, and reporting of WB-MRI scans for use in the specific case of advanced prostate cancer.

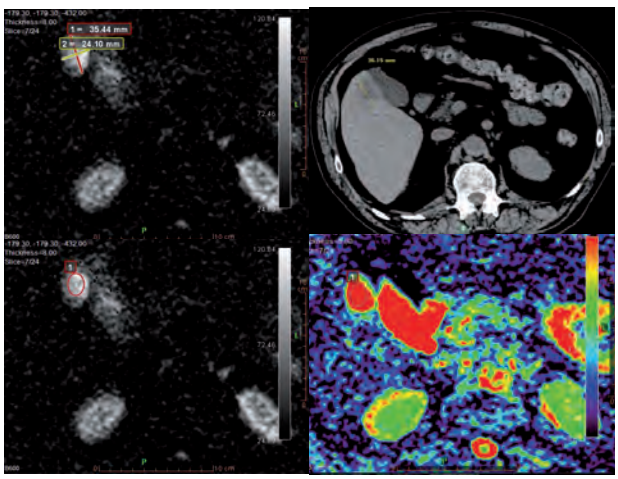

Figure 5: Same patient as in Figure 3, 2 months after chemotherapy. Mass showing the same size on DWI b-600 and CT exam and DWI, but a signal loss on axial DWI images and a still higher ADC value (3.2 x10^{-3} mm^2/s), consistent with therapeutic necrosis process and loss of cellularity.

This is the first (but surely not the last) global and specific recommendations considering specific neoplasia.

Among many purposes, this group proposed evidence recommendations to establish minimum acceptable technical parameters for WB-DWI data, develop standardized data collection methods that enable detailed descriptions of the disease phenotype based on imaging patterns of metastases, develop comprehensive response criteria that assess bones, soft tissues, and local diseases, summarize the likelihood of response in bones, soft tissues, and local diseases that may be used to direct patient management, enable data collection for outcome monitoring in the context of clinical trials and allow the education of radiologists on WB-MRI reporting in order to reduce variability in imaging interpretations [3].

No doubt that in a near future, these types of evidence reviews and recommendations will be enlarged to other categories of cancer with improved data acquisition [4] and quantitative assessments [5].

Trevor La Folie, MD
Radiologist at HIA Sainte Anne, Toulon, France

References

1. Koh DM, Collins DJ. Diffusion-weighted MRI in the body: applications and challenges in oncology. Am J Roentgenol. 2007 Jun; 188 (6):1622-35.
2. Padhani AR, Liu G, Koh DM, Chenevert TL, Thoeny HC, Takahara T, Dzik-Jurasz A, Ross BD, Van Cauteren M, Collins D, Hammoud DA, Rustin GJ, Taouli B, Choyke PL. Diffusion-weighted magnetic resonance imaging as a cancer biomarker: consensus and recommendations. Neoplasia. 2009 Feb; 11 (2):102-25.
3. Padhani AR, Lecouvet FE, Tunariu N, Koh DM, De Keyzer F, Collins DJ, Sala E, Schlemmer HP, Petralia G,Vargas HA, Fanti S, Tombal HB, de Bono J. METastasis Reporting and Data System for Prostate Cancer: Practical Guidelines for Acquisition, Interpretation, and Reporting of Whole-body Magnetic Resonance Imaging-based Evaluations of Multiorgan Involvement in Advanced Prostate Cancer. Eur Urol 2016.
4. Taouli B, Beer AJ, Chenevert T, Collins D, Lehman C, Matos C, Padhani AR, Rosenkrantz AB, Shukla-Dave A, Sigmund E, Tanenbaum L, Thoeny H, Thomassin-Naggara I, Barbieri S, Corcuera-Solano I, Orton M, Partridge SC, Koh DM. Diffusion-weighted imaging outside the brain: Consensus statement from an ISMRM-sponsored workshop. J Magn Reson Imaging. 2016 Sep; 44 (3): 521-40.
5. Rosenkrantz AB, Padhani AR, Chenevert TL, Koh DM, De Keyzer F, Taouli B, Le Bihan D. Body diffusion kurtosis imaging: Basic principles, applications, and considerations for clinical practice. J Magn Reson Imaging. 2015 Nov; 42 (5):1190-202.

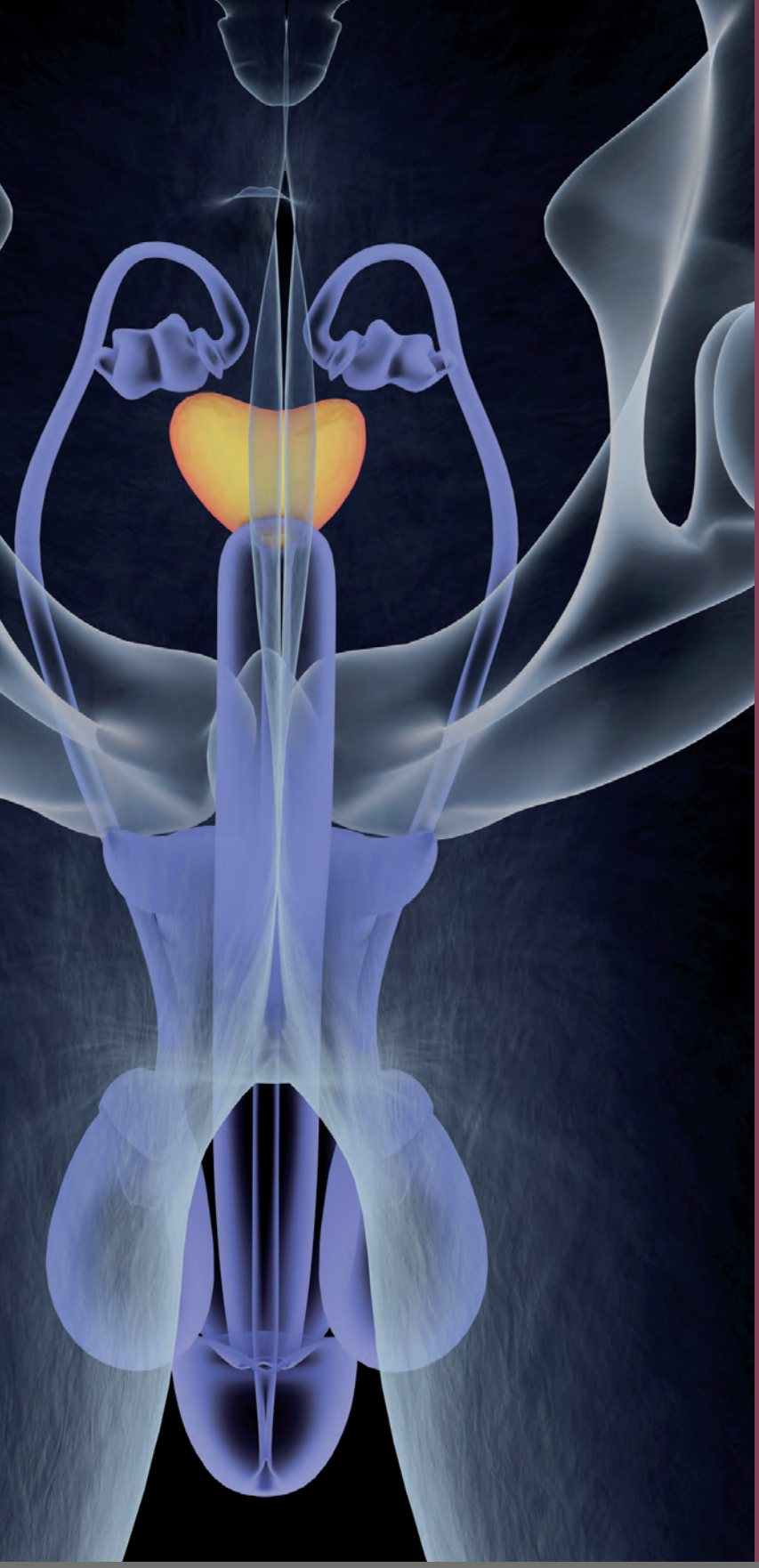

DWI of the Prostate:

should we use quantitative metrics to better characterize focal lesions originating in the peripheral zone?

François Cornud, MD
Thibaut Pierre
Paul Legmann, MD

1. Weinreb JC, Barentsz JO, Choyke PL, Cornud F, Haider MA, Macura KJ, et al. PI-RADS Prostate Imaging - Reporting and Data System: 2015, Version 2. Eur Urol. 2016;69(1):16-40.
2. Jung SI, Donati OF, Vargas HA, Goldman D, Hricak H, Akin O. Transition zone prostate cancer: incremental value of diffusion-weighted endorectal MR imaging in tumor detection and assessment of aggressiveness. Radiology. 2013;269(2):493-503.
3. Rosenkrantz AB, Kim S, Campbell N, Gaing B, Deng FM, Taneja SS. Transition zone prostate cancer: revisiting the role of multiparametric MRI at 3 T. AJR Am J Roentgenol. 2015;204(3):W266-72.
4. Mertan FV, Greer MD, Shih JH, George AK, Kongnyuy M, Muthigi A, et al. Prospective Evaluation of the Prostate Imaging Reporting and Data System Version 2 for Prostate Cancer Detection. J Urol. 2016.
5. Abd-Alazeez M, Kirkham A, Ahmed HU, Arya M, Anastasiadis E, Charman SC, et al. Performance of multiparametric MRI in men at risk of prostate cancer before the first biopsy: a paired validating cohort study using template prostate mapping biopsies as the reference standard. Prostate cancer and prostatic diseases. 2013.
6. Afaq A, Koh DM, Padhani A, van As N, Sc Clinical utility of diffusion-weighted magr nance imaging in prostate cancer. BJU inte 2011;108(11):1716-22.
7. Vargas HA, Akin O, Franiel T, Mazaheri Y Moskowitz C, et al. Diffusion-weighted er MR imaging at 3 T for prostate cancer: tur tion and assessment of aggressiveness. Ra 2011;259(3):775-84.

DW-MRI of the prostate plays a central role in prostate MRI. It is considered as the dominant sequence in the peripheral zone (PZ) [1]. If combined with T2W images, it also improves the accuracy of MRI for the detection of transitional zone cancer (TZ Ca) [2,3].

To characterize a focal lesion visible on MRI, a 1 to 5 scale is used. A score of 4 or 5 results in a cancer detection rate of 70-100% [4], whereas a score of 1 or 2 has been found to generally represent benign tissue [4]. As a result, it is now recommended to routinely perform MR-targeted biopsy of score 4 or 5 lesions, while considering deferment of biopsy for low-probability lesions.

However, management of score 3 lesions remains unclear, because the visual assessment of the combination of the Signal Intensity (SI) on the apparent diffusion coefficient (ADC) map and source DW images (dark on the ADC map and bright on source DW images), which characterizes score 4 and 5 lesions, is not straightforward in score 3 lesions. Visual assessment of these lesions is labelled "mildly hypointense" on the ADC map and "iso or mildly hyperintense" on the DW source images at a b-value >1000 s/mm^2 (i.e 1500 or 2000 in most studies), which entails a part of subjectivity.

Currently, targeted biopsies of score 3 lesions are recommended, but the cancer detection rate is low, approximately 20% [4], which contributes largely to the low specificity of the Likert or PIRADS scoring systems, lower than 50% [5]. The value of DW-MRI metrics deserved thus to be explored to improve the specificity of DW-MRI to characterize focal prostatic lesions, especially score 3 lesions. The most often used parameter has been the absolute value of the ADC, but several studies have proposed other parameters derived from the ADC map to improve the diagnostic and prognostic values of ADC metrics.

This review aims to show the different quantitative parameters available to evaluate the performance of quantitative MRI with a special focus on score 3 lesions.

QUANTITATIVE DWI AND DETECTION OF PZ PCA

The ADC map

Numerous publications have established that the mean ADC value was significantly lower in prostate cancer (PCa) than in benign tissue [6]. However, the reported values of ADC in PCa showed great variations, ranging from 0.98 $\pm$ 0.22 x10^{-3} mm^2/s to 1.39 $\pm$ 0.23 x10^{-3} mm^2/s. One factor contributing to these variations is the selection of the maximal b-value among the studies. The higher the b-value, the lower the ADC value [7,8]. Also, the ADC value varies with the number of intermediate b-values [9] between 0 and 1000 s/mm ^{2} and with the inclusion of the b0 value, often discarded to avoid the perfusion effect (pseudo-diffusion).

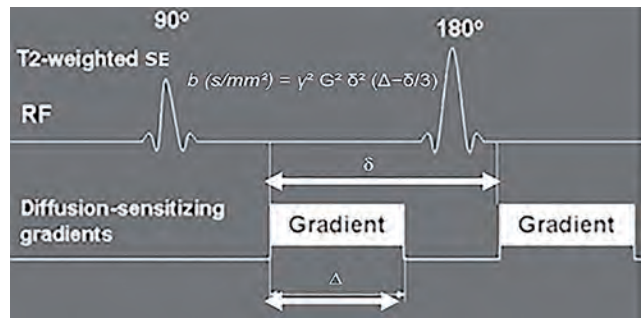

Figure 1: Water Diffusion Metrics (modified from [64]). Two rectangular gradient pulses of equal strength are applied before and after the 180-refocusing pulse of the turbo fast spin echo sequence. δ (diffusion time) is the time interval between the two gradient lobes, and Δ is the overall time interval during which the gradients are applied (gradient duration). The b-value (formula in brackets) is linearly related to Δ, but also to the square of δ. The values should thus be the same in every patient to have a valid comparison of ADC values across patients.

8. Kitajima K, Takahashi S, Ueno Y, Yoshikawa T, Ohno Y, Obara M, et al. Clinical utility of apparent diffusion coefficient values obtained using high b-value when diagnosing prostate cancer using 3 tesla MRI: comparison between ultra-high b-value (2000 s/mm(2)) and standard high b-value (1000 s/mm(2)). Journal of magnetic resonance imaging : JMRI. 2012;36(1):198-205.
9. Thormer G, Otto J, Reiss-Zimmermann M, Seiwerts M, Moche M, Garnov N, et al. Diagnostic value of ADC in patients with prostate cancer: influence of the choice of b values. European radiology. 2012;22(8):1820-8.
10. Nagel KN, Schouten MG, Hambrock T, Litjens GJ, Hoeks CM, ten Haken B, et al. Differentiation of prostatitis and prostate cancer by using diffusion-weighted MR imaging and MR-guided biopsy at 3 T. Radiology. 2013;267(1):164-72.
11. Scheenen TW, Rosenkrantz AB, Haider MA, Futterer JJ. Multiparametric Magnetic Resonance Imaging in Prostate Cancer Management: Current Status and Future Perspectives. Invest Radiol. 2015.
12. Rosenkrantz AB, Khalef V, Xu W, Babb JS, Taneja SS, Doshi AM. Does normalisation improve the diagnostic performance of apparent diffusion coefficient values for prostate cancer assessment? A blinded independent-observer evaluation. Clin Radiol. 2015;70(9):1032-7.
13. Barrett T, Priest AN, Lawrence EM, Goldman DA, Warren AY, Gnanapragasam VJ, et al. Ratio of Tumor to Normal Prostate Tissue Apparent Diffusion Coefficient as a Method for Quantifying DWI of the Prostate. AJR Am J Roentgenol. 2015;205(6):W585-93.

Another finding shared by all studies is that, despite the significant difference of ADC values between cancer and benign tissue, an overlap could be noted between benign and malignant focal lesions [10]. Lastly, the two parameters used to measure the ADC value, diffusion time (Figure 1) and duration of application of the gradients [11] should theoretically be the same to compare ADC values across patients, but they are currently integrated together into one b-value. As a result, quantitative ADC metrics should be used with caution to better characterize focal prostatic abnormalities. To circumvent this limitation, the only reliable alternative would be for each center to define its own cut-off ADC value to differentiate PCa from benign tissue, according to the local DW protocol and MR platform used.

For example, in our routine practice, the mean ADC value is measured at the upper, mid and lower part of the lesion and the lowest value is the reference value. With regards to score 3 lesions (Table 1), we confirmed that cancer lesions had a lower mean ADC value than benign lesions (0.978 ± 0.146 vs 1.120 ± 0.115 x10^{-3} mm^2/s, p=0.02). The value of the area under the curve (Az) of the ADC value to differentiate PCa from benign tissue was 0.795. A sensitivity (Se) of 89% could be obtained at a cut-off value of 1.080x10^{-3} mm^2/s achieving a specificity (Sp) of 50%. This finding may help for the biopsy decision making in score 3 lesions, allowing for the deferral of 25% of immediate biopsies.

The ADC ratio

The ADC ratio consists of calculating the ratio of the mean tumor ADC value to that of a surrounding reference tissue. This intra-patient normalized ADC may compensate for equipment-related variations and improve the discrepant performance of absolute ADC values. To measure the ADC ratio, a region of interest (ROI) is placed in the contralateral benign PZ, in mirror position to the tumor.
A mean ADC ratio value of around 0.60-0.65 is the most often reported cut-off to differentiate PCa from benign tissue [12]. However, as for ADC metrics,

Table 1: ADC metrics and derivates in 41 score 3 lesions (Cornud et al., unpublished data).

	Benign (32)	any Ca (9)	GS 3+3 (4)	GS 3+4 (5)
ADC (x10^{-3} mm^2/s)	1.12 ± 115	0.9- ± 0.136 (p=0.003)	0.937 ± 0.15	1.01 ± 0.013 (p=0.45)
ADC ratio				
Mirror	0.61 ± 0.1	0.57 ± 0.07 (p=0.26)	0 59 ± 0.06	0.56 ± 0.08 (p=0.14)
Whole Prostate	0.72 ± 0.09	0.6 ± 0.06 (p=0.0002)	0.53 ± 0.08	0.63 ± 0.03 (p=0.03)
WL ADC (x10^{-3} mm^2/s)				
Mean	1.2 ± 0.0.155	1.06 ± 0.93 (p=0.02)	1.04 ± 0.59	1.08 ± 117 (p=0.5)
10 %	1.08 ± 0.143	0.95 ± 0.15 (p=0.37)	0.93 ± 0.75	0.97 ± 0.19 (p>0.07)
25%	1.17 ± 0.142	0.99 ± 0.11 (p=0.10)	0.97 ± 0.74	1.01 ± 0.15 (p>0.05)
50%	1.17 ± 0.14	1.07 ± 0.106 (p=0.055)	1.04 ± 0.62	1.10 ± 0.13 (p>0.05)
SI ratio				
1500	1.7 ± 0.33	1.8 ± 0.39 (p=0.13)	1.8 ± 0.3	1.9 ± 0.5 (p>0.05)
3000	2.84 ± 0.95	4 ± 1.26 (p=0.005	4.1 ± 1.4	4 ±1.3 (p>0.05
6000	6.49 ± 4.5	15.7 ± 12.7 (p=0.001	18 ± 19	13 ± 6 (p>0.05)

14. Donati OF, Mazaheri Y, Afaq A, Vargas HA, Zheng J, Moskowitz CS, et al. Prostate cancer aggressiveness: assessment with whole-lesion histogram analysis of the apparent diffusion coefficient. Radiology. 2014;271(1):143-52.
15. Hoang Dinh A, Melodelima C, Souchon R, Lehaire J, Bratan F, Mege-Lechevallier F, et al. Quantitative Analysis of Prostate Multiparametric MR Images for Detection of Aggressive Prostate Cancer in the Peripheral Zone: A Multiple Imager Study. Radiology. 2016:151406.
16. Peng Y, Jiang Y, Antic T, Giger ML, Eggener SE, Oto A. Validation of quantitative analysis of multiparametric prostate MR images for prostate cancer detection and aggressiveness assessment: a cross-imager study. Radiology. 2014;271(2):461-71.
17. Rosenkrantz AB, Triolo MJ, Melamed J, Rusinek H, Taneja SS, Deng FM. Whole-lesion apparent diffusion coefficient metrics as a marker of percentage Gleason 4 component within Gleason 7 prostate cancer at radical prostatectomy. J Magn Reson Imaging. 2015;41(3):708-14.
18. Rosenkrantz AB, Meng X, Ream JM, Babb JS, Deng FM, Rusinek H, et al. Likert score 3 prostate lesions: Association between whole-lesion ADC metr pathologic findings at MRI/ultrasound fusion ed biopsy. J Magn Reson Imaging. 2016;43(2):32
19. Maas MC, Futterer JJ, Scheenen TW. Quant tive evaluation of computed high B value diff sion-weighted magnetic resonance imaging o prostate. Investigative radiology. 2013;48(11):77
20. Grant KB, Agarwal HK, Shih JH, Bernardo M Pang Y, Daar D, et al. Comparison of calculate acquired high b value diffusion-weighted ima; prostate cancer. Abdom Imaging. 2014.

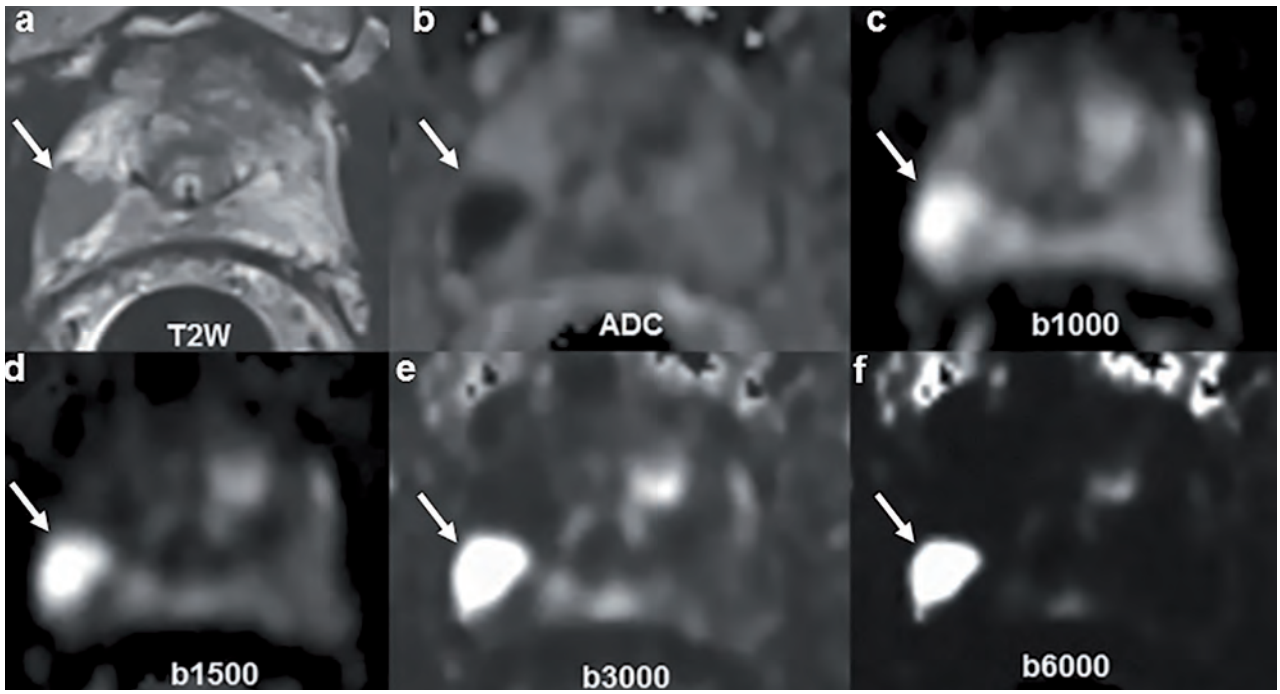

Figure 2: Very high computed b-values in a score 4 lesion. Right focal hypointensity on T2W (arrow, a) in the right lobe, dark on the ADC map (b), extracted from a b-50-500-1000 DW acquisition, and bright on the acquired b1000 images (c). As the computed b-value increases (d,e,f), the benign prostate is more and more suppressed, while the tumor remains bright.

the discriminant value of the ADC ratio showed conflicting results. Some studies [13] reported that the correlation coefficient with the presence of tumor was higher (0.883) for the ADC ratio compared with that obtained when the absolute ADC values were used alone (0.873). Other studies showed the opposite [12] by reporting that for PZ tumor detection the ADC value achieved a significantly higher Az value and specificity than the ADC ratio. With regard to score 3 lesions, our experience (Table 1) showed that the mean value of ADC ratio of tumors was not significantly different from that of benign lesions (0.57 ± 0.07 vs 0.61 ± 0.1). These discrepancies may be due to the fact that the benign PZ commonly shows variations of signal intensity related to the frequency of PZ benign changes such as prostatitis, fibrosis or atrophy [12]. As a result, we thought it could be more appropriate to define a more reproducible ROI to average the heterogeneity of the benign prostate (Figures 2 and 3). We thus calculated the Az of the ADC ratio by choosing the rest of the entire surface of the benign prostate, including the PZ and the TZ as the ROI of reference. In score 3 lesions (Table 1), the ADC ratio with this metric was significantly lower in Ca (0.6 ± 0.06) than in benign focal lesions (0.73 ± 0.09) ($p<0.0002$). The Az value was 0.89 and a cut-off value of 0.66 could detect any prostate cancer with a sensitivity of 90% and a specificity of 75% (Table 1).

Whole lesion ADC with values of the 10th, 25th, and 50th percentiles

Recent studies have shown that the prognostic value of more sophisticated ADC metrics derived from whole-lesion histogram assessment [14-17] (see below).

21. Rosenkrantz AB, Chandarana H, Hindman N, Deng FM, Babb JS, Taneja SS, et al. Computed diffusion-weighted imaging of the prostate at 3 T: impact on image quality and tumour detection. European radiology. 2013;23(11):3170-7.
22. Metens T, Miranda D, Absil J, Matos C. What is the optimal b value in diffusion-weighted MR imaging to depict prostate cancer at 3T? Eur Radiol. 2012;22(3):703-9.
23. Katahira K, Takahara T, Kwee TC, Oda S, Suzuki Y, Morishita S, et al. Ultra-high-b-value diffusion-weighted MR imaging for the detection of prostate cancer: evaluation in 201 cases with histopathological correlation. Eur Radiol. 2011;21(1):188-96.
24. Vural M, Ertas G, Onay A, Acar O, Esen T, Saglican Y, et al. Conspicuity of Peripheral Zone Prostate Cancer on Computed Diffusion-Weighted Imaging: Comparison of cDWI1500, cDWI2000, and cDWI3000. BioMed research international. 2014;2014:768291.
25. Feuerlein S, Davenport MS, Krishnaraj A, Merkle EM, Gupta RT. Computed high b-value diffusion-weighted imaging improves lesion contrast and conspicuity in prostate cancer. Prostate Cancer Prostatic Dis. 2015;18(2):155-60.
26. Rosenkrantz AB, Parikh N, Kierans AS, Kong MX, Babb JS, Taneja SS, et al. Prostate Cancer Detection Using Computed Very High b-value Diffusion-weighted Imaging: How High Should We Go? Acad Radiol. 2016.
27. Zhang K, Shen Y, Zhang X, Ma L, Wang H, An N, et l. Predicting Prostate Biopsy Outcomes: A Preliminary Investigation on Screening with Ultrahigh B-Value Diffusion-Weighted Imaging as an Innovative Diagnostic Biomarker. PLoS One. 2016;11(3):e0151176.

Such metrics may also represent an aid for the management decisions in score 3 lesions. A software is required for the segmentation of the lesion by placing a 3D volume of interest involving all slices showing the lesion. Whole-lesion ADC metrics (mean value and mean values determined by the 10th, 25th, and 50th percentiles) are then computed.

These metrics are supposed to provide a more robust assessment of the presence of low ADC values within the lesion than does the absolute minimum ADC value within any single voxel. In score 3 lesions, a study [18] showed that, in naïve biopsy patients, a whole lesion ADC value at the 25th percentile ≤1.04 x10^{-3} mm^2/s achieved a 90% sensitivity and 50% specificity to suspect the presence of a Gleason score (GS) >6 tumor. Comparison with the accuracy of the mean non-whole lesion ADC value was not available in the article.

In our practice (Table 1), we found that the mean whole-lesion ADC value of score 3 cancer lesions was significantly lower than that of benign lesions. The Az value was 0.76 and a cut-off value of 1.18x$10^{-3}$$mm^2/s$ could detect any tumor with a sensitivity of 89% and a specificity of 47%. However, the 10th and 25th percentiles were not significantly different between both groups.

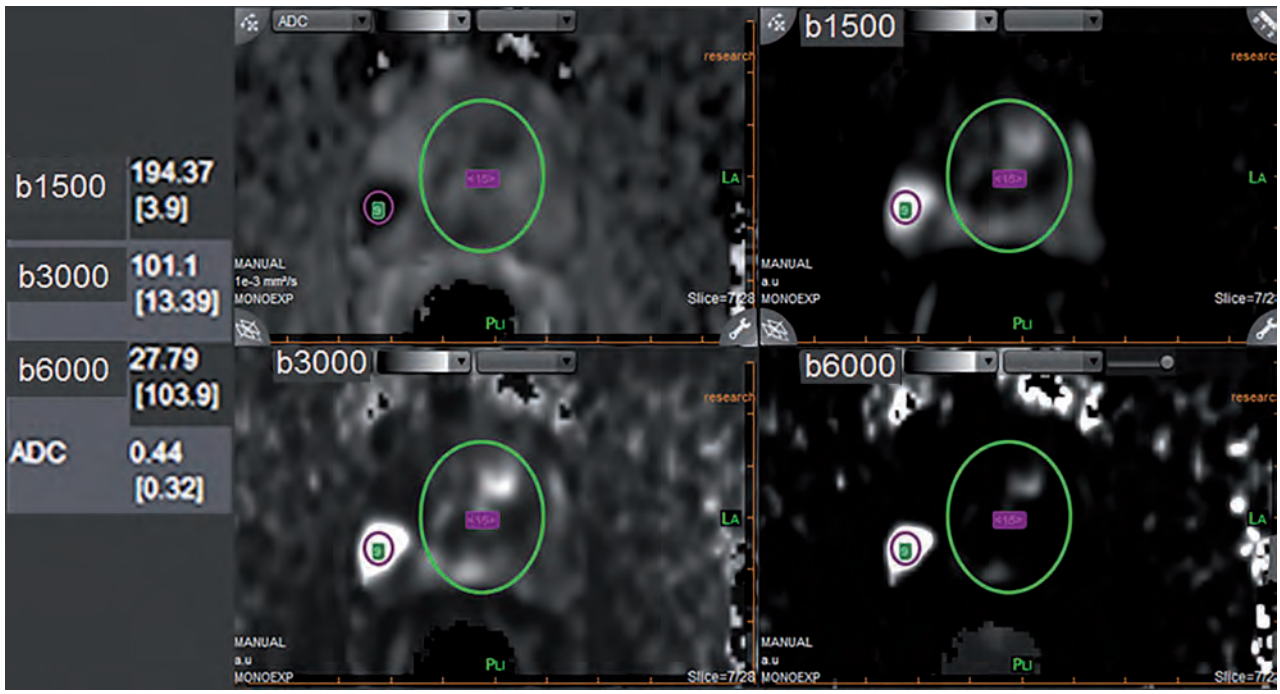

Figure 3: Signal Intensity Ratio metrics (same patient as in Figure 2). A reference ROI is placed on the tumor and a second one on the rest of the benign prostate. The ROIs are automatically propagated to all b-values and to the ADC map. The SI ratios are automatically calculated by the software. The value steadily increases from 4 to 104, as the b-values increase from 1500 to 6000 s/mm^2. Of note the low value of the ADC (0.44 x10^{-3} mm^2/s) and of the ADC ratio (0.32) measured with the rest of the prostate as the reference ROI. Targeted biopsies showed a Gleason score 4+3 tumor with 70% G4.

28. Gudbjartsson H, Patz S. The Rician distribution of noisy MRI data. Magn Reson Med. 1995;34(6):910-4.
29. Dyvorne HA, Galea N, Nevers T, Fiel MI, Carpenter D, Wong E, et al. Diffusion-weighted imaging of the liver with multiple b values: effect of diffusion gradient polarity and breathing acquisition on image quality and intravoxel incoherent motion parameters--a pilot study. Radiology. 2013;266(3):920-9.
30. Neil JJ, Bretthorst GL. On the use of Bayesian probability theory for analysis of exponential decay data: an example taken from intravoxel incoherent motion experiments. Magn Reson Med. 1993;29(5):642-7.
31. Chamie K, Sonn GA, Finley DS, Tan N, Margolis DJ, Raman SS, et al. The role of magnetic resonance imaging in delineating clinically significant prostate cancer. Urology. 2014;83(2):369-75.
32. Donati OF, Afaq A, Vargas HA, Mazaheri Y, Zheng J, Moskowitz CS, et al. Prostate MRI: Evaluating Tumor Volume and Apparent Diffusion Coefficient as Surrogate Biomarkers for Predicting Tumor Gleason Score. Clin Cancer Res. 2014;20(14):3705-11.
33. Futterer JJ, Verma S, Hambrock T, Yakar D, Barentsz JO. High-risk prostate cancer: value of multi-modality 3T MRI-guided biopsies after previous negative biopsies. Abdominal imagin 2012;37(5):892-6.
34. Itatani R, Namimoto T, Kajihara H, Katahira Kitani K, Hamada Y, et al. Triage of Low-Risk P Cancer Patients With PSA Levels 10 ng/mL or Comparison of Apparent Diffusion Coefficien and Transrectal Ultrasound-Guided Target Bi AJR Am J Roentgenol. 2014;202(5):1051-7.
35. Itou Y, Nakanishi K, Narumi Y, Nishizawa Y Tsukuma H. Clinical utility of apparent diffusi coefficient (ADC) values in patients with pros

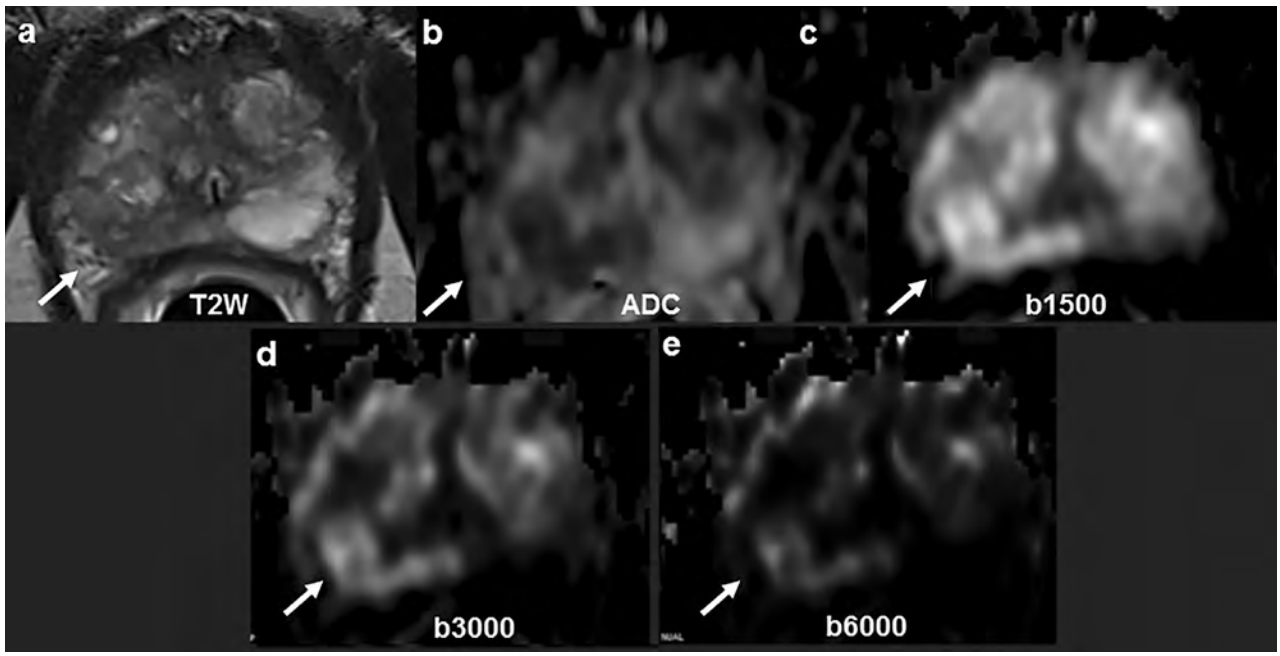

Figure 4: Very high computed b-values in a score 3 lesion. 67 y/o man. PSA: 18 ng/ml. Two series of systematic negative biopsies. Right focal hypointensity on T2W images (arrow, a) in the right lobe, dark on the ADC map (b) and isointense on the acquired b-value of 1500 s/mm^2 (c). As the computed b-value increases (d,e), both the benign prostate and the lesion are increasingly suppressed.

Very high b-values images

To increase the conspicuity of tumor foci, the use of computed b-values of 1500 or 2000 s/mm^2 is recommended [19-23]. Computed high b-values images increase diffusion-weighting, allowing for a greater suppression of benign prostate, and thus improve the sensitivity of source DW-MR images for the detection of PCa (Figures 2 and 3).

More recently, several studies have reported a greater contrast between tumor and benign tissue at still higher computed b-values of 2500 to 4000 s/mm^2 [19,24-27], considering that b-values ›2000 s/mm^2 can show a continual greater degree of benign tissue suppression. All these studies have evaluated the increase of the tumor conspicuity visually, so that no quantitation has been evaluated to define a cut-off value to differentiate PCa from benign tissue. However, in one of these studies [26], the ratio between the signal intensity of the PZ tumor and the rest of the PZ has been shown to steadily increase as the b-value was increasing, thus potentially defining a quantitative parameter to differentiate PCa from benign lesions. The rationale for such an approach is that computed DWI at very high b-values, up to 6000 s/mm^2, synthetized from measured images with b-values between 0 and 800 s/mm^2, yield a high contrast to noise ratio, because computed values are theoretically noise-free, hence not affected by the noise floor effect due to the non-normal Rician distribution of the noise [28].

These metrics can be evaluated using the Bayesian theory which has been successfully applied to improve the performance of ADC metrics [29,30]. This probabilistic approach is used in Olea Sphere® software to calculate more robustly, with regards to the noise level, the ADC value and to synthetize very high b-values.

cancer: can ADC values contribute to assess the aggressiveness of prostate cancer? J Magn Reson Imaging. 2011;33(1):167-72.
36. Baco E, Rud E, Eri LM, Moen G, Vlatkovic L, Svindland A, et al. A Randomized Controlled Trial To Assess and Compare the Outcomes of Two-core Prostate Biopsy Guided by Fused Magnetic Resonance and Transrectal Ultrasound Images and Traditional 12-core Systematic Biopsy. Eur Urol. 2015.
37. Kitajima K, Takahashi S, Ueno Y, Miyake H, Fujisawa M, Kawakami F, et al. Do apparent diffusion coefficient (ADC) values obtained using high b-values with a 3-T MRI correlate better than a transrectal ultrasound (TRUS)-guided biopsy with true Gleason scores obtained from radical prostatectomy specimens for patients with prostate cancer? Eur J Radiol. 2013;82(8):1219-26.
38. Nagarajan R, Margolis D, Raman S, Sheng K, King C, Reiter R, et al. Correlation of Gleason scores with diffusion-weighted imaging findings of prostate cancer. Advances in urology. 2012;2012:374805.
39. Oto A, Yang C, Kayhan A, Tretiakova M, Antic T, Schmid-Tannwald C, et al. Diffusion-weighted and dynamic contrast-enhanced MRI of prostate cancer: correlation of quantitative MR parameters with Gleason score and tumor angiogenesis. AJR Am J Roentgenol. 2011;197(6):1382-90.
40. Somford DM, Hambrock T, Hulsbergen-van de Kaa CA, Futterer JJ, van Oort IM, van Basten JP, et al. Initial experience with identifying high-grade prostate cancer using diffusion-weighted MR imaging (DWI) in patients with a Gleason score ‹/= 3 + 3 = 6 upon schematic TRUS-guided biopsy: a radical prostatectomy correlated series. Investigative radiology. 2012;47(3):153-8.

Quantitative very high b-value DWI may thus represent an adjunct to the ADC map, especially in score 3 lesions, to differentiate PCa from benign tissue, at least in the PZ.

In our practice (Table 1), we studied the Signal Intensity Ratio (SIR) between the lesion and the rest of benign prostate on the same MRI slice including, as for the ADC ratio, the TZ and the PZ. Olea Sphere® software allows for a computation of an array of very high b-values. As shown in Figure 2, the benign prostate is more and more suppressed as the b-value increases and results in an increase of the SIR. With regard to score 3 lesions (Figure 3), we found that the SIR was significantly greater in cancer than in benign lesions at b-3000 (4 ± 1.26 vs 2.84 ± 0.95, p=0,005) and still significantly greater at b-6000 (15.7 ± 12.7 vs 6.49 ± 4.5, p=0,0012), but not at b-1500 s/mm^2. At b-3000, the value of the Az was 0.78 and a cut-off of 2.7 achieved a sensitivity of 100% and a specificity of 53% for the detection of any cancer. At a b-value of 6000 s/mm^2, the Az was 0.82 and a cut-off value of 7.6 achieving a sensitivity of 100% and a specificity of 66%, although the difference was not significant with results at a b-value of 3000 s/mm^2.

QUANTITATIVE DWI AND ASSESSMENT OF GLEASON SCORE OF PZ CANCER

Numerous studies have shown an inverse relationship between the ADC value and the surgical Gleason score of PCa with an overall correlation coefficient which varies from 0.32 (weak correlation) to 0.50 (fair correlation). The ADC value of Gleason 6 tumors is above 1 x10^{-3}mm^2/s in all studies [7,17,31-43] but one [44] (range: 1.04-1.3), and is higher than that of Gleason score ›7 tumors (range: 0.69-0.88 x10^{-3} mm^2/s). All studies share showed a substantial overlap between the different subclasses, as indicated by the high values of reported standard deviations. Similarly, whole-tumor ADC metrics [14,45] showed that the mean and/or the mean 10th percentile ADC values were lower in Gleason 6 vs ›6 tumors.

Table 2: Correlation of the %G4 component of TRUS-MRI image fusion targeted biopsies (TB%G4) with the pathological %G4 component of radical prostatectomy specimen (RP%G4) (from reference [52]). The %G4 detected on TB is upgraded to a higher rate in 15-43% of cases, depending of the %G4 category.

TB %G4 / RP %G4	0%G4 GS6	>0-25% G4 GS 3+4	>25-50% G4 GS 3+4	>50% G4 GS 4+3
0%G4 GS 6	45%	4%	4%	0
>0-25% G4 GS 3+4	43%	54%	18%	0
>25-50% G4 GS 3+4	10%	27%	48%	8%
>50% G4 GS 4+3	2%	15%	30%	92%

41. Thormer G, Otto J, Horn LC, Garnov N, Do M, Franz T, et al. Non-invasive estimation of prostate cancer aggressiveness using diffusion-weighted MRI and 3D proton MR spectroscopy at 3.0 T. Acta Radiol. 2015;56(1):121-8.
42. Verma S, Rajesh A, Morales H, Lemen L, Bills G, Delworth M, et al. Assessment of aggressiveness of prostate cancer: correlation of apparent diffusion coefficient with histologic grade after radical prostatectomy. AJR Am J Roentgenol. 2011;196(2):374-81.
43. Vos EK, Kobus T, Litjens GJ, Hambrock T, Hulsbergen-van de Kaa CA, Barentsz JO, et al. Multiparametric Magnetic Resonance Imaging for Discriminating Low-Grade From High-Grade Prostate Cancer. Invest Radiol. 2015.
44. Bittencourt LK, Barentsz JO, de Miranda LC, Gasparetto EL. Prostate MRI: diffusion-weighted imaging at 1.5T correlates better with prostatectomy Gleason Grades than TRUS-guided biopsies in peripheral zone tumours. European radiology. 2012;22(2):468-75.
45. Wu CJ, Wang Q, Li H, Wang XN, Liu XS, Shi HB, et al. DWI-associated entire-tumor histogram analysis for the differentiation of low-grade prostate cancer from intermediate-high-grade prostate cancer. Abdom Imaging. 2015.
46. Lebovici A, Sfrangeu SA, Feier D, Caraiani C, Suciu M, et al. Evaluation of the normal-to-eased apparent diffusion coefficient ratio as a indicator of prostate cancer aggressiveness. B medical imaging. 2014;14:15.
47. De Cobelli F, Ravelli S, Esposito A, Giganti na A, Montorsi F, et al. Apparent diffusion coe value and ratio as noninvasive potential biom to predict prostate cancer grading: comparisc prostate biopsy and radical prostatectomy sp men. AJR Am J Roentgenol. 2015;204(3):550-7.

Results of ADC ratio metrics were discrepant, probably for the same reasons as for the diagnostic value of the ADC ratio (see above). Some authors [41,46] found a mean ADC ratio ‹0.50 in GS›6 tumors vs ›0.50 in GS=6 tumors. In another study [47], using an unusual set of acquired b-values (0-800-1600), the Az value was 0.92 (p=0.12) for the ADC value and 0.86 for the ADC ratio (p=0.42), indicating no incremental value of the ADC ratio compared to that of the ADC value.

Several studies aimed to be more accurate and addressed the more specific challenge of intermediate grade tumors (Gleason score 7) which probably represents the true challenge of DW-MRI. Tumor aggressiveness is strongly related to the percent of Gleason grade 4 (%G4) components present within the tumor [48]. Stamey et al [49] demonstrated that biological progression after radical prostatectomy increased for each 10% increment of %G4 and the poorer prognosis of Gleason score 4+3 vs 3+4 [50] has been well-established [51].

The accuracy for the detection of the %G4 has been significantly increased these past years thanks to MR-targeted biopsies, but some limitations, namely the detection of small amounts of Gleason grade 4 and the determination of the primary grade of Gleason 7 tumors can still be noted [52] (Table 2). Several studies [7,17,33,35,38,42] compared ADC values of Gleason score 74+3 vs 73+4 and discrepancies could be noted. Some authors [17,42] failed to show a significant difference between both groups, while four studies [7,33,35,38] found the difference to be significant. Whole-lesion ADC metrics similarly failed to find a significant difference between the two categories of Gleason Score [17,53].

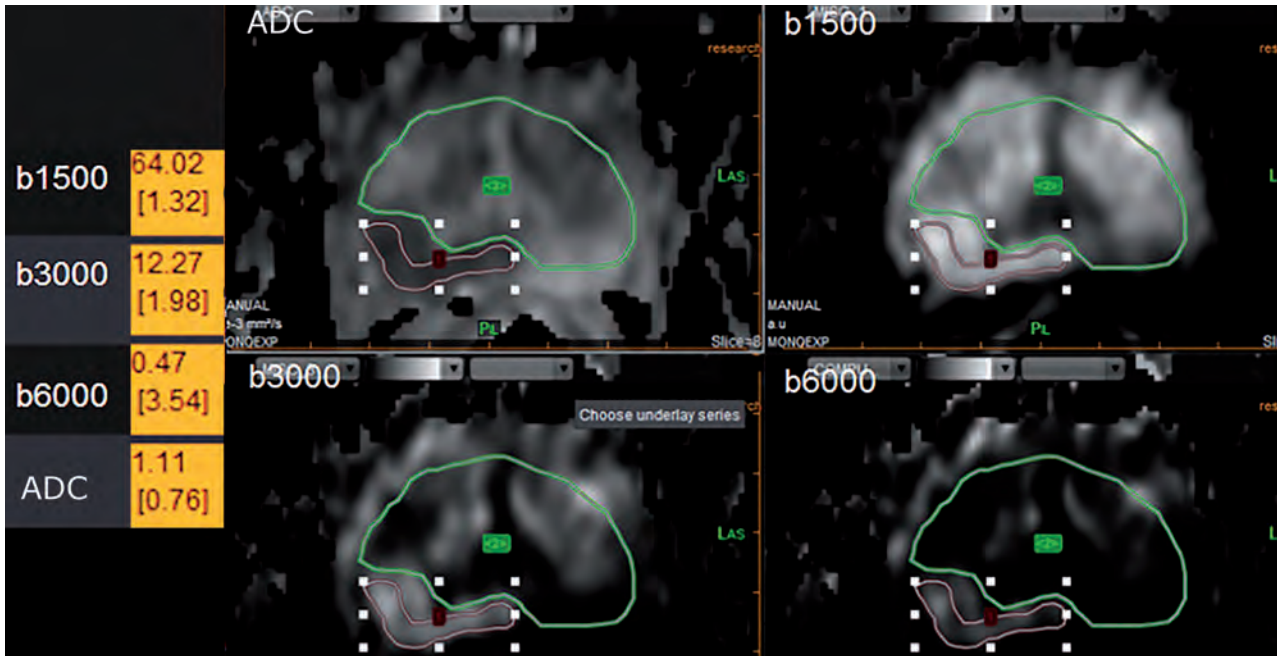

Fiugre.5: Signal Intensity Ratio metrics (same patient as in Figure 4). The SI ratio is of 2 at b-3000 and of 3.5 at b-6000 s/mm^2, suggesting benign tissue. Note however that the value of the ADC (1.1 x10^{-3} mm^2/s) and of the ADC ratio (0.76) also suggest benign tissue. Sixty template transperineal biopsies showed benign tissue.

48. Cheng L, Koch MO, Juliar BE, Daggy JK, Foster RS, Bihrle R, et al. The combined percentage of Gleason patterns 4 and 5 is the best predictor of cancer progression after radical prostatectomy. J Clin Oncol. 2005;23(13):2911-7.
49. Stamey TA, McNeal JE, Yemoto CM, Sigal BM, Johnstone IM. Biological determinants of cancer progression in men with prostate cancer. JAMA. 1999;281(15):1395-400.
50. Chandra RA, Chen MH, Zhang D, Loffredo M, D'Amico AV. Age, Comorbidity, and the Risk of Prostate Cancer-Specific Mortality in Men With Biopsy Gleason Score 4+3: Implications on Patient Selection for Multiparametric MRI. Clinical genitourinary cancer. 2015.
51. Cole AI, Morgan TM, Spratt DE, Palapattu GS, He C, Tomlins SA, et al. Prognostic Value of Percent Gleason Grade 4 at Prostate Biopsy in Predicting Prostatectomy Pathology and Recurrence. J Urol. 2016.
52. Lanz C, Cornud F, Beuvon F, Lefevre A, Legmann P, Zerbib M, et al. Gleason Score Determination with Transrectal Ultrasound-Magnetic Resonance Imaging Fusion Guided Prostate Biopsies-Are We Gaining in Accuracy? J Urol. 2016;195(1):88-93.
53.Rozenberg R, Thornhill RE, Flood TA, Hakim SW, Lim C, Schieda N. Whole-Tumor Quantitative Apparent Diffusion Coefficient Histogram and Texture Analysis to Predict Gleason Score Upgrading in Intermediate-Risk 3 + 4 = 7 Prostate Cancer. AJR Am J Roentgenol. 2016;206(4):775-82.
54. Le Bihan D, Breton E, Lallemand D, Aubin ML, Vignaud J, Laval-Jeantet M. Separation of diffusion and perfusion in intravoxel incoherent motion MR imaging. Radiology. 1988;168(2):497-505.

These discrepancies may be due to the enrollment of score 73+4 tumors with varying amounts of grade 4 across studies. Intuitively, it may indeed be expected that tumors with small amounts of grade 4 (up to 20-25%) have a mean ADC value similar to that of Gleason 6 tumors, because the distribution of grade 4 components is diffuse, making thus impossible to detect an area within the tumor with a more restricted diffusion supposed to contain the Gleason grade 4 (G4) component. Moreover, between 40 and 60% of G4, evaluation of the %G4 may vary across pathologists. It can thus also be expected that, in the range of 40-60 %G4, the ADC value may not be significantly different to differentiate Gleason score 3+4 from 4+3 tumors.

In score 3 lesions, the use of ADC metrics to predict the presence signs of aggressiveness may thus be challenging. Nevertheless, it should be noted that the cancer detection rate of Gleason score >6 lesions in score 3 lesions by MR-targeted biopsies is low. It varies between 0 [4] and 8.8 % [18]. Also, in our experience, the percent of Gleason grade 4 observed in score 3 cancer lesions is low, no greater than 20% at surgical histology, similar to that observed in non-visible Gleason score 3+4 tumors, characterized by a low volume and a %G4 not greater than 20% [52]. It may thus be questioned if an immediate diagnosis of these tumors is required as a radical treatment.

In one study [18], a whole-lesion ADC value at the 25th percentile ≤1.04 x10^{-3} mm^2/s achieved a 90% sensitivity and 50% specificity for the detection of GS > 6 tumors. In our experience, the only factor which could discriminate Gleason score 3+4 from Gleason score 3+3 tumors in score 3 lesions was the ADC ratio using the whole benign prostate as the reference ROI (0.53±0.08 vs 0.63±0.03, respectively, p=0.03) (Table 1). The Az value to detect GS 3+4 tumors was 0.8 and a cut-off value of 0.63 provided on the ROC curve a sensitivity of 80% and a specificity of 78% to predict the presence of a >0-20% grade 4 component. Values of the other factors (mean ADC, whole-lesion mean ADC value whatever the percentile, signal intensity ratio whatever the b-value) were not significantly different between both groups.

ADVANCED DW-MRI TECHNIQUES

Bi-exponential diffusion (IntraVoxel Incoherent Motion, IVIM) or how to separate the perfusion and the diffusion effects in DW-MRI.

In the capillary compartment of the model originally described by Le Bihan et al [54], the movement of water molecules mimics a diffusion process (pseudo-diffusion), evaluated by perfusion parameters (D*, or ADC$_{fast}$), derived from the weighting by several low b-values (0-100) (Figure 6). D* is represented by the initial portion of the curve which has a steep slope, because of the greater ^1H_2O distance motion when diffusion gradients are applied.

> “ D has the highest accuracy to discriminate PCa from benign tissue ”

The second part of the curve is evaluated with higher b-values. The slope is less steep and reflects tissue diffusion (D or ADC$_{slow}$). f corresponds to the blood volume derived from water protons flowing through pseudo-randomly oriented micro-capillaries and has been labelled perfusion fraction in the study by Le Bihan et al. [54].

55. Dopfert J, Lemke A, Weidner A, Schad LR. Investigation of prostate cancer using diffusion-weighted intravoxel incoherent motion imaging. Magn Reson Imaging. 2011;29(8):1053-8.
56. Kuru TH, Roethke MC, Stieltjes B, Maier-Hein K, Schlemmer HP, Hadaschik BA, et al. Intravoxel Incoherent Motion (IVIM) Diffusion Imaging in Prostate Cancer - What Does It Add? J Comput Assist Tomogr. 2014;38(4):558-64.
57. Pang Y, Turkbey B, Bernardo M, Kruecker J, Kadoury S, Merino MJ, et al. Intravoxel incoherent motion MR imaging for prostate cancer: an evaluation of perfusion fraction and diffusion coefficient derived from different b-value combinations. Magnetic resonance in medicine : official journal of the Society of Magnetic Resonance in Medicine / Society of Magnetic Resonance in Medicine. 2013;69(2):553-62.
58. Quentin M, Blondin D, Klasen J, Lanzman RS, Miese FR, Arsov C, et al. Comparison of different mathematical models of diffusion-weighted prostate MR imaging. Magn Reson Imaging. 2012;30(10):1468-74.
59. Shinmoto H, Oshio K, Tanimoto A, Higuchi N, Okuda S, Kuribayashi S, et al. Biexponential a ent diffusion coefficients in prostate cancer. Reson Imaging. 2009;27(3):355-9.
60. Valerio M, Zini C, Fierro D, Giura F, Colari A, Giuliani A, et al. 3T multiparametric MRI o the prostate: Does intravoxel incoherent mc diffusion imaging have a role in the detectio stratification of prostate cancer in the perip zone? Eur J Radiol. 2016;85(4):790-4.
61. Zhang YD, Wang Q, Wu CJ, Wang XN, Zha J, Liu H, et al. The histogram analysis of diffu sion-weighted intravoxel incoherent motion

Several studies [55-59] showed that, among the three parameters (D, D* and f), D has the highest accuracy to discriminate PCa from benign tissue, but all the studies showed that D and ADC values performed equally to discriminate tumor from benign tissue (AUC: 0.9). Some studies [56,60] found that the value of D could discriminate low- (Gleason score ‹7) from high-grade (Gleason score ›7) PCa.

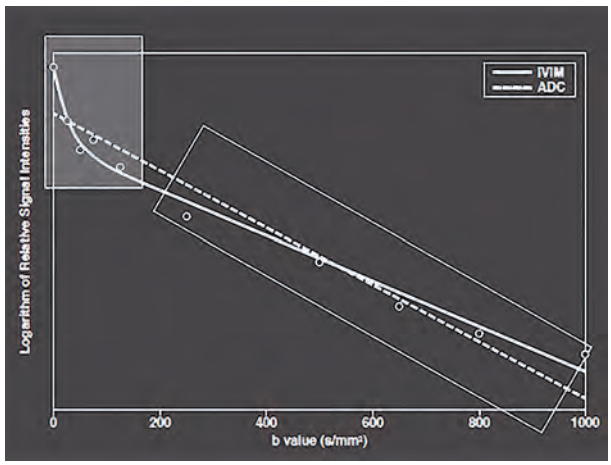

Figure 6: Bi-exponential decay of the DW signal, modified from [65]. The initial portion of the curve is steep for plotted signal intensity values at low b-values (within the rectangular light grey box). However, at higher b-values (dark grey rectangular box), the slope is less steep. The hockey stick shape of the bi-exponential curve provides a better fitting to the acquired DW data than the mono-exponential model used to generate the ADC map (dotted line).

The other parameters of the bi-exponential model (D* and f) showed a great variation of values with very large standard deviations and were thus not discriminant between Ca and benign tissue in all studies, but one [60]. The conclusion was that exclusion of this highly variable perfusion component may increase the diagnostic and prognostic values of the D parameter. Our experience at 1.5T with a reusable rectal coil (In Vivo) with a 10 b-values (0,10,20,30,40,50,80,100,500,1000) sequence showed that D and ADC values performed equally (AUC 0.89 and 0.91 respectively). The optimal cut-off value, regardless of the PIRADS score, to differentiate Ca from benign foci was 1070 for the ADC value (Se: 84%, Sp: 83%) and 1190 for the D value (Se: 86%, Sp: 83%).

Thus, although the bi-exponential model may provide a better fitting when multiple small b-values are used, further studies are required to confirm its potential incremental value over that of the mono-exponential model in the detection of PCa. In this regard, a study [61] showed that when measuring the whole lesion value of the ADC and that of D, D performed better, especially the 10th percentile value to differentiate GS6 tumors vs GS›6 tumors.

Kurtosis Diffusion Imaging

Overlap of quantitative ADC values derived from higher and lower grade PCa as well as from benign tissue may be due to another limitation of the mono-exponential DWI-based estimation of ADC, which assumes a Gaussian distribution of the displacements of the water molecules. However, when cellularity increases and restricts water diffusion, displacement of water molecules is assumed to become non Gaussian. The term Kurtosis describes the deviation of a non-Gaussian distribution compared with a Gaussian distribution. Using Diffusion-Kurtosis MRI (DK-MRI), it is possible to quantify this deviation. The Kurtosis is extracted from DW images acquired with a multi-b DW sequence including two b-values above 1000 s/mm^2 (b1500 and b2000) and may allow for a better differentiation between Ca and benign tissue. A high b-value of about 2000 s/mm^2 is needed to have a sufficiently large effect on the DW signal when a non Gaussian distribution is tested.

Only few clinical applications of DK-MRI of the prostate have been published. In the initial study [62], K values were higher (0.96 $\pm$ 0.24) in Ca than in benign PZ (0.57 $\pm$ 0.07) and also higher in Gleason score ›6 tumors (1.05 $\pm$ 0.26) than in Gleason score 6 tumors (0.89 $\pm$ 0.20, p‹.001).

imaging for differentiating the gleason grade of prostate cancer. Eur Radiol. 2015;25(4):994-1004.
62. Rosenkrantz AB, Sigmund EE, Johnson G, Babb JS, Mussi TC, Melamed J, et al. Prostate cancer: feasibility and preliminary experience of a diffusional kurtosis model for detection and assessment of aggressiveness of peripheral zone cancer. Radiology. 2012;264(1):126-35.
63. Roethke MC, Kuder TA, Kuru TH, Fenchel M, Hadaschik BA, Laun FB, et al. Evaluation of Diffusion Kurtosis Imaging Versus Standard Diffusion Imaging for Detection and Grading of Peripheral Zone Prostate Cancer. Invest Radiol. 2015.
64. Koh DM, Collins DJ. Diffusion-weighted MRI in the body: applications and challenges in oncology. AJR American journal of roentgenology. 2007;188(6):1622-35.
65. Koh DM, Collins DJ, Orton MR. Intravoxel incoherent motion in body diffusion-weighted MRI: reality and challenges. AJR Am J Roentgenol. 2011;196(6):1351-61.

The sensitivity of K was greater than that of the ADC for differentiating Ca from benign PZ (93.3% vs 78.5%, p<.001) without loss of specificity (95.7%, p>0.99) and showed a comparable value of the AUC (68.6% vs 51.0%) for differentiating Gleason score 6 tumors from Gleason score >6 tumors.

Interestingly, a second study from another group [63] did not reveal a significant difference between K and standard ADC for the detection of any cancer and of Gleason >6 tumors. The discrepancy between both studies was probably related to the ADC metrics which were extracted, in the first study [62], from the DW-Kurtosis sequence which requires an increased echo time to acquire the b-2000 images (81ms). In this second study [63] a separate standard DWI sequence was used, with a shorter TE (58ms) to calculate the ADC.

It was concluded in the second study that the value of the ADC metrics in a DK sequence may be underestimated. DK-MRI may thus show promise to improve the performance of a standard ADC map, both for diagnosis and assessment of tumor aggressiveness, but further studies are required to reconcile findings of both studies detailed above.

CONCLUSION

In summary, quantitative DW-MRI of the PZ may improve the specificity of DW-MRI scoring system of the PIRADS. Currently, there is not enough data to suggest that the value of the ADC metrics could be improved by more sophisticated parameters. Whole lesion ADC metrics and advanced DW sequences are under evaluation. However, they are time-consuming and labor intensive. They are thus not yet adapted for routine practice and more automatic workflows are required to incorporate them in workstations. Therefore, it seems useful to suggest simple recommendations.

The first is the use of a standardized protocol with three b-values (the high b-value should not exceed b-1000 s/mm^2) and with comparable acquisition parameters across platforms. This step should aid to standardize the ADC value across centers and most probably help to better characterize score 3 or 4 prostatic PZ lesions. It may thus help the biopsy decision making in routine clinical practice in an effort to upgrade or downgrade as much as possible score 3 lesions, to switch to a binary choice which would indicate biopsy or not.

The second recommendation is the use of high and very high computed b-values which increase the conspicuity of PCa and may help to differentiate it from benign tissue. A maximal value of b-3000, if available, has been suggested (26) to visually increase the conspicuity of prostatic tumors.

> “The second recommendation is the use of high and very high computed b-values”

The third is to use the rest of the benign prostate as the reference ROI, instead of the contra-lateral PZ, for ADC ratio and signal intensity ratio metrics which may improve the diagnostic accuracy of ADC metrics.

Determination of Gleason score by quantitative DW-MRI should take into account the fact that the underestimation rate of Gleason score, which was a major limitation of systematic biopsies, can be considerably decreased if MR-targeted biopsies are routinely used. These biopsies still show limitations to detect small amounts of grade 4 and to accurately predict the primary Gleason grade of score 7 lesions. This information may be an important requirement before including patients in active surveillance or focal therapy protocols. The true challenge of quantitative MRI may thus be to assess if it can predict an upgrade in the %G4 detected on a MR-targeted biopsy. Further research is definitively required to determine if this goal is achievable.

François Cornud, MD
Radiologist at Cochin hospital; and Professor at Paris-Descartes University, Paris, France
Thibaut Pierre
Resident in Radiology at Cochin hospital, Paris, France
Paul Legmann, MD
Head of the Radiology Department at Cochin hospital; and Professor at Paris-Descartes University, Paris, France

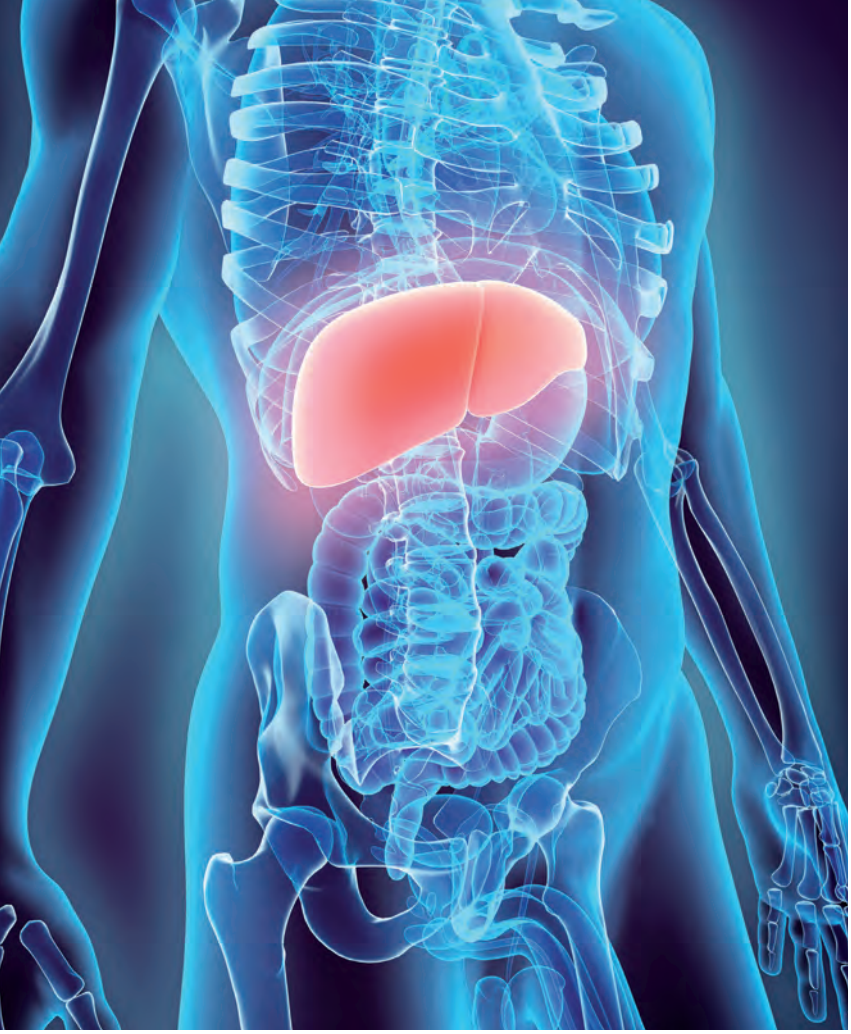

Article

Diffusion-weighted imaging in the liver: role of IVIM approach

| Mathilde Wagner, MD, PhD

Diffusion-weighted imaging (DWI) is a magnetic resonance imaging (MRI) technique using the microscopic thermal motion of water molecules in biologic tissues [1,2]. Because of technique development improving the image quality, DWI is now used worldwide in liver MRI for focal liver lesion detection and characterization, assessment of post-treatment tumor response and for evaluation of diffuse liver disease. Advanced diffusion methods like intravoxel incoherent motion (IVIM) have the potential to improve DWI accuracy for diffuse liver diseases and focal liver lesion assessment, but to date, the IVIM approach still belongs in the research field.

IVIM APPROACH

The IVIM approach is an advanced DWI technique initially described by Le Bihan et al. who showed that the signal intensity decay versus b-value has more than one exponential component, being mostly influenced by microcirculation at low b-values (100-150 s/mm^2) and by true extra- and intracellular diffusion at high b-values [3]. The IVIM approach assumes that the signal decrease is bi-exponential, with a fast component of the diffusion linked to the perfusion effect, called pseudo-diffusion, and a slow component linked to the water diffusion or true diffusion. A bi-exponential function is used to fit the signal intensity decay (Figure 1), as described in the following equation:

$$S_b = S0\,[(1-f)\,e^{-b\,D} + f\,e^{-b\,D^*}]$$

where $S0$ and S_b represent the signal intensity at baseline (b=0 s/mm^2) and at a specified b-value, f the perfusion fraction, D the tissue diffusion coefficient, and D^* the pseudo-diffusion coefficient. In this approach, the acquisition of multiple b-values is performed in order to accurately sample the signal decrease with the increase of the b-values.

1. Le Bihan D. Molecular diffusion nuclear magnetic resonance imaging. Magn Reson Q. 1991;7(1):1–30.
2. Bammer R. Basic principles of diffusion-weighted imaging. Eur J Radiol. 2003;45(3):169–184.
3. Le Bihan D, Breton E, Lallemand D, Aubin ML, Vignaud J, Laval-Jeantet M. Separation of diffusion and perfusion in intravoxel incoherent motion MR imaging. Radiology. 1988;168(2):497–505.
4. Dyvorne H, Jajamovich G, Kakite S, Kuehn B, Taouli B. Intravoxel incoherent motion diffusion imaging of the liver: optimal b-value subsampling and impact on parameter precision and reproducibility. Eur J Radiol. 2014;83(12):2109–2113.
5. Leporq B, Saint-Jalmes H, Rabrait C, et al. Optimization of intra-voxel incoherent motion imaging at 3.0 Tesla for fast liver examination. J Magn Reson Imaging JMRI. 2015;41(5):1209–1217.
6. Jerome NP, Orton MR, d' Arcy JA, Collins DJ, Koh D-M, Leach MO. Comparison of free-breathing with navigator-controlled acquisition regimes in abdominal diffusion-weighted magnetic resonance images: Effect on ADC and IVIM statistics. J Magn Reson Imaging JMRI. 2014;39(1):235–240.
7. Lee Y, Lee SS, Kim N, et al. Intravoxel incoherent motion diffusion-weighted MR imaging of the liver: effect of triggering methods on regional variability and measurement repeatability of quantitative parameters. Radiology. 2015;274(2):405–415.
8. Jajamovich GH, Dyvorne H, Donnerhack C, Taouli B. Quantitative liver MRI combining phase contrast imaging, elastography, and DWI: assessment of reproducibility and postprandial effect at 3.0 T. PloS One. 2014;9(5):e97355.
9. Barbieri S, Donati OF, Froehlich JM, Thoeny HC. Comparison of Intravoxel Incoherent Motion Parameters across MR Imagers and Field Strengths: Evaluation in Upper Abdominal Organs. Radiology. 2016;279(3):784–794.

IVIM acquisition parameters:

The typical and most widely used protocol involved fat-saturated single shot echo planar (EPI) diffusion-weighted imaging sequence. Currently, there is no consensus on the number of b-values to use for liver application, and published studies have used distributions of 5 to 16 b-values that sample both perfusion and diffusion regimes. An increased number of b-values may allow a better sampling of the signal intensity decrease, but this involves a longer scan time; its use is therefore limited. Recently, Dyvorne et al. showed that an optimized distribution with 4 b-values yields parameter deviations within the test-retest reproducibility of a 16 b-values acquisition, while reducing scan time by up to 75% compared to 16 b-values [4]. Leporq et al. also found that the acquisition of 4 b-values is sufficient to determine the IVIM parameters [5].

As any DWI acquisition, either breath hold, free breathing, respiratory triggering, or cardiac triggering techniques may be used. Breath hold technique allows the shortest acquisition time but limits the number of acquired b-values and is therefore not performed for IVIM acquisition. Furthermore, compared to free breathing technique, it is unclear if there is an advantage to respiratory triggering. When comparing respiratory triggering and free breathing, the triggering offers no advantage in fitted diffusion parameters with greater confidence and few outliers with free breathing and no improvement of the regional variability [6,7].

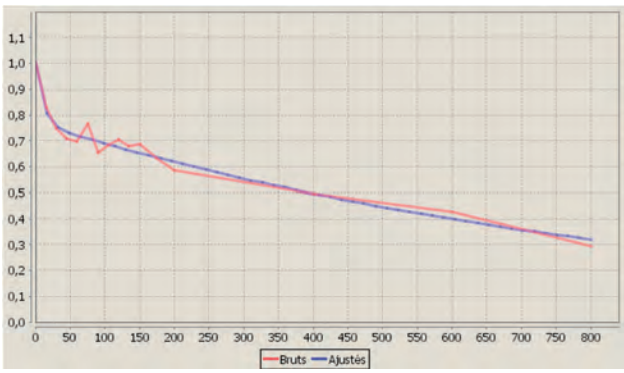

Figure 1: Example of bi-exponential fit

However, cardiac triggering can reduce cardiac motion artifacts, cardiac motion-induced errors in the measurements and therefore reduce the variability between right and left lobes values [7]. Finally, IVIM acquisition does not need to be performed in a controlled fasting state. Indeed, liver D, D*, f and apparent diffusion coefficient (ADC) do not significantly change after caloric intake [8].

Reproducibility:

The main drawback of the IVIM approach is its low reproducibility. Indeed, the reproducibility of the IVIM parameters, especially in the left lobe, is quite low, with a coefficients of variation (CV) around 20% within subject; with large 95% Bland and Altman limits of agreement [9]. In the liver parenchyma, a higher reproducibility for D (CV ‹10-20%), compared to f (CV›15%) and D* (CV › 20-30%) within subject, between sequences and between platforms has been reported [4,9–14].

> “Reproducibility of IVIM parameters and ADC has been reported generally better in liver parenchyma compared to focal liver lesion”

In abdominal lesions, few studies have reported the reproducibility of IVIM parameters and have found that D seems to be the most reproducible parameter with variability around 20% [12,13,15].

The variability of perfusion-related IVIM parameters is much higher, with reported values of coefficient of repeatability as high as 158% for f and 1104% for D* in liver metastasis [12] and of coefficient of variation as high as 37% for f and 61% for D* in hepatocellular carcinoma (HCC) [13]. Reproducibility of IVIM parameters and ADC has been reported generally better in liver parenchyma compared to focal liver lesion [12,13].

10. Dyvorne HA, Galea N, Nevers T, et al. Diffusion-weighted imaging of the liver with multiple b values: effect of diffusion gradient polarity and breathing acquisition on image quality and intravoxel incoherent motion parameters--a pilot study. Radiology. 2013;266(3):920–929.
11. Patel J, Sigmund EE, Rusinek H, Oei M, Babb JS, Taouli B. Diagnosis of cirrhosis with intravoxel incoherent motion diffusion MRI and dynamic contrast-enhanced MRI alone and in combination: preliminary experience. J Magn Reson Imaging JMRI. 2010;31(3):589–600.
12. Andreou A, Koh DM, Collins DJ, et al. Measurement reproducibility of perfusion fraction and pseudodiffusion coefficient derived by intravoxel incoherent motion diffusion-weighted MR imaging in normal liver and metastases. Eur Radiol. 2013;23(2):428–434.
13. Kakite S, Dyvorne H, Besa C, et al. Hepatocellular carcinoma: short-term reproducibility of apparent diffusion coefficient and intravoxel incoherent motion parameters at 3.0T. J Magn Reson Imaging JMRI. 2015;41(1):149–156.
14. Cui Y, Dyvorne H, Besa C, Cooper N, Taouli B. IVIM Diffusion-weighted Imaging of the Liver at 3.0T: Comparison with 1.5T. Eur J Radiol Open. 2015;2:123–128.
15. Koh D-M, Blackledge M, Collins DJ, et al. Reproducibility and changes in the apparent diffusion coefficients of solid tumours treated with combretastatin A4 phosphate and bevacizumab in a two-centre phase I clinical trial. Eur Radiol. 2009;19(11):2728–2738.
16. Yoon JH, Lee JM, Baek JH, et al. Evaluation of hepatic fibrosis using intravoxel incoherent motion in diffusion-weighted liver MRI. J Comput Assist Tomogr. 2014;38(1):110–116.
17. Moteki T, Horikoshi H. Evaluation of hepatic lesions and hepatic parenchyma using diffusion-weighted echo-planar MR with three values of gradient b-factor. J Magn Reson Imaging. 2006;24(3):637–645.
18. Luciani A, Vignaud A, Cavet M, et al. Liver cirrhosis: intravoxel incoherent motion MR imaging--pilot study.

IVIM AND DIFFUSE LIVER DISEASE

IVIM and fibrosis:

As some studies have shown that liver fibrosis is associated with progressive restriction of diffusion motion and decreased ADC (computed with the mono-exponential approach), the IVIM method was also evaluated in liver fibrosis in order to assess if the decrease of the ADC is linked to the increase in connective tissue or to the decreased perfusion associated with liver fibrosis. Results are unclear. Some studies have reported that D, D*, f, and ADC values were reduced as liver fibrosis increased [11,16], while others have reported no difference in the D value in hepatic fibrosis [17–19]. Moreover, negative correlations between liver fibrosis stage (METAVIR score) and perfusion related parameters (D* and f) and between liver fibrosis stage and ADC have been found, while the correlation with D remains uncertain [19,20].

Compared to the mono-exponential approach, the IVIM approach has been found to be more accurate for the evaluation of fibrosis stages, with either greater correlation for D* or higher area under the curve of the association of the IVIM parameters than of the ADC [19,20]. The decrease of D* is expected as the liver perfusion is reduced in liver fibrosis (decrease of the portal flow, not compensated by the increase of the arterial flow). Indeed, D* in the liver is influenced by perfusion changes related to portal venous flow [3,21,22]. The decreases of f and D could be explained by the increased proportion of extracellular matrix (collagen), which reduces the volume of hepatic sinusoid and free extracellular space. Overall, the reduced ADC associated with advanced fibrosis/cirrhosis seems reflecting decreased liver perfusion and possibly some restricted molecular diffusion in the liver parenchyma. However, even if the IVIM approach is more accurate than ADC for liver fibrosis staging, it has lower discriminative capacity than liver stiffness determined by magnetic resonance elastography [19].

IVIM and steatosis:

The effect of fat on liver DWI is a subject of debate. Some studies have suggested that ADC decreased significantly in patients with hepatic steatosis [23,24]. Similarly, some studies have found that D and D* decreased in cases of steatosis while f increased [25,26]. However, Lee et al. concluded that hepatic steatosis does not affect measurement of perfusion or diffusion and therefore is unlikely a confounding factor for the use of diffusion to evaluate liver fibrosis [27].

More recently, Joo et al. have shown in an animal model that the IVIM approach could be relevant to the differentiation of non-alcoholic fatty liver disease (NAFLD) and non-alcoholic steatohepatitis (NASH). Indeed, they found that ADC, D, and D* were not significantly different between the NAFLD and NASH groups, but f was significantly different [28]. In a cohort of type 2 diabetic patients, Parente et al. found that D and the D* were significantly lower in patients with steatohepatitis, and that f was also lower in patients with steatohepatitis, but did not reach statistical significance [29].

Overall, the IVIM approach is almost entirely absent from steatosis assessment, because of the existence of other accurate MRI tools (MR spectroscopy, proton density fat fraction (PDFF), ...) [30], but in the future, the IVIM approach might be a useful non-invasive tool for the diagnosis of the severity of fatty liver disease, which is still an unsolved clinical question.

Radiology. 2008;249(3):891–899.
19. Ichikawa S, Motosugi U, Morisaka H, et al. MRI-based staging of hepatic fibrosis: Comparison of intravoxel incoherent motion diffusion-weighted imaging with magnetic resonance elastography. J Magn Reson Imaging JMRI. 2015;42(1):204–210.
20. Hu G, Chan Q, Quan X, et al. Intravoxel incoherent motion MRI evaluation for the staging of liver fibrosis in a rat model. J Magn Reson Imaging JMRI. 2015;42(2):331–339.
21. Regini F, Colagrande S, Mazzoni LN, et al. Assessment of Liver Perfusion by IntraVoxel Incoherent Motion (IVIM) Magnetic Resonance-Diffusion-Weighted Imaging: Correlation With Phase-Contrast Portal Venous Flow Measurements. J Comput Assist Tomogr. 2015;39(3):365–372.
22. Lee JH, Cheong H, Lee SS, et al. Perfusion Assessment Using Intravoxel Incoherent Motion-Based Analysis of Diffusion-Weighted Magnetic Resonance Imaging: Validation Through Phantom Experiments. Invest Radiol. 2016;51(8):520–528.
23. Poyraz AK, Onur MR, Kocakoç E, O□ur E. Diffusion-weighted MRI of fatty liver. J Magn Reson Imaging JMRI. 2012;35(5):1108–1111.
24. Anderson SW, Soto JA, Milch HN, et al. Effect of disease progression on liver apparent diffusion coefficient values in a murine model of NASH at 11.7 Tesla MRI. J Magn Reson Imaging JMRI. 2011;33(4):882–888.
25. Guiu B, Petit J-M, Capitan V, et al. Intravoxel incoherent motion diffusion-weighted imaging in nonalcoholic fatty liver disease: a 3.0-T MR study. Radiology. 2012;265(1):96–103.
26. Dijkstra H, Handayani A, Kappert P, Oudkerk M, Sijens PE. Clinical implications of non-steatotic hepatic fat fractions on quantitative diffusion-weighted imaging of the liver. PloS One. 2014;9(2):e87926.
27. Lee JT, Liau J, Murphy P, Schroeder ME, Sirlin CB, Bydder M. Cross-sectional investigation of correlation between hepatic steatosis and IVIM perfusion on MR imaging. Magn Reson Imaging. 2012;30(4):572–578.

IVIM and liver function:

Zhang et al. recently showed that IVIM may be a useful image-based method for assessing liver function. They found that D* and f values significantly decreased with increasing Child–Pugh scores and that Child–Pugh scores were inversely correlated with D* and f values (r = -0.423, r = -0.620, respectively) [31]. Those results need to be confirmed and compared to other non-invasive biomarkers of liver function.

IVIM AND FOCAL LIVER LESIONS

Focal liver lesions characterization:

The IVIM approach has been evaluated for liver lesion characterization, with variable results, but there was a significant overlap in IVIM parameters values of benign and malignant lesions. As with ADC, D has been found to be significantly higher in benign lesions compared to malignant lesions [32–37].

The performance of D compared to ADC is variable, either lower, similar or higher [32–34,37].The role of perfusion-related IVIM parameters, f and D*, for differentiating benign and malignant lesions is controversial, in that it was found not to be significantly different between benign and malignant lesions in Doblas et al., while a higher f was found in malignant lesion in Yamada et al. [33,35]. However, perfusion-related IVIM parameters have been shown to be able to separate hypervascular and hypovascular lesions, with higher f and D* in hypervascular lesions compared to hypovascular lesions [32].

Moreover, the IVIM approach has been shown to be useful for the differentiation between viable tumor tissue and intratumoral necrotic and fibrotic zones in focal liver lesions [38].

Hepatocellular carcinoma (HCC):

In HCC, a correlation between D and histologic grade has been found with a higher area under the ROC curve value for D than for ADC for differentiating high-grade HCC from low-grade HCC [39]. Kakite et al. found a significant negative/positive correlation between D/f and enhancement ratio and a significant positive/negative correlation between D/f and tumor necrosis [40]. Beyond those results, the role of IVIM parameters is controversial in HCC treated by Sorafenib: Lewin et al. found that f significantly increased in responder patients and decreased in non-responder patients while Shirota et al. found that D at baseline may be a useful parameter for predicting the therapeutic outcome of Sorafenib for advanced HCC [41,42].

Yang at al. in an animal study have shown that D was higher and increased in the treated group while f decreased initially and increased secondly in this group [43].

Overall, the IVIM approach may provide useful biomarkers for evaluating the therapeutic effects of Sorafenib on HCC but its place is still unclear.

Liver metastases:

In treated colorectal liver metastases, Chiaradia et al. have shown that both D (r=0.36, p=0.035) and ADC (r=0.4, p=0.02) correlated significantly with the degree of tumor necrosis while D* and f did not [44] (Figure 2).

Similarly, ADC and D measured in the periphery area of the lesion have been shown to be higher in colorectal liver metastases with major pathological response [45]. Comparing responder and non responder, variation of IVIM parameters have been variable among the studies [46,47]. In breast liver metastases treated by radio-embolization, early change (4-6 weeks) of f has been showed to be predictive of patient outcome [48].

28. Joo I, Lee JM, Yoon JH, Jang JJ, Han JK, Choi BI. Nonalcoholic fatty liver disease: intravoxel incoherent motion diffusion-weighted MR imaging-an experimental study in a rabbit model. Radiology. 2014;270(1):131–140.
29. Parente DB, Paiva FF, Oliveira Neto JA, et al. Intravoxel Incoherent Motion Diffusion Weighted MR Imaging at 3.0 T: Assessment of Steatohepatitis and Fibrosis Compared with Liver Biopsy in Type 2 Diabetic Patients. PloS One. 2015;10(5):e0125653.
30. Reeder SB, Sirlin CB. Quantification of liver fat with magnetic resonance imaging. Magn Reson Imaging Clin N Am. 2010;18(3):337–357, ix.
31. Zhang J, Guo Y, Tan X, et al. MRI-based estimation of liver function by intravoxel incoherent motion diffusion-weighted imaging. Magn Reson Imaging. 2016;34(8):1220–1225.
32. Yoon JH, Lee JM, Yu MH, Kiefer B, Han JK, Choi BI. Evaluation of hepatic focal lesions using diffusion-weighted MR imaging: comparison of apparent diffusion coefficient and intravoxel incoherent motion-derived parameters. J Magn Reson Imaging JMRI. 2014;39(2):276–285.
33. Doblas S, Wagner M, Leitao HS, et al. Determination of malignancy and characterization of hepatic tumor type with diffusion-weighted magnetic resonance imaging: comparison of apparent diffusion coefficient and intravoxel incoherent motion-derived measurements. Invest Radiol. 2013;48(10):722–728.
34. Watanabe H, Kanematsu M, Goshima S, et al. Characterizing focal hepatic lesions by free-breathing intravoxel incoherent motion MRI at 3.0 T. Acta Radiol Stockh Swed 1987. 2014;55(10):1166–1173.
35. Yamada I, Aung W, Himeno Y, Nakagawa T, Shibuya H. Diffusion coefficients in abdominal organs and hepatic lesions: evaluation with intravoxel incoherent motion echo-planar MR imaging. Radiology. 1999;210(3):617–623.
36. Coenegrachts K, Delanote J, Ter Beek L, et al. Evaluation of true diffusion, perfusion factor, and

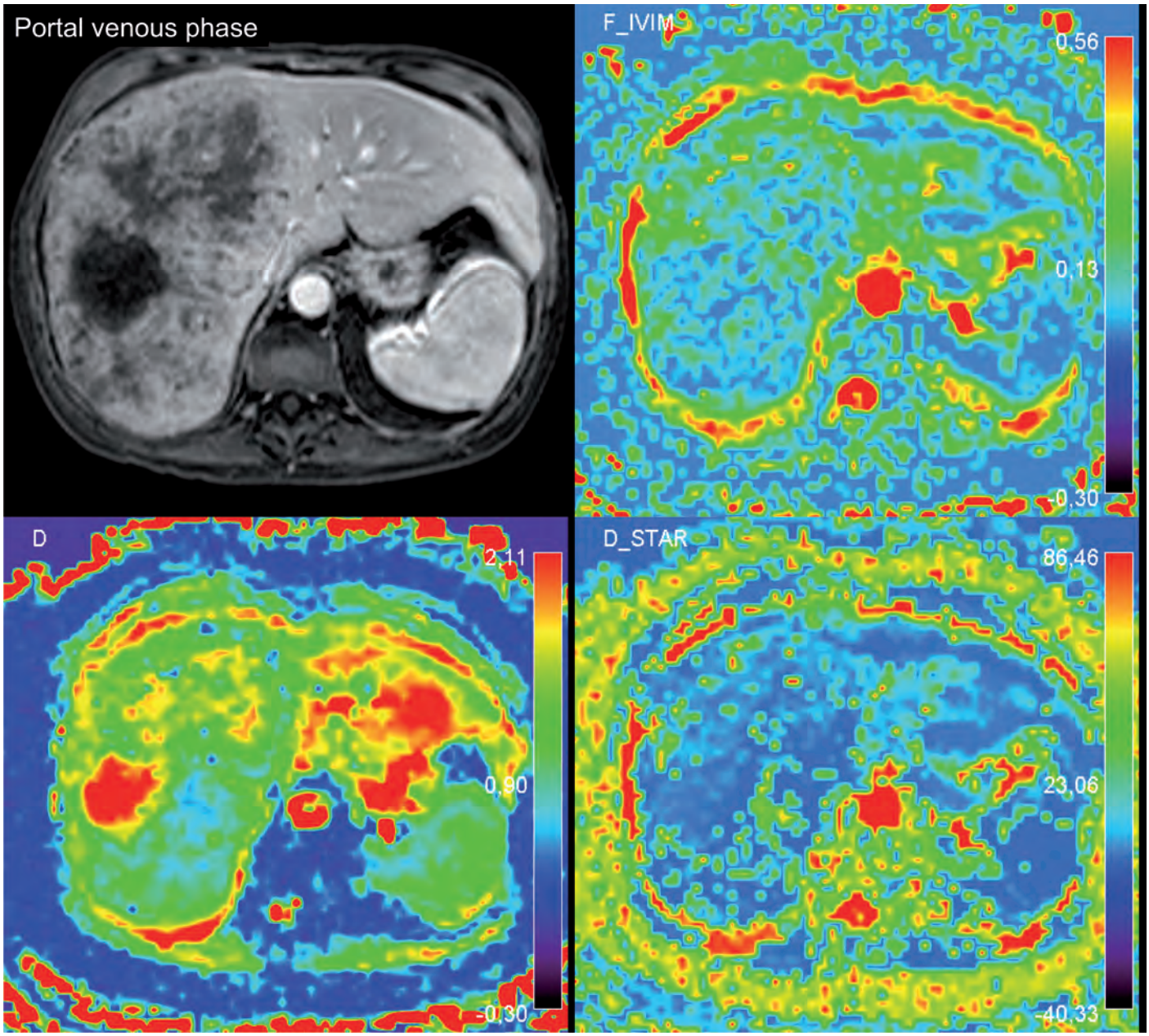

Figure 2: Example of colorectal liver metastasis, in a 60 yo male patient. The D map shows the lesion heterogeneity, while the D* and F maps do not

apparent diffusion coefficient in non-necrotic liver metastases and uncomplicated liver hemangiomas using black-blood echo planar imaging. Eur J Radiol. 2009;69(1):131–138.
37. Zhu L, Cheng Q, Luo W, Bao L, Guo G. A comparative study of apparent diffusion coefficient and intravoxel incoherent motion-derived parameters for the characterization of common solid hepatic tumors. Acta Radiol Stockh Swed 1987. 2015;56(12):1411–1418.
38. Wagner M, Doblas S, Daire J-L, et al. Diffusion-weighted MR imaging for the regional characterization of liver tumors. Radiology. 2012;264(2):464–472.
39. Woo S, Lee JM, Yoon JH, Joo I, Han JK, Choi BI. Intravoxel incoherent motion diffusion-weighted MR imaging of hepatocellular carcinoma: correlation with enhancement degree and histologic grade. Radiology. 2014;270(3):758–767.
40. Kakite S, Dyvorne HA, Lee KM, Jajamovich GH, Knight-Greenfield A, Taouli B. Hepatocellular carcinoma: IVIM diffusion quantification for prediction of tumor necrosis compared to enhancement ratios. Eur J Radiol Open. 2016;3:1–7.
41. Lewin M, Fartoux L, Vignaud A, Arrivé L, Menu Y, Rosmorduc O. The diffusion-weighted imaging perfusion fraction f is a potential marker of sorafenib treatment in advanced hepatocellular carcinoma: a pilot study. Eur Radiol. 2011;21(2):281–290.
42. Shirota N, Saito K, Sugimoto K, Takara K, Moriyasu F, Tokuuye K. Intravoxel incoherent motion MRI as a biomarker of sorafenib treatment for advanced hepatocellular carcinoma: a pilot study. Cancer Imaging. 2016 Jan 29;16:1.
43. Yang S-H, Lin J, Lu F, et al. Evaluation of antiangiogenic and antiproliferative effects of sorafenib by sequential histology and intravoxel incoherent motion diffusion-weighted imaging in an orthotopic hepatocellular carcinoma xenograft model. J Magn Reson Imaging JMRI. 2016 Jun 14.

ROLE OF CALCULATED B-VALUE

Computed DWI MR imaging is a mathematical technique which computes any b-value image (usually a high b-value) from diffusion-weighted images obtained with at least 2 different b-values [49]. A mono-exponential or bi-exponential approach can be used, based on the number of the acquired b-values.

> “computed b-value images (...) improved visualization of small hepatic metastases”

Obtaining high b-value images in the liver is challenging because of the T2 of the liver and poor signal to noise ratio (SNR), but also because of higher distortion with high b-values. As calculated DWI MR images are simulated, they are less affected by poor SNR and image distortion that degrade acquired images and they allow a suppression of the background signal while maintaining the original lesion signal. In a preliminary study, Blackhedge et al. have shown that computed b-value images are possible in the liver and that the technique also improved visualization of small hepatic metastases [49].

CONCLUSION

IVIM approach has been shown to be useful for the evaluation of liver fibrosis and focal hepatic lesions and may be useful for the evaluation of non-alcoholic fatty liver disease and liver function. However, despite all the promising results, this technique still belongs in the research field. Indeed, its low reproducibility currently prevents it from being a valid, unbiased and reliable clinical tool. In the future, technical improvement, standardization and consensus on an optimal protocol could allow its wide scale use.

Mathilde Wagner MD, PhD
Associate Professor,
Radiology Department,
Pitié-Salpêtrière Hospital,
Paris, France

44. Chiaradia M, Baranes L, Van Nhieu JT, et al. Intravoxel incoherent motion (IVIM) MR imaging of colorectal liver metastases: are we only looking at tumor necrosis? J Magn Reson Imaging JMRI. 2014;39(2):317–325.
45. Wagner M, Ronot M, Doblas S, et al. Assessment of the residual tumour of colorectal liver metastases after chemotherapy: diffusion-weighted MR magnetic resonance imaging in the peripheral and entire tumour. Eur Radiol. 2016;26(1):206–215.
46. Kim JH, Joo I, Kim T-Y, et al. Diffusion-Related MRI Parameters for Assessing Early Treatment Response of Liver Metastases to Cytotoxic Therapy in Colorectal Cancer. AJR Am J Roentgenol. 2016;207(3):W26–32.
47. Granata V, Fusco R, Catalano O, et al. Early Assessment of Colorectal Cancer Patients with Liver Metastases Treated with Antiangiogenic Drugs: The Role of Intravoxel Incoherent Motion in Diffusion-Weighted Imaging. PloS One. 2015;10(11):e0142876.
48. Pieper CC, Meyer C, Sprinkart AM, et al. The value of intravoxel incoherent motion model-based diffusion-weighted imaging for outcome prediction in resin-based radioembolization of breast cancer liver metastases. OncoTargets Ther. 2016;9:4089–4098.
49. Blackledge MD, Leach MO, Collins DJ, Koh D-M. Computed diffusion-weighted MR imaging may improve tumor detection. Radiology. 2011;261(2):573–581.

IVIM in Liver

Mathilde Wagner MD, PhD
Associate Professor, Radiology Department, Pitié-Salpêtrière Hospital, Paris, France

The following case report illustrates an application of IVIM in liver metastases.

Patient history:

A 69-year-old male patient with a metastatic pancreatic cancer was included in a phase 1 study. A MRI was performed before and after treatment, including diffusion-weighted imaging with 6 b-values (0, 50, 200, 400, 600 and 800 s/mm^2).

MRI before treatment

The MRI exam showed multiple liver metastases. The addition of functional imaging allowed for the highlighting of the heterogeneity of the disease, as shown in Figure 1.

MRI after treatment

The metastases were stable after treatment according to RECIST 1.1 criteria (97+90=187 mm vs. 89+84=173 mm, +8%). However, the analysis of the IVIM data showed that ADC and D increased and D* and f decreased (Table 1 and Figure 2).

Those results suggested that both the cellularity and the perfusion decreased after treatment, which may reflect a response to treatment.

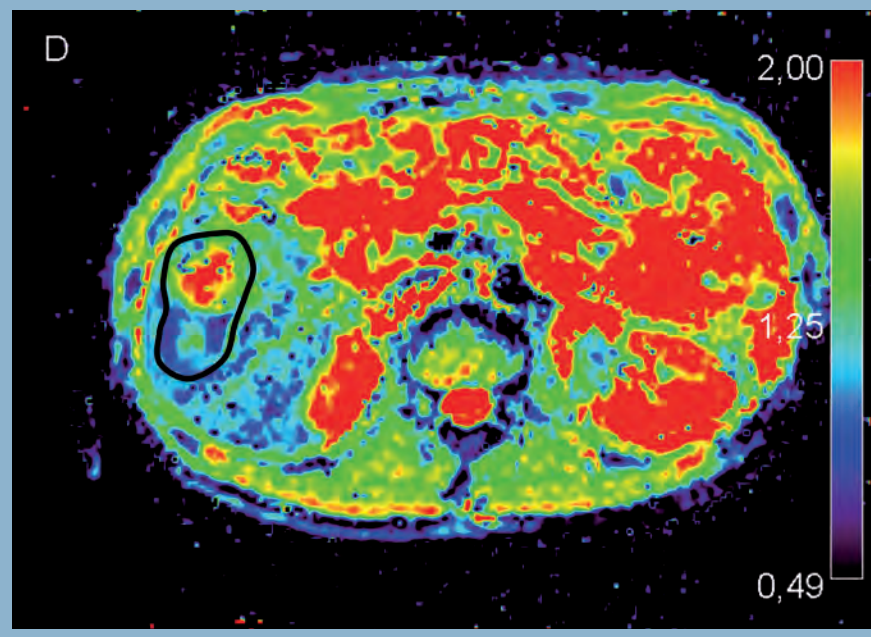

Figure 1: D map of a liver metastasis in segment 5, with 2 components: the posterior component, which was less necrotic and more cellular than the anterior one.

Table 1: ADC and IVIM parameters of the 2 target lesions.

	26/09	17/10
Lesion 1		
ADC	1,81	2,15
D	1,57	1,96
D*	9,01	6,65
f	0,1	0,07
Lesion 2		
ADC	1,73	1,84
D	1,37	1,54
D*	17,94	6,56
f	0,2	0,14

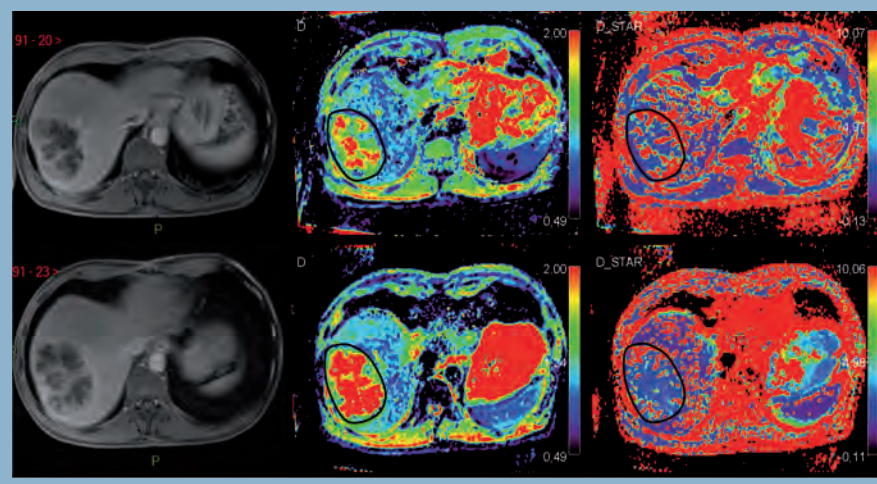

Figure 2: T1-weighted post-contrast imaging (left column), D map (middle column) and D* map (right column) before (upper row) and after treatment (lower row). The size of the lesion was stable while the IVIM parameters changed after treatment suggesting a response to treatment.

IVIM for Head & Neck application

Jan W. Casselman, MD
Chair of the Department of Radiology
at A.Z. Sint-Jan Hospital in Bruges, Belgium

Once a week, he is a Head and Neck "consultant radiologist" at the A.Z. Sint Augustinus Hospital in Antwerp and further has Academic teaching activities at the University of Ghent. His main field of interest is Neuroradiology and Head & Neck Radiology which explains why he spends most of his time on MR.

Olea Imagein: Could you simply explain what IVIM is?

Jan Casselman: Routine DW-MRI measures motion of water protons and in tissues this motion will be modified by their interactions with macromolecules and cell membranes. Hence, cellularity, integrity of the cell membranes, tortuosity of the extracellular space and viscosity of fluids will alter the apparent diffusion. This apparent diffusion can be quantified using a simple mono-exponentional apparent diffusion coefficient (ADC) evaluation for which only two b-values are needed, routinely b-0 and b-1000.

However, at low b-values below 100-200 s/mm^2 the measured signal attenuation in well perfused tissue arises not only from water diffusion in tissues (water diffusivity) but also from microcirculation within the normal capillary network (tissue perfusion). When several low b-values below 200 s/mm^2 are used a more complex bi-exponentional function is used to describe the DW-MRI data and allows calculation of

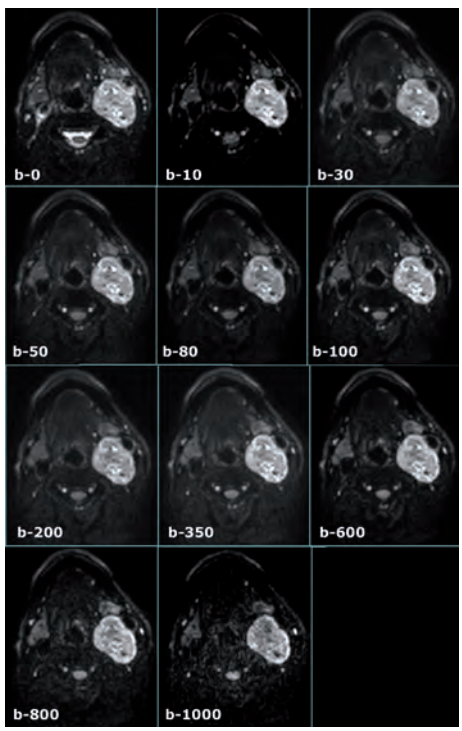

Figure 1: DWI acquisition with 6 b-values (b0,50, 100, 500, 750, 1000)

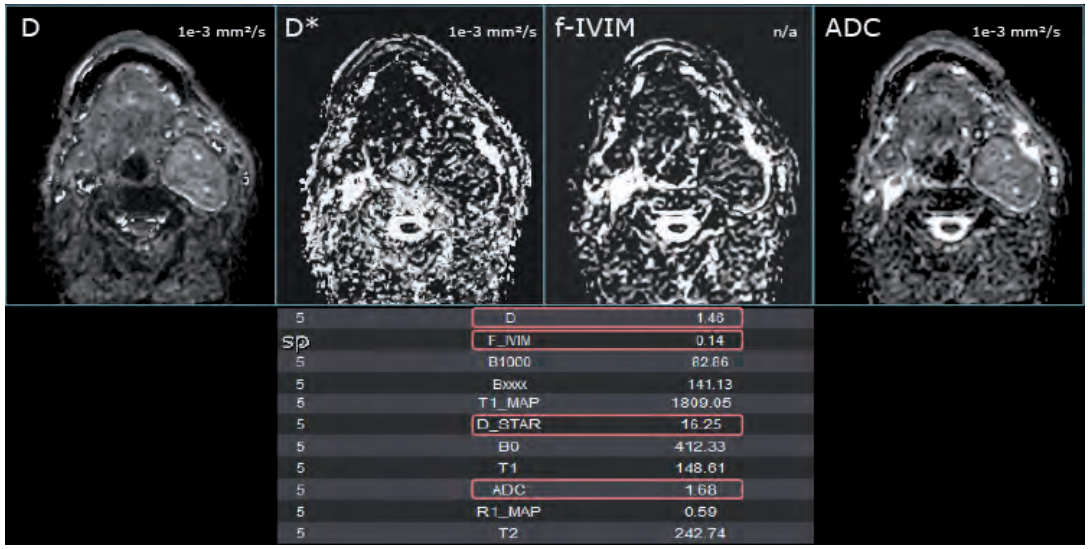

Figure 2: IVIM maps (D, D* and f) computed using the 6 b-values

the water diffusivity (D or diffusion coefficient), microcapillary perfusion (D* or pseudo-diffusion coefficient, which depends on the vascular architecture and velocity of the flowing blood – correlates with relative blood flow) and the perfusion fraction (f, which correlates with relative blood volume). This principle of taking into account both tissue diffusivity and tissue microcapillary perfusion within imaging voxels was called Intravoxel Incoherent Motion (IVIM) by Le Bihan.

> “Therefore a single technique “IVIM” provides both information about Brownian water molecular diffusion and blood perfusion.”

Therefore a single technique “IVIM” provides both information about Brownian water molecular diffusion and blood perfusion.

O.I: Do you use it in clinical routine or only in research?

J.C: We started to use it in research, more specifically in the evaluation of all head and neck tumors. However, as the first data became available on the use of IVIM in the head and neck region we also started to use it in clinical routine. Today a PubMed search on “IVIM head and neck” results in 19 publications but many new studies are on the way of which the preliminary results have been shown at meetings.

O.I: In your opinion, what are the main clinical interests of this technique?

J.C: The potential of IVIM is huge. First, it can be used to characterize tumors and studies showed for instance that Warthin tumors, pleomorphic adenomas and malignant tumors of the salivary glands can be distinguished by looking at the relation of the D, D* and f values. The same biomarkers can be used to try to differentiate malignant from benign lesions. Secondly, IVIM can be used for therapy monitoring. Treatment response to chemoradiation and prediction of treatment outcome are two of the main areas of interest but the technique can also be used to evaluate radiation induced changes in the treated organs as well. The fact that D* and f are related to the vascular architecture, velocity of the flow and relative blood flow and volume explains that one can start to predict if the treatment will easily reach the tumor or not.

O.I: How are our solutions embedded in your daily routine?

J.C: Today standard vendor software doesn’t allow to perform these more complicated bi-exponential analyses. It is clear that we would not have access to these new IVIM applications if we wouldn’t have the Olea Sphere® software. The workflow was also tailored to our specific needs, reducing the “interaction time” during the calculation to a minimum. This is crucial as long as procedures and calculation times would hinder routine use of the IVIM technique.

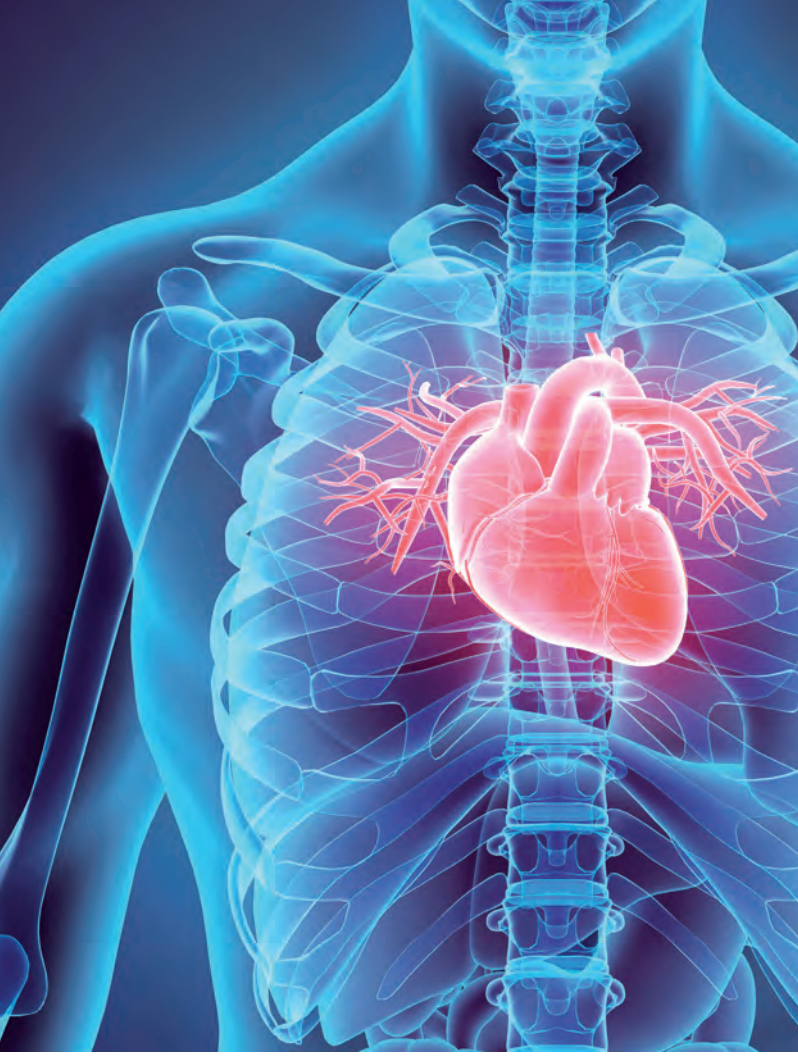

IVIM in the Human Heart:
A promising approach

Pierre Croisille, MD
Timothé Boutelier, PhD
Kévin Moulin
Magalie Viallon, PhD

CARDIOVASCULAR DISEASES ARE A GLOBAL CONCERN

In 2008, the leading causes of non-communicable disease (NCD) deaths were: cardiovascular diseases (17 million deaths, or 48% of NCD deaths); cancers (7.6 million, or 21% of NCD deaths); and respiratory diseases (4.2 million), including asthma and chronic obstructive pulmonary disease (COPD), and in 2020, they will become the first cause of death in the world burdens. Behavioral risk factors, including tobacco use, physical inactivity, and unhealthy diet, are responsible for about 80% of coronary heart disease and cerebrovascular disease [Global status report NCD WHO (2010)].

Cardiac Magnetic Resonance (CMR) imaging has greatly expanded with a broader availability of routine clinical MR equipment, to explore and help in the management of cardiac disease. It provides gold-standard regional and global function quantification as well as advanced tissue characterization (scar/fibrosis imaging), is 100% radiation-free and less expensive than alternative approaches, but like most modalities except PET imaging fails to provide quantitative perfusion measurements.

Macrocirculation (coronary arteries) and microcirculation perfusion abnormalities are met in most if not all cardiac diseases, from metabolic heart disease to diabetes, in systemic hypertension, coronary heart disease to heart failure. Both are accompanied by alterations in basal conditions and/or during maximal load conditions (effort), that require quantification of local perfusion in absolute units (ml/g/min), both at rest and stress with the resulting absolute perfusion reserve measurement. It is essential to develop tools allowing accurate quantification of these parameters for accurate diagnosis without ambiguous scenarios and for optimal treatment decisions, as well as during the patient follow-up during and/or after treatment.

In vivo cardiac Intravoxel Incoherent Motion (IVIM) imaging, as an all-in-one method, both sensitive to the diffusion (at b-values > 200 s/mm^2) and perfusion (at low b-values < 50 s/mm^2) and intrinsically quantitative in contrast, is of particular interest as a promising alternative to map myocardial perfusion without the need for contrast agent administration [1]. Indeed, the IVIM model is more complex than when considering pure diffusion only, but is able to separate the diffusion compartment from the micro capillaries' blood flow [2]. On the other side, the quantification of inflammatory (edema) or infiltrative (fibrosis) processes is a main interest in cardiology sciences, motivating recent

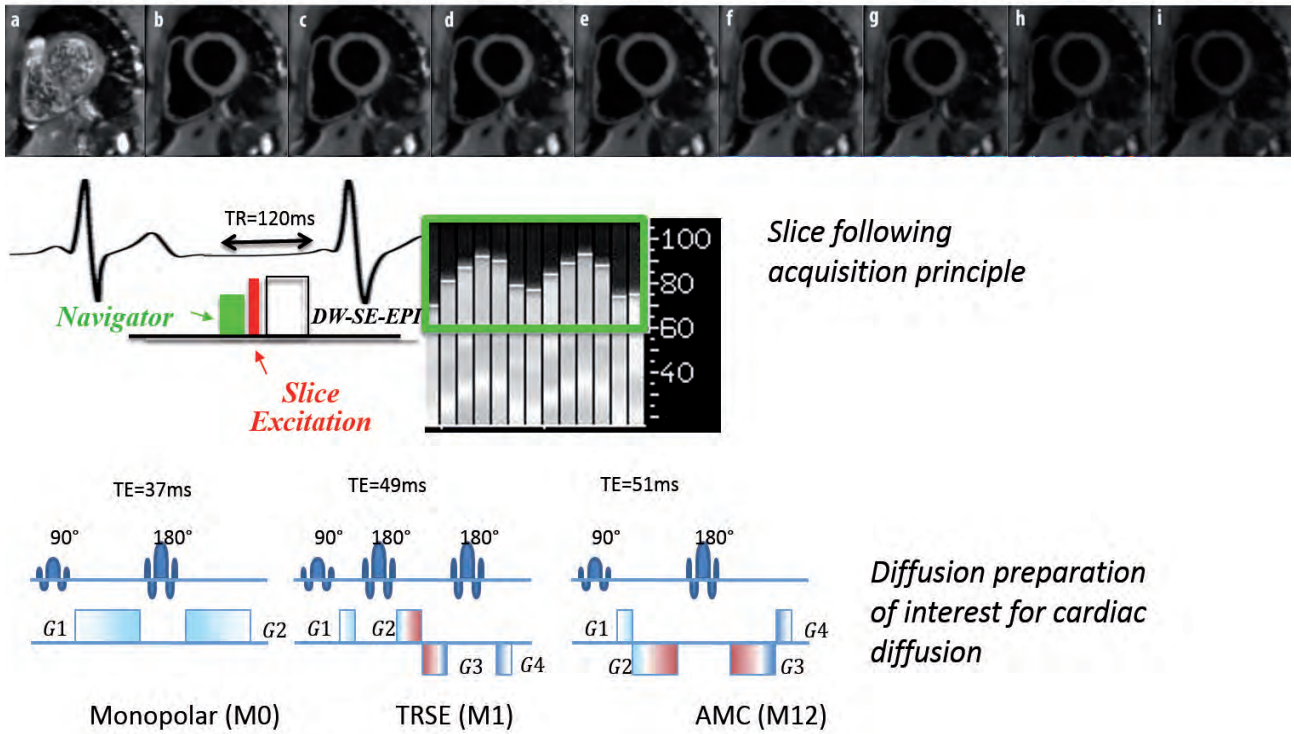

Figure 1: Diffusion weighted images and the sequence diagram of dedicated slice-following DW-SE-EPI acquisition for cardiac diffusion.

developments of quantitative methods such as T1 mapping [3] and T2 mapping. Like in the brain, diffusion is expected to be a crucial indicator and a key differentiator of paramount importance for patient management. The motivation is therefore high to explore the potential of IVIM biomarkers for cardiac disease investigations.

Nevertheless, Cardiac IVIM imaging is also particularly challenging due to cardiac and respiratory motion, but also low signal-to-noise ratio. This technique requires longer duration acquisitions, even more challenging in the context of fast motion, with multiple b-value diffusion-weighted (DW)-MRI to encompass the wide range of fast diffusion decay due to perfusion, and similarly, slow diffusion decay due to pure diffusion. Before considering the application of the IVIM approach in clinical scenarios at a given time-point to assess the integrity of healthy and diseased cardiac tissue (e.g. myocardial ischemia or infarction) or in the patient follow-up, one needs to address the challenge of acquiring diffusion data in a very mobile organ. First of all, the spin-echo (SE) based sequence originally proposed by Le Bihan needs several adaptations and improvements [4-7].

Our group has shown that it is possible to acquire DW and IVIM data in the heart using powerful acquisition strategies (real-time slice-followed SE-EPI navigator-based sequence) and a dedicated post-processing pipeline to achieve a good reproducibility in healthy volunteers [8-10]. Figure 1 shows IVIM diffusion weighted images and the sequence diagram of dedicated slice-following DW-SE-EPI acquisition for cardiac diffusion.

Currently, the post-processing involves several steps: denoising using principal component analysis (PCA), motion artefacts removal using temporal Maximum Intensity Projection (tMIP), fitting... The fitting of the data by the bi-exponential model is particularly challenging and prone to errors, strongly depending on the noise level and on the acquisition protocols (number of b-values). Bayesian estimation is of evident and particular interest to improve the accuracy and the precision (i.e. reduce significantly the intra-subject variation [11,12] of the quantification of the physiological indexes: f, the perfusion fraction, D the diffusion coefficient, and D*, the pseudo-diffusion coefficient [11,13,14].

Figure 2 shows the results obtained using a Bayesian approach [15,16] compared to a classical multiple parameters fitting approach: the Bayesian approach provides higher resolution maps due to its higher intrinsic robustness to lower signal to noise ratio.

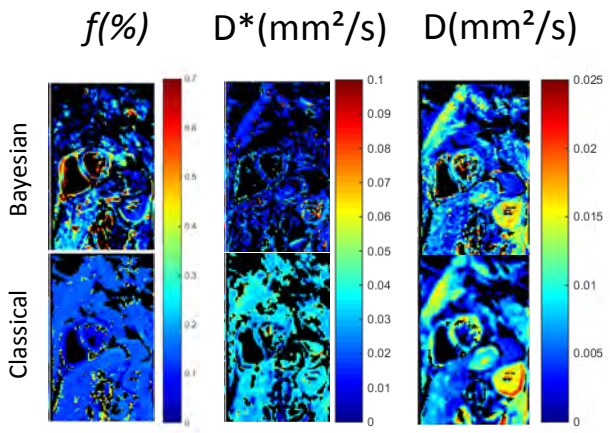

Figure 2: IVIM maps obtained using a Bayesian approach (first row) compared to a classical approach (second row), showing that the Bayesian approach provides higher resolution maps.

WHAT ABOUT DYNAMIC CONTRAST-ENHANCED IMAGING AS AN ALTERNATIVE METHOD FOR CMR PERFUSION QUANTIFICATION?

Attempts to quantify myocardial perfusion using cardiovascular magnetic resonance (CMR) were first proposed >20 years ago [17,18] and consisted in imaging in real time contrast kinetics signal changes of the MR signal during the first pass of a gadolinium-based paramagnetic contrast agent, injected intravenously.

Dynamic perfusion imaging combined with pharmacologic challenge is of major interest for the detection of myocardial ischemia in the context of coronary artery disease. The expected result is a precise localization of one or more ischemic areas, the measure of their extension and significance (severity), in order to identify and ultimately guide the decision to treat culprit vessels.

The images are acquired during free-breathing of the patient and registration of the dynamic images is needed first to facilitate state-of-the-art visual analysis of the signal by the radiologist or cardiologist. The radiologist is looking for a transient or a persistent hyposignal, namely a range of the myocardium in which the signal is enhanced to a lower extent, since a lesser amount of contrast medium reaches it during the first pass of the tracer. This hypoperfusion documents the hemodynamic impact of stenosis located further upstream in the vessels supplying the identified territory. The visual comparison with the images obtained at rest used by mimicking cardiac scintigraphy for evaluating the reversible or irreversible anomalies is now usefully replaced by the associated analysis of the perfusion images under stress with those of delayed enhancement. These latter allow real ischemic lesions to be revascularized (which will necessitate the absence of scarring range or an extension that goes beyond the scarred area) to be differentiated of a sequel hypoperfusion involvement within a scar range that will not require any treatment. Delayed enhancement methods focus on the tracer persisting in the myocardium approximately ten minutes after injection of the contrast agent [19,20]. Delayed enhancement reflects a relative excess of gadolinium in pathological tissues compared to healthy tissues where the agent has been eliminated and in necrotic regions that have not been reached by the agent. It is used to characterize and quantify the size of infarcted regions. In the case of the detection of myocardial ischemia, only the size and the localization of lesions are reported and will be decisive for therapeutic decision and for prognosis, not the precise value of the flow in the ischemia area.

Some help is further brought to the clinician by means of the online calculation of the parametric mapping of simple indices such as slopes (up-slope) in order to help the classification of affected sectors of the myocardium, and correct for coil sensitivity variations. This qualitative and semi- quantitative analysis comes in addition to the visualization of native images, which nevertheless still provides far more precise information about the localization and the extent of the lesion. Recent technology and software developments have led to significant improvements in image quality, and clinically available techniques now offer a satisfactory spatial coverage of all the myocardial segments under pharmacologic stress. Nevertheless, MR myocardial perfusion imaging sequences and analysis techniques are currently not answering all the clinical needs and cannot provide a robust quantification of blood delivery to the tissue yet, and therefore this is still an active area of research.

Indeed, quantification of blood flow by CMR remains challenging in many aspects. First of all, there is a wide range of sequence designs and parameters to consider when optimizing an acquisition protocol that directly

impact on the signal to tracer concentration conversion and thus the modeling. The interdependence of these parameters with patient geometry forces the user to make compromises and these technical issues result in patient-specific and sequence-design specific signal to concentration conversion, with various performance tradeoffs that are associated with the large variety of T1-weigthing acquisition schemes. Artifact mechanisms are also related to sequence design and parameters, and are numerous. Last but not least, if different analysis models of myocardial perfusion were described in the literature to quantify absolute myocardial blood flow (F or MBF) in ml/min/g, all are based on advanced "in-house" post-processing.

While imaging technologies are potentially offering quantitative measures, their true impact in clinical practice in cardiology is in fact limited to qualitative analysis only due to inappropriate image processing technology with prohibitive computing time and lack of integration in medical software. And this is really the strength of Olea Medical® to accompany the development of imaging technologies with advanced and integrated solutions, so that the newly and jointly developed technology ultimately aims at serving as objective image-guided clinical decision tools, with a true impact in cardiovascular patient management.

CONCLUSION

Bayesian fitting of IVIM model for multi-b DWI data is considered a promising approach to map myocardial perfusion fractions without the need for contrast agent administration. But, of course, further work is warranted to study the potential outcomes in clinical routine, notably the local perfusion changes during both rest and pharmacologically induced stress in ischemic patients, or large cohorts of patients with myocardial diseases.

Pierre Croisille, MD
Professor of Radiology; Chairman Department of Radiology at CHU Saint-Etienne; Deputy Director of CREATIS Medical Imaging Research Center, Lyon, France

Timothé Boutelier, PhD
Research & Innovation Director at Olea Medical®

Kévin Moulin
PhD candidate at CREATIS, France

Magalie Viallon, PhD
MR physicist and Senior Researcher at CREATIS, France

References

1. Callot V, Bennett E, Decking UK, Balaban RS, Wen H. In vivo study of microcirculation in canine myocardium using the IVIM method. Mag. Reson Med. 2003 Sep;50(3):531-40.
2. Bihan D, Turner R. The capillary network: a link between IVIM and classical perfusion. Magn Reson Med. 1992 Sep;27(1):171-8.
3. Cernicanu A, Axel L. Theory-based signal calibration with single-point T1 measurements for first-pass quantitative perfusion MRI studies. Acad Radiol. 2006 Jun;13(6):686-93.
4. Noehren B, Andersen A, Feiweier T, Damon B, Hardy P. Comparison of twice refocused spin echo versus stimulated echo diffusion tensor imaging for tracking muscle fibers. J Magn Reson Imaging. 2015 Mar;41(3):624-32.
5. Froeling M, Strijkers GJ, Nederveen AJ, Chamuleau SA, Luijten PR. Diffusion Tensor MRI of the Heart – In Vivo Imaging of Myocardial Fiber Architecture. Curr Cardiovasc Imaging Rep. July 2014, 7:9276.
6. Welsh CL, DiBella EV, Hsu EW. Higher-Order Motion-Compensation for In Vivo Cardiac Diffusion Tensor Imaging in Rats. IEEE Trans Med Imaging. 2015 Sep;34(9):1843-53.
7. Stoeck CT, von Deuster C, Genet M, Atkinson D, Kozerke S. Second-order motion-compensated spin echo diffusion tensor imaging of the human heart. Magn Reson Med. 2016 Apr;75(4):1669-76.
8. Rapacchi S, Wen H, Viallon M, Grenier D, Kellman P, Croisille P, Pai VM. Low b-value Diffusion-Weighted Cardiac Magnetic Resonance Imaging. Invest Radiol. 2011 Dec;46(12):751-8.
9. Moulin K, Croisille P, Feiweier T, Delattre BM, Wei H, Robert B, Beuf O, Viallon M. In vivo free-breathing DTI and IVIM of the whole human heart using a real-time slice-followed SE-EPI navigator-based sequence: A reproducibility study in healthy volunteers. Magn Reson Med. 2016 Jul;76(1):70-82.
10. Delattre BM, Viallon M, Wei H, Zhu YM, Feiweier T, Pai VM, Wen H, Croisille P. In vivo cardiac diffusion-weighted magnetic resonance imaging: quantification of normal perfusion and diffusion coefficients with intravoxel incoherent motion imaging. Invest Radiol. 2012 Nov;47(11):662-70.
11. Dyvorne HA, Galea N, Nevers T, Fiel MI, Carpenter D, Wong E, Orton M, de Oliveira A, Feiweier T, Vachon ML, Babb JS, Taouli B. Diffusion-weighted Imaging of the Liver with Multiple bValues: Effect of Diffusion Gradient Polarity and Breathing Acquisition on Image Quality and Intravoxel Incoherent Motion Parameters—A Pilot Study. Radiology. 2013 Mar;266(3):920-9.
12. Jeffreys H. An Invariant Form for the Prior Probability in Estimation Problems. Proc R Soc Lond A Math Phys Sci. 1946;186(1007):453-61.
13. Neil JJ, Bretthorst GL. On the use of Bayesian probability theory for analysis of exponential decay data: An example taken from intravoxel incoherent motion experiments. Magn Reson Med. 1993 May;29(5):642-7.
14. Spinner G, von Deuster C, Stoeck CT, Kozerke S. Bayesian Intravoxel Incoherent Motion Imaging to Map Perfusion in the Human Heart. Proceedings ISMRM 2016, Singapour, Indonesia.
15. Boutelier T, Kudo K, Pautot F, Sasaki M. Bayesian Hemodynamic Parameter Estimation by Bolus Tracking Perfusion Weighted Imaging. IEEE Trans Med Imaging. 2012 Jul;31(7):1381-95.
16. Orton MR, Collins DJ, Koh DM, Leach MO. Improved intravoxel incoherent motion analysis of diffusion weighted imaging by data driven Bayesian modeling. Magn Reson Med. 2014 Jan;71(1):411-20.
17. McNamara MT, Higgins CB, Ehman RL, Revel D, Sievers R, Brasch RC. Acute myocardial ischemia: magnetic resonance contrast enhancement with gadolinium-DTPA. Radiology. 1984 Oct;153(1):157-63.
18. Atkinson DJ, Burstein D, Edelman, RR. First-pass cardiac perfusion: evaluation with ultrafast MR imaging. Radiology. 1990 Mar;174(3 Pt 1):757-62.
19. Kim RJ, Shah DJ, Judd RM. How we perform delayed enhancement imaging. J Cardiovasc Magn Reson. 2003 Jul;5(3):505-14.
20. Kim,RJ, Fieno DS, Parrish TB, Harris K, Chen EL, Simonetti O, Bundy J, Finn JP, Klocke FJ, Judd RM. Relationship of MRI Delayed Contrast Enhancement to Irreversible Injury, Infarct Age, and Contractile Function. Circulation. 1999 Nov 9;100(19):1992-2002.

DWI and IVIM in the Orbit at 3T

How-to session

Augustin Leeler, MD
Department of Radiology, Fondation Ophtalmologique A.Rothschild, Paris, France

The following case report highlights a potential great interest of IVIM applied in the orbit.

Patient history

A 38-year-old woman presented with rapidly worsening, painless monocular vision loss of her left eye, which began six months prior to the encounter. The clinical exam revealed a visual acuity of 1.4/10 and a central scotoma in the left eye. Oculomotricity was normal. A MRI was performed.

Morphological findings

The MRI protocol included an axial unenhanced T1-weighted spin echo sequence, a coronal T2-weighted Dixon, a dynamic-contrast enhancement perfusion sequence, a coronal fat sat post-contrast T1-weighted spin echo sequence, an axial high resolution post-contrast proton density-weighted spin echo sequence and an IVIM acquisition based on DW images acquired using 15 b-values (0, 10, 20, 40, 80, 110, 140, 170, 200, 300, 400, 600, 800, 1000, 2000 s/mm^2) at 3T.

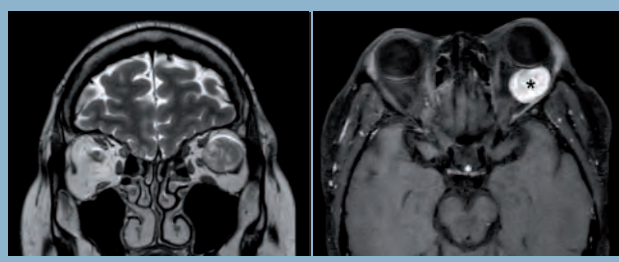

Figure 1: Left orbital mass pointed out on coronal T2-WI Dixon series and on axial post-contrast T1-WI series (asterisk)

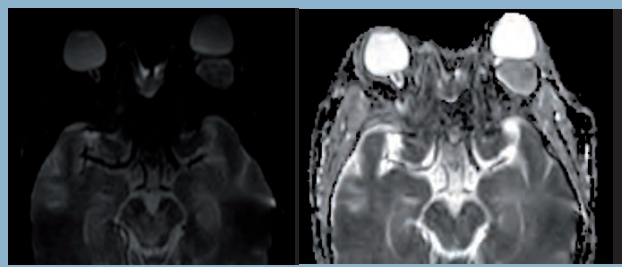

Figure 2: b0 image and ADC map

The patient was asked to look at a fixed point during the acquisitions in order to prevent kinetic artifacts from eye movements. Conventional MRI showed a 30 mm mass located in the left orbit, displacing the eye anteriorly, with a high intensity on T2-WI and progressive filling of the lesion after contrast injection on DCE acquisitions, suggesting the diagnosis of cavernous hemangioma (Figure 1).

Post-treatment and analysis

ADC and IVIM maps were computed and analyzed using Olea Sphere® software (Olea Medical®, La Ciotat, France). A multiparametric display (b0, b2000, T1 gado, ADC, D, D*, PF) was used to draw regions of interest (ROIs) and to provide quantitative values of the mass metrics.

Diffusion-weighted imaging (DWI)

The orbital mass was detected by a hyperintense signal on the axial b0 image and a large freehand ROI encompassing the largest area inside the lesion was placed and automatically propagated on all available maps. Apparent diffusion coefficient (ADC) map showed a high ADC value of 1.26 x 10^{-3} mm^2/s, confirming a probably benign lesion (Figure 2).

Intravoxel incoherent motion (IVIM) imaging

The true diffusion coefficient (D), the pseudo-diffusion coefficient (D*) and the perfusion fraction (PF) maps also showed the left orbital mass with mean values of 1.02 x 10^{-3} mm^2/s, 14.6 x 10^{-3} mm^2/s and 0.18 respectively. In addition, voxels inside the lesion presented a bi-exponential behavior, confirming the presence of both diffusional and perfusional components of the IVIM imaging (Figure 3).

Histopathology diagnosis

The biopsy confirmed the diagnosis of cavernous hemangioma which is the most frequent benign lesion in the orbit.

Conclusion

Diffusion-weighted imaging has been used in a variety of organs, with a few studies in the orbit. They showed that a restricted diffusion in orbital tumors during MR imaging with echo-planar DWI was associated with malignancy, especially in lymphoid lesions such as lymphoma [1-3]. Moreover, the association of ADC with dynamic contrast-enhanced (DCE) perfusion helped to predict malignancy in another recent studies [4], with ADC alone yielding the optimal sensitivity in differentiating malignant from benign orbital lymphoproliferative disorders [3].

However, no study has previously evaluated the performances of IVIM imaging on orbital diseases, especially in orbital tumor characterization, despite a potential great interest since orbital tumors are highly vascularized. Acquisition of IVIM parameters could potentially be useful in the characterization of orbital masses, since more quantitative DWI parameters are acquired, some of them reflecting tissue perfusion. It could also serve as a potential biomarker to evaluate therapeutic responses under treatment such as chemotherapy in lymphomas or proton therapy in ocular melanomas.

References

1. Sepahdari AR, Aakalu VK, Setabutr P, Shiehmorteza M, Naheedy JH, Mafee MF. Indeterminate orbital masses: restricted diffusion at MR imaging with echo-planar diffusion-weighted imaging predicts malignancy. Radiology 2010; 256:554–564.
2. Haradome K, Haradome H, Usui Y, Ueda S, Kwee TC, Saito K, Tokuuye K, Matsubayashi J, Nagao T, Goto H. Orbital lymphoproliferative disorders (OLPDs): value of MR imaging for differentiating orbital lymphoma from benign OPLDs. AJNR Am J Neuroradiol 2014; 35:1976–1982.
3. Xu X-Q, Hu H, Liu H, Wu JF, Cao P, Shi HB, Wu FY. Benign and malignant orbital lymphoproliferative disorders: Differentiating using multiparametric MRI at 3.0T. J Magn Reson Imaging JMRI 2016.
4. Ro S-R, Asbach P, Siebert E, Bertelmann E, Hamm B, Erb-Eigner K. Characterization of orbital masses by multiparametric MRI. Eur J Radiol 2016; 85:324–336.

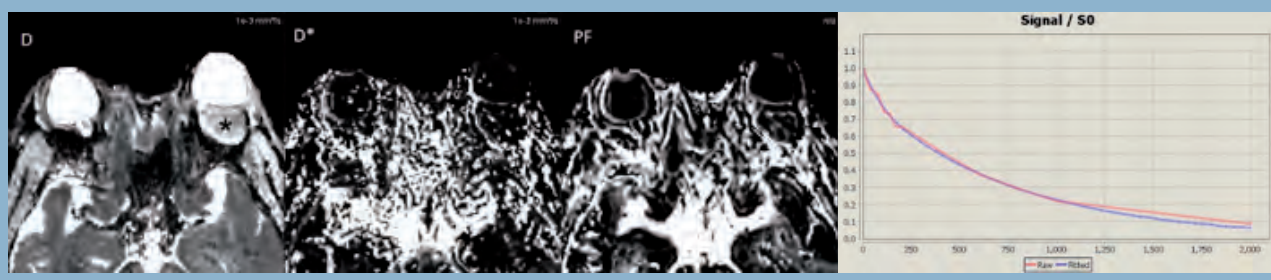

Figure 3: Left orbital mass pointed out on D, D* and PF maps (asterisk) with bi-exponential fitting curves showing signal intensity as a function of b-values (red: raw data; blue: fitted data)

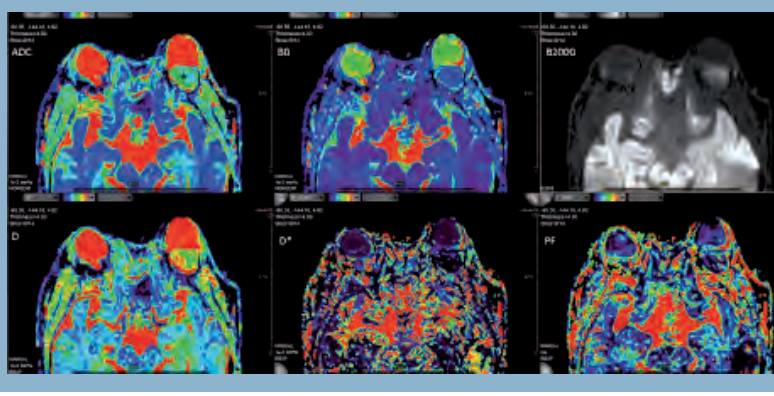

Figure 4: Multiparametric display with diffusion maps (ADC, b0, b2000, D, D* and PF)

State of the art in Diffusion MRI & beyond

6 FAQs to summarize Diffusion MRI

Denis Le Bihan, MD, PhD

1 WHAT ARE THE BASIC TISSUE FEATURES AT THE ORIGIN OF THE DIFFUSION CONTRAST?

With diffusion MRI one investigates the diffusion of water molecules in tissue (diffusion of other molecular moieties may also be studied with MR diffusion spectroscopy). One may consider water molecules as spies which will probe the tissues for us, giving an imprint into the diffusion MRI signal of what they have 'seen' during their Brownian motion driven displacements, fibers, macromolecules, cell membranes, all obstacles which have prevented them to diffuse freely. Hence, although the images are acquired at a millimetric scale, one gets information on the tissue structure at a microscopic scale, a kind of virtual biopsy. Of course, one should not forget that this microscopic information is averaged out within each voxel, although one may still get information on the degree of homogeneity or heterogeneity of the diffusion process within each voxel.

This concept, inferring information on tissue microstructure in images with a macroscopic resolution has proven extremely useful in clinical practice, providing exquisite contrast not readily available with other imaging modalities, including MRI. For instance, brain cell swelling which occurs right at the onset of ischemia is only revealed by diffusion MRI, well before any detectable changes in T1 or T2 may be observed, thus allowing diagnosis at the acute phase, which has completely changed our views on the management of acute stroke patients, drastically improving many patients' clinical outcome and, often, saving their lives.

2 WHAT ARE THE B-VALUES, HOW DO I CHOOSE THEM?

Diffusion-driven displacements of water molecules are encoded in the MRI signal through variations of the magnetic field in space caused by magnetic field gradient pulses. The degree of sensitivity to diffusion is described by the so-called b-value which was introduced in 1985 to take into account the intensity and time profile of the multiple gradient pulses used in MRI sequences. The overall effect of diffusion in the presence of gradient pulses is a signal attenuation and the MRI signal becomes "diffusion-weighted". The signal attenuation is more pronounced when using large b-values and when diffusion is fast.

As diffusion-weighted images also depend on other parameters, such as T1 and T2, one may prefer to use "calculated" diffusion images where contrast solely depends on diffusion, through a parameter called ADC (Apparent Diffusion Coefficient). The ADC can be obtained from images acquired using only 2 different b-values. In theory the ADC does not depend on b-values, so the choice of b-values is set just to provide the best accuracy on the ADC, depending on expected ADC values. For instance, in the brain, the optimal pair of b-values is 0 and 1000 s/mm^2, while in most body tissues one may prefer 0 and 600 s/mm^2.

Unfortunately, this is true only to some extent, only with free (also called Gaussian) diffusion, such as in liquids. In most tissues diffusion becomes non-Gaussian as many obstacles hinder water diffusion, and the amount of diffusion driven signal attenuation decreases when the b-value increases, in other words the ADC value decreases when high b-values are used. It is thus mandatory to indicate which b-values have been used to acquire data, if one wishes to make meaningful comparisons across literature or centers. In fact, not only the b-values, but the precise timing of the gradient pulses (which set the "diffusion time") used for diffusion encoding must be provided, as different time profiles could lead to different diffusion effects, while sharing the same b-value. This is due to the fact that water molecules will have more chances to interact with tissue microscopic features when using long diffusion times than short diffusion times.

3 WHAT IS IVIM MRI, SHALL I USE IT FOR PERFUSION MRI?

Flow of blood water in randomly oriented capillaries (at voxel level) mimics a random walk which results in a pseudo-diffusion effect when using diffusion MRI. The effect is seen at very low b-values only, because the pseudo-diffusion coefficient, D*, associated with blood flow is higher than the water diffusion coefficient. For this reason, true diffusion and pseudo-diffusion can be separated using dedicated algorithms and software.

> "IVIM MRI is increasingly used to assess perfusion, especially in the field of cancer imaging."

The idea to use diffusion MRI to get images of perfusion has been found ground-breaking, and IVIM MRI is increasingly used to assess perfusion, especially in the field of cancer imaging. A key feature of IVIM diffusion MRI is that it does not involve contrast agents, and it may serve as an interesting alternative to contrast-enhanced perfusion MRI in some patients with contraindications for contrast agents, such as patients with renal failure, at risk for Nephrogenic Systemic Fibrosis (NSF) or patients requiring multiple MRI examinations, as gadolinium has been shown to accumulate in the brain. One has to keep in mind, though, that IVIM MRI is a bit challenging, as separation of perfusion from diffusion requires high signal-to-noise ratios.

4 WHAT IS DIFFUSION ANISOTROPY, SHOULD I CARE, HOW DOES IT RELATE TO TRACTOGRAPHY?

With the MRI encoding process diffusion, although a three-dimensional process, is only measured along one direction at a time determined by the orientation in space of the gradient pulses. Most often diffusion is "isotropic" (the same in all directions), so that this spatial orientation does not matter. This is the case for most tissues in the body (liver, prostate, breast).

However, in some tissues, such as brain, white matter or heart/muscle fibers, diffusion is "anisotropic", and diffusion results strongly depend on the direction of the gradient pulse.
Proper handling of anisotropic diffusion requires the acquisition of diffusion-weighted images along with at least 6 different directions (and not 3), through the Diffusion Tensor Imaging (DTI) method. With DTI one can get the "trace" of the diffusion tensor which represents the true mean diffusivity, indices of the degree of anisotropy (such as Fractional Anisotropy) and so-called "eigenvectors" which point to the directions along which diffusion is the fastest, corresponding in general to the directions parallel to tissue fibers. DTI has served as the basis for brain white matter tractography, in conjunction with algorithms connecting voxels based on their fiber orientations, but more advanced techniques are currently used, such as HARDI, to take into account voxels with multiple fiber orientations.

DTI must be used in tissues where water diffusion is anisotropic, mainly in the heart, muscle and brain white matter, but also in other tissues showing signs of anisotropy, such as the kidney. Diffusion anisotropy may also appear only when spatial resolution gets sufficiently high, as in the brain cortex or the breast.

5 WHAT CAN I EXPECT FROM POST-PROCESSING OF DIFFUSION-WEIGHTED MR IMAGES?

Diffusion is a genuine physical process occurring in tissues on its own, as opposed to T1 or T2 which are only defined in the MRI context. Post-processing is a very important step to get full information, not readily visible on raw diffusion-weighted images which are also T1- and T2-weighted. For instance, one can get diffusion-calculated images, which only depends on the ADC.

But other very useful parameters can also be extracted from diffusion-weighted MR signals, such as perfusion from the IVIM effect. When processing a set of images acquired with multiple b-values, including high b-values, one may get additional information on non-Gaussian diffusion, that is on the degree of hindrance of water diffusion by obstacles present in tissues, amount of fibers and most importantly cell membranes, an extremely valuable information to identify and characterize malignant tissues. To do so, signals from images are combined through algorithms and evaluated with mathematical and physical diffusion models which have been devised to handle non-gaussian diffusion, such as the Kurtosis model.

Model outputs are finally transformed into a series of parametric maps, showing means, but also heterogeneity of parameters across tissues and organs. Once those diffusion-related parameters have been estimated, one may also generate a posteriori virtual diffusion-weighted image mimicking contrast which could be obtained at any b-value. Post-processing is, obviously, the cornerstone of tractography, providing 3D maps of brain connections from DTI images, but also information on axon fiber diameter or orientation coherence. Another important mission of post-processing software is to "clean" raw data, realigning images affected by organ motion, correcting geometric distortions induced by gradient pulses or extracting meaningful signals from background noise. In summary, post-processing is the key one needs to fully exploit the benefits of IVIM and diffusion MRI.

6 WHAT IS BEYOND THE CORNER?

First, as diffusion MRI is becoming more and more sophisticated we are counting on algorithms and software to make clinicians' life easier. Instead of separately analyzing many parameters, IVIM, ADC, Kurtosis, etc. software might digest the overwhelming information to provide semi-automatic analysis of lesions, through synthetic diffusion indices or scores, up to diagnosis or staging, of course under final clinician guidance. For instance, each parameter may have a given threshold to segregate benign and malignant tissues.

> "MRI might also provide information on tissue elasticity."

Those parameters may be combined to give a summary diagnostic score based on the number of parameters "voting" for malignancy. Score maps can be generated giving diagnosis, but also showing which areas of lesions are likely to be most malignant, suggesting best locations for biopsies. With the Bayesian approach one may, instead, weight each parameter value with population based statistics to provide an overall probability for each tissue type (e.g., malignant versus benign or malignant stages). One may also calculate a signature index from the "proximity" of the full diffusion MRI signal profile (obtained from a set of key b-values) of an examined tissue to a databank of "signature" signal profiles, e.g. from established malignant and benign tissues of a given organ. With this signature index, diagnosis or tissue staging can be obtained directly and automatically with great accuracy without calculating any parameter model. With IVIM, the signature index may identify voxels exhibiting fast flow. Those voxels can then be connected using algorithms similar to those used for tractography to generate IVIM based angiograms without using contrast agents.

Secondly, we have to realize that the information buried in diffusion MRI signal is incredibly rich, so it takes up to our imagination to devise new ideas, methods or algorithms to dig into this gold mine. For instance, the exquisite sensitivity of diffusion MRI to minute changes in cell size (e.g. swelling) makes diffusion MRI a completely new approach for functional MRI, as neural activation is associated to cell swelling, a much more direct approach than BOLD fMRI which relies on the neurovascular coupling principle.

As another example, taking into consideration that diffusion MRI is intimately linked to tissue microstructure, it should not be surprising that diffusion MRI might also provide information on tissue elasticity. Indeed, diffusion features, especially through the synthetic indices presented above, have been successfully converted quantitatively into tissue shear stiffness (in kPa) with great accuracy, and without the need for the vibration devices or the phase sensitive MR sequences used with conventional MR Elastography (MRE). Furthermore, the intravoxel phase dispersion which would result from propagating shear waves induced by mechanical vibrations can be emulated and transformed into virtual elastograms through the IVIM effect for any organ and for any combination of vibration frequency or amplitude, not readily available with conventional MRE hardware, producing new and exciting contrast. Clearly, diffusion MRI will keep Olea Medical® busy for years to come, integrating those very promising innovations into their software for the benefit of patients and health professionals alike.

Denis Le Bihan
MD, PhD

Director of NeuroSpin, CEA Saclay-Center, Gif-sur-Yvette, France.
Professor at Human Brain Research Center, Kyoto University Graduate School of Medicine, Kyoto, Japan.

Meet Olea Medical® in 2017

January 31 – February 3
4th ESO-ESMINT-ESNR
Stroke Winter School
Bern, Switzerland

February 22-24
International Stroke Conference **(ISC)**
Houston, USA

March 1-5
European Congress of Radiology **(ECR)**
Vienna, Austria

March 22-24
American Society of Neuroradiology **(ASNR)**
55th Annual Meeting
California, USA

April 22-27
International Society for Magnetic Resonance in Medicine **(ISMRM)**
25th Annual Meeting Honolulu, USA

May 4-7
Jornadas Paulistas de Radiologia **(JPR)**
Sao Paulo, Brazil

June
Atelier prostate du Docteur Cornud
Paris, France

August 24-27
Eastern Neuroradiological Society **(ENRS)**
29th Annual Meeting
Toronto, Canada

August 30 - September 1

44th Annual Meeting and Musculo-skeletal Imaging Course: Fundamentals to Advanced Concepts **(ISS)**
New York, USA

September 16-20

American Society of Head & Neck **(ASHNR)**
Las Vegas, USA

October 13-16

Journées Françaises de Radiologie **(JFR)**
Paris, France

October 25-28

49th Annual Meeting of Western Neuroradiological Society **(WNRS)**
Koloa, USA

October

British Society of Neuroradiologists **(BSNR)**
Annual Conference
York, England

October

Atelier prostate du Docteur Cornud
Paris, France

November 27 – December 2

Radiological Society of North America **(RSNA)**
Chicago, USA

Word scramble

L	U	O	X	C	W	N	X	N	A	S	Y	E	Y	J
Y	T	T	U	U	U	L	K	F	W	D	L	T	U	L
W	I	Ç	S	I	O	P	T	S	O	K	U	A	J	B
F	B	W	T	S	A	E	R	B	O	D	I	T	F	A
U	P	K	I	V	I	M	E	B	N	D	T	S	X	Y
S	K	V	N	C	P	L	V	I	I	N	C	O	J	E
T	U	I	M	V	O	A	C	F	E	P	O	R	A	S
R	R	A	N	H	L	Y	F	I	J	U	M	P	X	I
O	T	S	W	U	N	U	D	H	Z	F	P	Q	O	A
K	O	P	E	O	S	A	R	E	O	B	U	I	G	N
E	S	O	B	I	R	E	J	A	G	D	T	Z	Ç	C
Ç	I	A	O	G	V	B	W	R	E	A	E	L	O	L
W	S	N	Z	I	I	Z	I	T	Q	K	D	K	N	F
M	B	M	L	L	X	H	H	T	G	M	Z	G	J	K
J	D	N	R	S	H	E	A	D	N	E	C	K	R	L

- DIFFUSION
- BVALUE
- GRADIENT
- IVIM
- KURTOSIS
- OLEA
- BAYESIAN
- STROKE
- BREAST
- WHOLEBODY
- HEADNECK
- ORBIT
- HEART
- PROSTATE
- LIVER
- COMPUTED

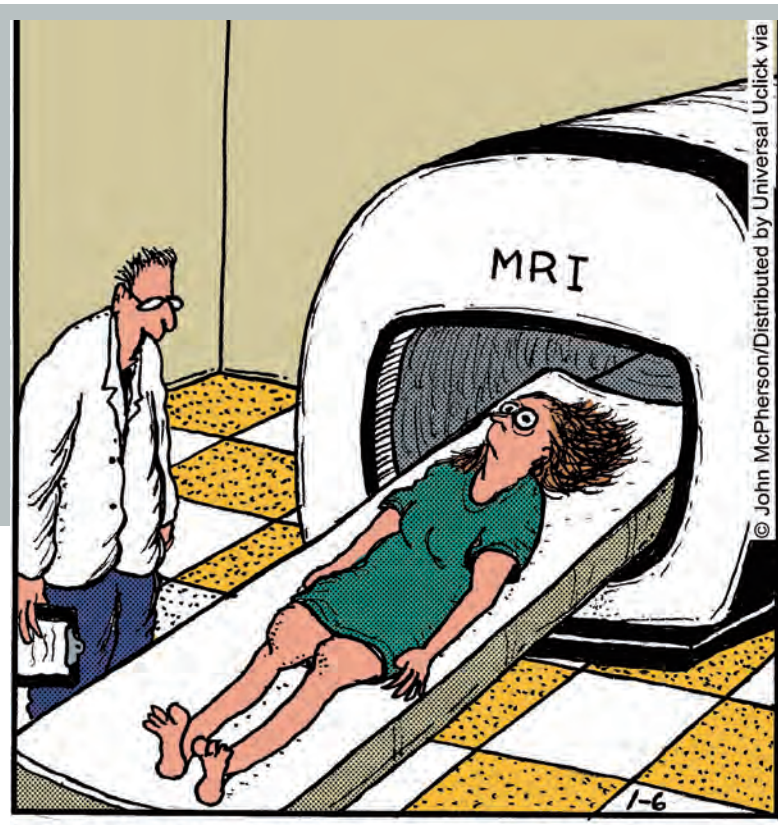

"OK, Mrs. Dunn. We'll slide you in there, scan your brain, and see if we can find out why you've been having these spells of claustrophobia."

TAKE PART IN THE 2nd OLEA INNOVATORS AWARDS

Are you working on an innovative project on MRI?

Subscribe to Olea Innovators Awards for:

- **Technological industrialization & commercialization of innovation**

OR

- **Innovation incubator (10,000 € research grant)**

TOPIC

Innovative MRI medical imaging techniques for diagnosis and follow-up of severe diseases

Apply on **www.olea-medical.com**, before **March 31th, 2017**

Competition details and rules available online

The award ceremony will be held during the Journées Francophones de la Radiologie, in Paris, in October 2017

Olea MEDICAL | Improved diagnosis for life™

Partner of Olea Innovators 2nd edition: Inria INVENTORS FOR THE DIGITAL WORLD

Coming next

Advanced Diffusion MRI models

Shigeki Aoki, MD, PhD
Professor and Chairman, Department of Radiology, Juntendo University; President of 43rd Japanese Society for Magnetic Resonance in Medicine.

Olea Imagein: Your remarkable research contributions cover broad clinical areas in MRI, with a special focus on Diffusion Tensor Analysis. Could you please share with our readers how your background and interests led you to select and develop this particular imaging process?

Shigeki Aoki: My research focus is on Diffusion Tensor MRI, and on next generation sequences including Diffusion Kurtosis or Neurite Orientation Dispersion and Density Imaging (NODDI).

Why select Diffusion? It is easy to explain since Diffusion process has two unique characteristics. First, it includes directions; there is no other imaging sequence that deals with directional data, except Phase Contrast imaging. Second, it can measure, this is a very unique MRI acquisition; diffusion tensor parameters such as fractional anisotropy are measurable everywhere and in every direction.

dMRI reveals the structure, it can display very precise and good-looking images; with brain tractography, it has the capacity to visualize white matter tracts.

O.I: What are your expectations about diffusion kurtosis imaging? Which potential new applications could benefit to the patient with this technique?

S.A: Kurtosis imaging is very sensitive, much more sensitive than any other diffusion technique. It gives information that are not available with any other technique.

What does Kurtosis reveal?

Kurtosis diffusion imaging can reveal very early infarction in stroke; this technique is better to see infarction, and make some measurements. It is also very sensitive for Parkinson's diseases.

As for kurtosis imaging evolution towards clinical practice, we are still not there yet. Though very helpful, the images are noisy and not easy to characterize. Also, the availability of Kurtosis is not so high; even for us, we have to transfer the data to other computers for processing and send them to the PACS. There is a necessity to make a DICOM image, online and of good quality to the PACS, before considering a clinical use. Therefore, today it is still time consuming and not easy to process.

to be continued in the next issue of Olea Imagein ...

Coming next

Would you like to learn more about the future of MRI? World experts will reveal their vision in the upcoming issue of Olea Imagein.

Subscribe Online to Olea Imagein upcoming edition at www.olea-medical.com

INTRODUCING
FULLY AUTOMATED
STROKE APPLICATIONS

Olea Sphere 3.0*

ZERO CLICK
Calculation of infarct penumbra & mismatch

AUTOMATED STROKE REPORT
(MRI & CT) by email

VENDOR-NEUTRAL
& easy integration into IT systems

Ask for a free trial
www.olea-medical.com

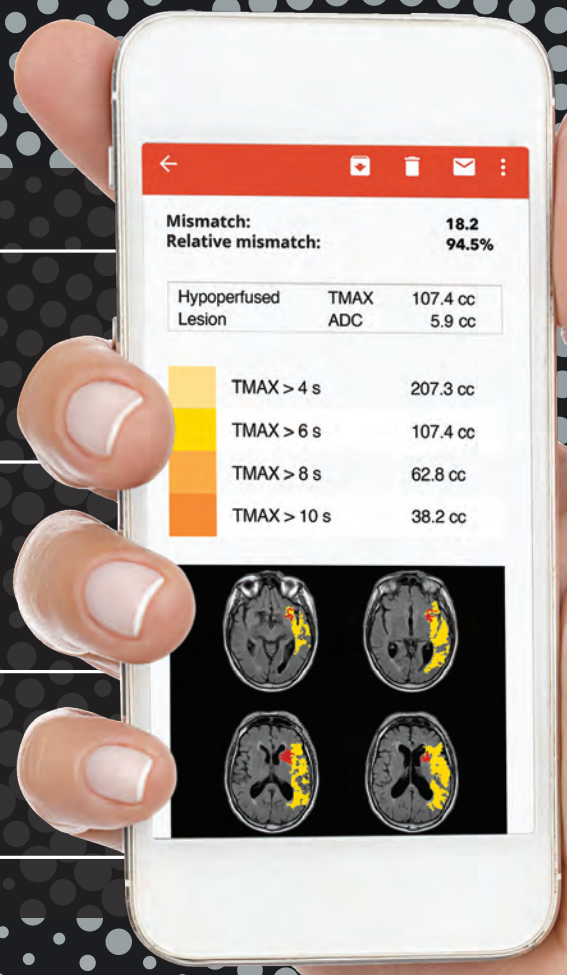

“ **Innovation** is in our **DNA.** ”

* FDA cleared

Olea MEDICAL

Improved diagnosis for life™